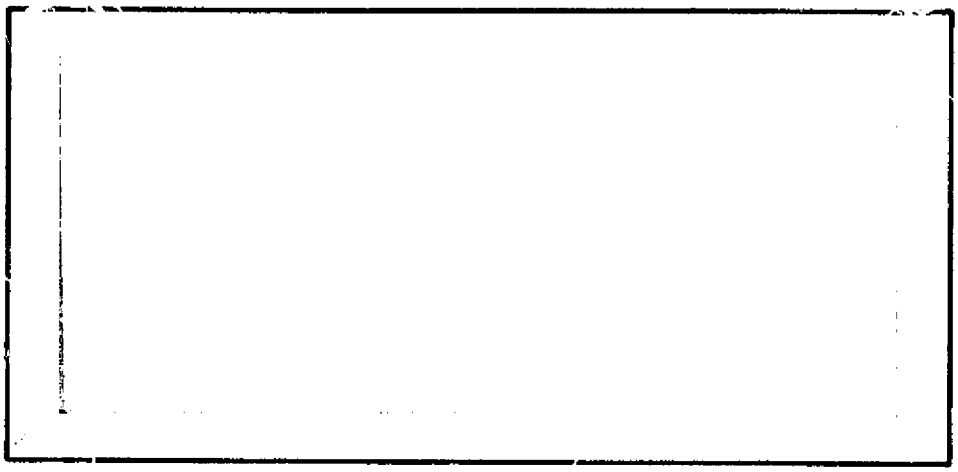

SCIENCE APPLICATIONS, INC.

Report No. SAI 1-120-580-T6

MERCURY ORBITER TRANSPORT STUDY

by

Alan L. Friedlander
Harvey Feingold

Science Applications, Inc.
1701 East Woodfield Road
Schaumburg, Illinois 60195

for

Lunar and Planetary Programs Division
Office of Space Sciences
NASA Headquarters
Washington, D.C. 20546

Contract No. NASW-2893

January 1977

FOREWORD

This study was conducted between March and October 1976 as part of the work performed by Science Applications, Inc. under Contract No. NASW-2893 for the Lunar and Planetary Programs Division, Code SL, of NASA Headquarters. The results are intended to assist NASA planners assess the trajectory/payload performance requirements of candidate flight modes in delivering spacecraft systems to orbit the planet Mercury.

TABLE OF CONTENTS

	Page
FOREWORD	ii
SUMMARY	v
1. INTRODUCTION	1
1.1 Mission Concepts and Payload Requirements	1
1.2 Study Objectives and Scope	3
2. TRANSPORT OPTION CAPABILITIES	9
2.1 Ballistic Mode (Venus Swingby)	9
2.2 Solar Electric Propulsion Mode	22
2.3 Solar Sailing Mode	29
3. PERFORMANCE COMPARISON	39
3.1 Payload and Flight Time Trades	39
3.2 Cost Implications	42
REFERENCES	49
APPENDIX A: Performance Curves for Ballistic Opportunities	51

Science Applications, Inc.
Schaumburg, Illinois

MERCURY ORBITER TRANSPORT STUDY

Contract No. NASW-2893

STAR Abstract

The objective of this task is to provide a data base and comparative performance analyses of alternative flight mode options for delivering a range of payload masses to Mercury orbit. Launch opportunities over the period 1980-2000 are considered. Extensive data trades are developed for the ballistic flight mode option utilizing one or more swingbys of Venus. Advanced transport options studied include solar electric propulsion and solar sailing. Study results show the significant performance tradeoffs among such key parameters as trip time, payload mass, propulsion system mass, orbit size, launch year sensitivity and relative cost-effectiveness. Handbook-type presentation formats, particularly in the case of ballistic mode data, provide planetary program planners with an easily used source of reference information essential in the preliminary steps of mission selection and planning.

SUMMARY

The objective of this task is to provide a data base and comparative performance analyses of alternative flight mode options for delivering a range of payload masses to Mercury orbit. Launch opportunities over the period 1980-2000 are considered. Extensive data trades are developed for the ballistic flight mode option utilizing one or more swingbys of Venus. Advanced transport options studied include solar electric propulsion and solar sailing. Study results show the significant performance tradeoffs among such key parameters as trip time, payload mass, propulsion system mass, orbit size, launch year sensitivity and relative cost-effectiveness. Handbook-type presentation formats, particularly in the case of ballistic mode data, provide planetary program planners with an easily used source of reference information essential in the preliminary steps of mission selection and planning.

A comparative summary of trajectory and payload characteristics for 16 ballistic launch opportunities is presented in Table S-1. The first four columns show the launch date, number of Venus swingbys, flight time to Mercury, and launch energy C_3 (10^d window). Post-launch retro mass and orbited payload data shown in the last two columns assume the Shuttle/IUS(III) launch vehicle, a space-storable retro system, and a 500 km circular orbit about Mercury. The 1986 V(3), 1988 (V2)-a, 1994 and 1996 launches are among the better opportunities from the mid-1980's through the end of the century. However, the payload capability with IUS upper stages is marginal in most cases and certainly insufficient for extensive science investigations, e.g., multiple lander deployment. Note that massive retro systems, more than six times the payload weight, are required for ballistic missions. Availability of a Tug upper stage would significantly improve payload transport capability. This is shown in Figure S-1 which is an example from the set of performance graphs presented in Appendix A. For a selected periapse altitude and orbit period (open circle intersection), the payload capability of each launch upper stage (solid circle intersection) is read off the left-hand scale; in the example a two-stage retro is assumed.

Figure S-2 compares payload/flight time performance of the three flight modes for achieving a 500 km circular orbit at Mercury. Use of the Shuttle/IUS(III) launch vehicle is assumed. The six sample ballistic opportunities shown on the graph span the range of ballistic mission performance, i.e., flight times between 750 and 1250 days and orbited payloads between 250 and 650 kg. Retro system capability, in order of increasing performance, is Earth-storable, solid/monopropellant and space-storable. Solar electric propulsion offers a considerable performance improvement in terms of reduced flight time (500-600 days) and payload increases to the level 500-1000 kg. This potential of low-thrust transport is further enhanced by the solar sailing concept which could deliver sufficient payload, up to 2000 kg, for multiple surface lander deployment missions.

Estimates were made for the recurring cost of the transport vehicle (SEP or solar sail) and the total costs of the chemical retro systems used for each mode of flight. Figure S-3 shows a comparison of the three flight modes in terms of a specific cost index, i.e., propulsion system cost per kilogram of delivered payload plotted as a function of flight time. Since low specific cost and short flight times are most desirable, it is seen that solar sailing provides the best performance, followed by SEP and then ballistic mode transport. In the ballistic case, the most cost-effective retro propulsion is generally the combined solid/mono system, followed closely by space-storable, with Earth-storable systems being least cost-effective.

In making the above comparison between SEP and solar sailing, the basic assumption used was a SEP recurring cost of $20M-$24M and a considerably lower sail recurring cost of $6M (FY'77 base period). Furthermore, the payload performance stated for SEP was based on current technology parameters. Since these assumptions are certainly subject to question, a sensitivity analysis was performed and the comparative results are shown in Figure S-4. One may conclude, for example, that a SEP vehicle of advanced design is more nearly comparable with a solar sail vehicle in terms of cost-effectiveness.

In summary, the results of this study have shown that low-thrust propulsion is far superior to the ballistic flight mode in transporting appreciable payloads to Mercury orbit. It also appears to be more cost-effective, provided that low-thrust systems are developed for and used across a wide spectrum of planetary mission applications. Solar sail vehicles have a performance advantage over SEP for Mercury missions. This might not be the case for other planetary targets beyond 1 AU distance. Although "conventional" ballistic missions can be flown to Mercury, the flight time tends to be quite long and the payload delivery marginal with IUS launches. Large payload delivery requires the equivalent of a Tug(E) launch vehicle and a very large retro propulsion system carried to Mercury. Also, good ballistic launch opportunities do not occur every year as they do for low-thrust propulsion.

Table S-1

COMPARATIVE SUMMARY OF BALLISTIC MODE MERCURY ORBITERS

Launch Date	Transfer Type	Flight Time (days)	C_3 $(km/sec)^2$	Retro* Mass (kg)	Orbited* Payload (kg)
2/26/80	V(3)	1126	30.90	3095	425
6/26/80	V(1)	657	34.20	2965	285
7/9/81	V(2)-a	1067	32.80	2930	450
10/22/81	V(2)-b	422	45.41	2425	125
3/6/83	V(2)	989	17.45	4075	500
7/8/83	V(3)	953	25.25	3550	350
6/24/85	V(1)	420	49.60	2150	190
7/18/86	V(2)	911	24.44	3790	200
7/29/86	V(3)	1247	19.17	3750	670
3/19/88	V(2)-a	741	25.80	3460	420
7/10/88	V(2)-b	621	28.05	3345	355
7/2/89	V(2)	792	43.25	2370	320
7/13/91	V(2)	1019	25.80	3505	365
7/25/94	V(2)	877	19.38	3770	630
2/9/96	V(3)	782	23.00	3630	470
7/13/99	V(4)	1177	26.35	3380	445

*Shuttle/IUS(III), space-storable retro (two stages), 500 km circular orbit.

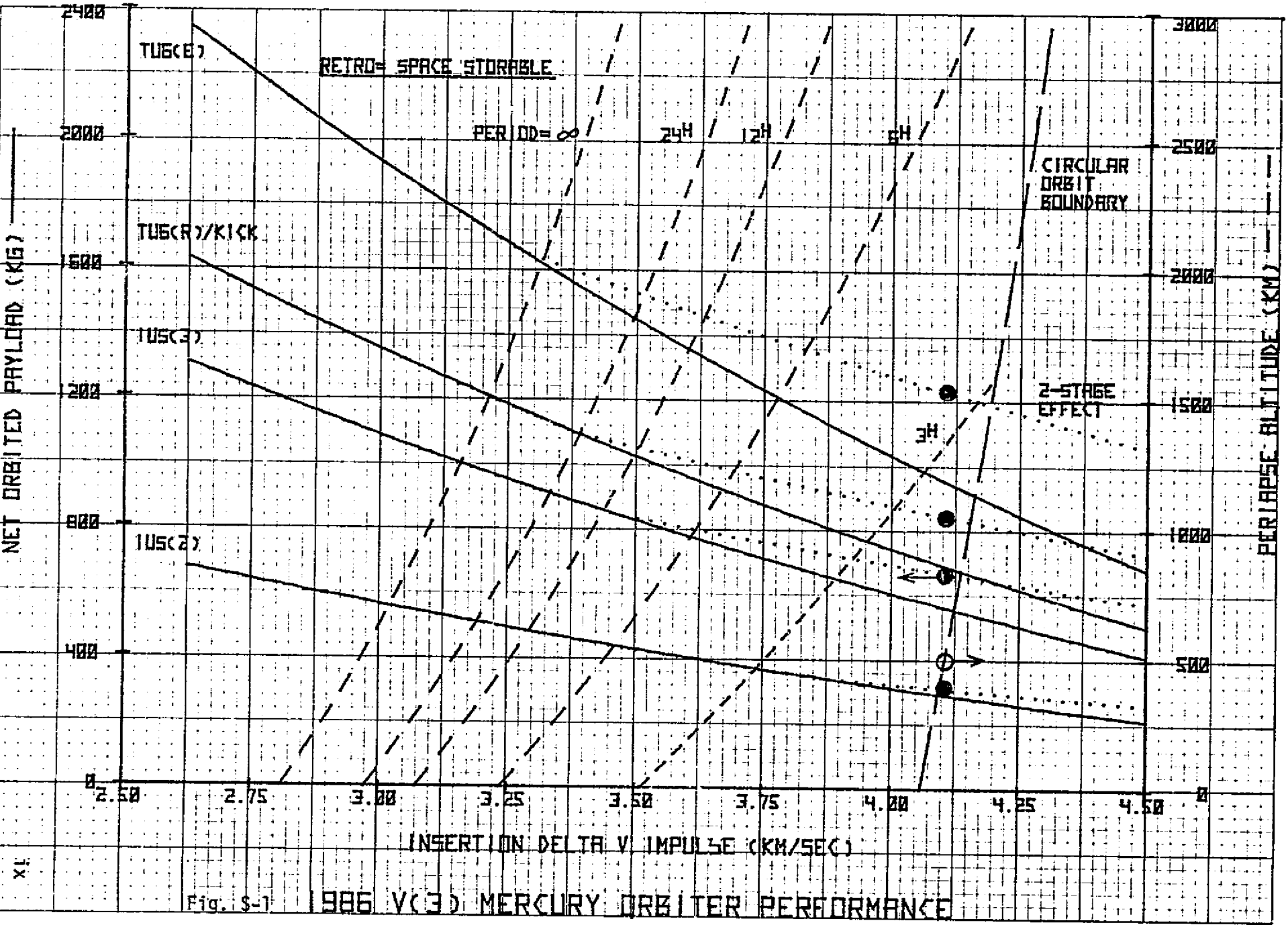

Fig. S-1 1986 V(3) MERCURY ORBITER PERFORMANCE

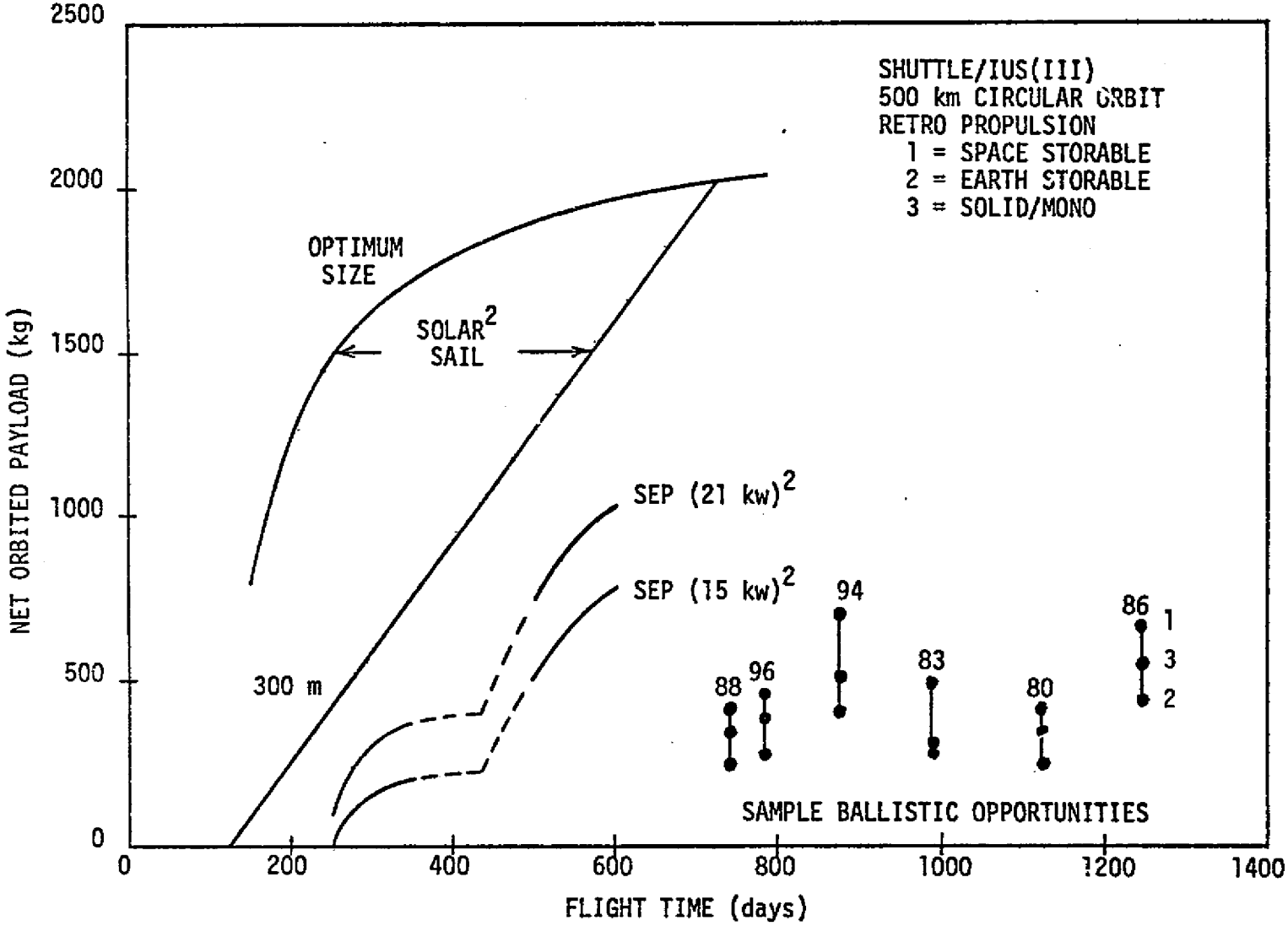

Fig. S-2 PAYLOAD PERFORMANCE COMPARISON FOR MERCURY ORBITER MISSIONS

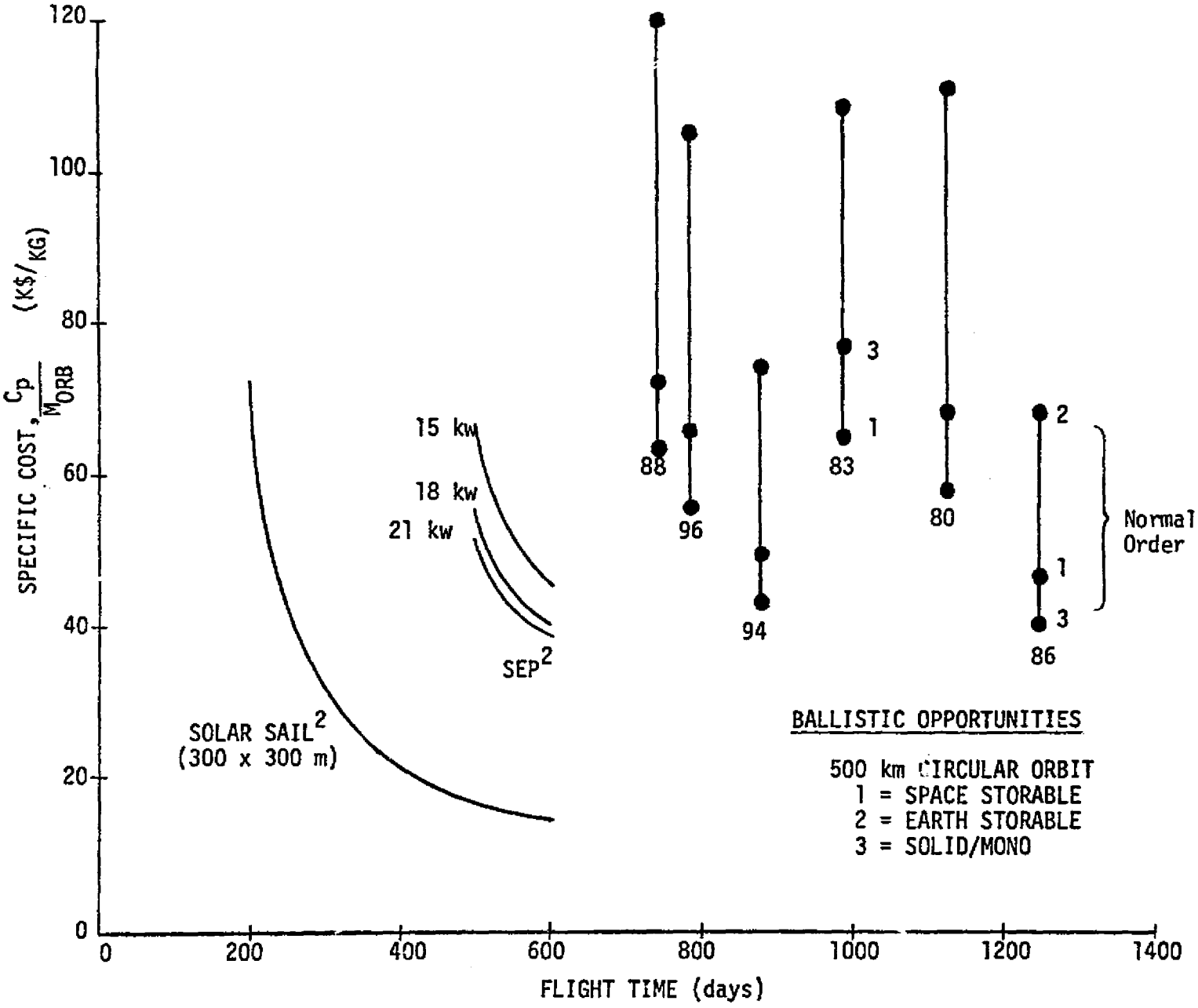

Fig. S-3 PROPULSION SYSTEM SPECIFIC COST COMPARISON FOR MERCURY ORBITER MISSIONS

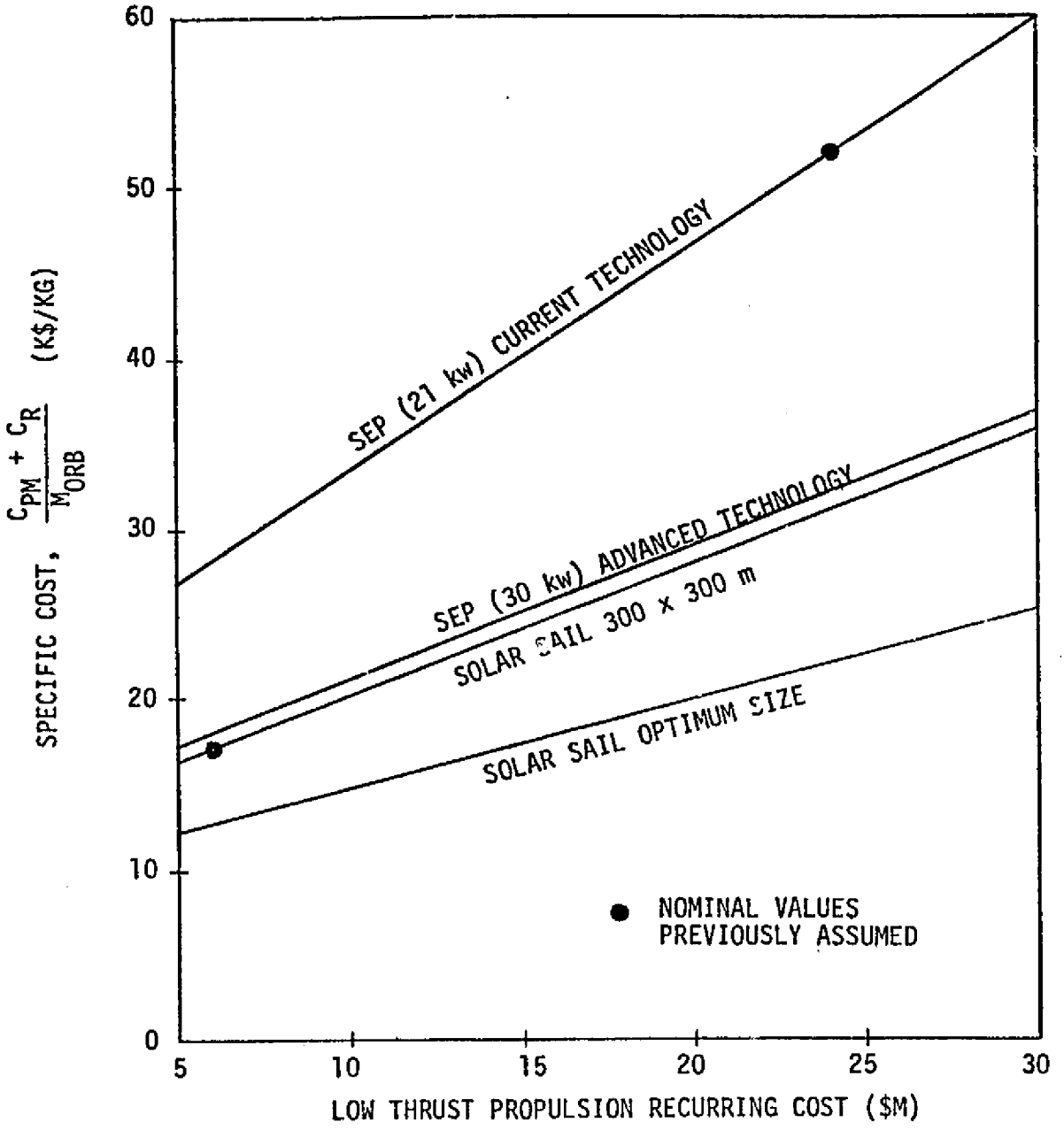

Fig. S-4 PARAMETRIC COST COMPARISON OF SEP AND SOLAR SAIL FOR MERCURY ORBITER MISSION TF = 500 days; 500 km CIRCULAR ORBIT EARTH-STORABLE RETRO

MERCURY ORBITER TRANSPORT STUDY

1. INTRODUCTION

1.1 Mission Concepts and Payload Requirements

Mercury is thought to occupy a unique place in the solar system because of its close proximity to the Sun, its high mass density, and the recently measured magnetic interaction with the solar wind. It is expected that increased knowledge about Mercury will provide the necessary clues to its internal evolution and consequently to the early history of the inner solar system. Scientific objectives and investigations fall into five broad categories: surface morphology, composition, magnetospheric physics, internal mass distribution, and external gravitational theories. The exploration of this planet has begun with the Mariner 10 mission which achieved three successive flyby encounters in 1974-75. A follow-on orbiter mission, perhaps in the mid-1980's, is considered to be an important next step in this exploration process.[1] Surface penetrators[2] and alternative lander[3] concepts have also been studied in conjunction with Mercury orbiter missions. Such a lander would be carried into orbit about Mercury by a spacecraft bus with subsequent deployment to a selected landing site. Hopefully, sufficient payload capability would exist to allow multiple surface probe deployments. Table 1-1 provides a reference list of expected mass requirements in Mercury orbit to conduct different levels of science investigation.

Mercury revolves about the Sun with an orbital period of 88 days, perihelion 0.308 AU, aphelion 0.467 AU, and inclination 7° relative to the ecliptic plane. Since its synodic period with Earth is 116 days there exists an average of three direct launch opportunities each calendar year. These opportunities vary in terms of trajectory/payload performance due to Mercury's orbital eccentricity and spatial orientation; one of these could be identified as a "best choice" in any given year taking into account all mission and spacecraft design features. If another planetary body such as Venus is included in the flight plan, then the transfer mode is no longer direct with the consequence that launch opportunities and performance depend

Table 1-1

PAYLOAD REQUIREMENTS FOR MERCURY ORBITER MISSIONS

Science Mission Type	Orbit Size	Orbited Payload Range (kg)[a]
Particles and Fields	Elliptical, 12^h-24^h	350-450
Planetology	Circular, p ≈ 1.8^h	400-600
Dual Orbiters	Each of above	1000-1400[b]
Orbiter and Small Lander(1)	Elliptical deployment Circular deployment	650-850 550-750
Orbiter and Small Landers(3)	Elliptical deployment Circular deployment	1150-1350 900-1100

[a] Includes science payload and spacecraft bus subsystems, but excludes retro propellant and inerts unless otherwise stated; science payload 40-60 kg; landers 150-250 kg.

[b] Mass in elliptical orbit prior to release of circular orbiter, hence includes retro system for circular orbit insertion.

strongly on the geometry and time phasing of the three planetary bodies. It is in fact the Earth-Venus-Mercury transfer mode employing a Venus gravity-assisted swingby which may allow the Mercury orbiter mission to be accomplished without advanced propulsion technology. However, it is recognized that advanced technology systems such as solar electric propulsion (SEP) or solar sailing offer greater flexibility in mission planning, launch vehicle selection, and mass delivery capability.

Capture into Mercury orbit can be relatively difficult from a propulsion standpoint because of the planet's small gravitational attraction. Figure 1-1 shows orbit insertion ΔV requirements as a function of orbit eccentricity over a range of hyperbolic approach speeds. Ballistic mode transfers have typical approach speeds in the range 5.5 to 7.0 km/sec. Insertion ΔV is 2.8-5.3 km/sec for close circular orbits. Very large retropropulsion systems may therefore be expected for the ballistic flight mode. Low-thrust transfers, by contrast, have typically low approach speeds in the range 0-2 km/sec, and hence have retro ΔV requirements no greater than 1.6 km/sec even for circular orbits. These characteristic results should be kept in mind as they bear strongly on the comparative payload capability data to be presented.

1.2 Study Objectives and Scope

The purpose of this study is to provide a data base and comparative analyses of alternative flight modes for delivering a range of payload mass to Mercury orbit. Launch opportunities over the period 1980-2000 are considered. Extensive data trades are developed for the ballistic flight mode option utilizing one or more swingbys of Venus. Advanced transport options studied include solar electric propulsion and solar sail vehicles. In the case of SEP, data is obtained only for conventional technology systems, i.e., flat arrays without concentrators and standard power processing units. Solar sail technology is considerably less developed than SEP at present, although extensive ongoing studies at JPL are providing the needed data base for sail trajectories and vehicle design.

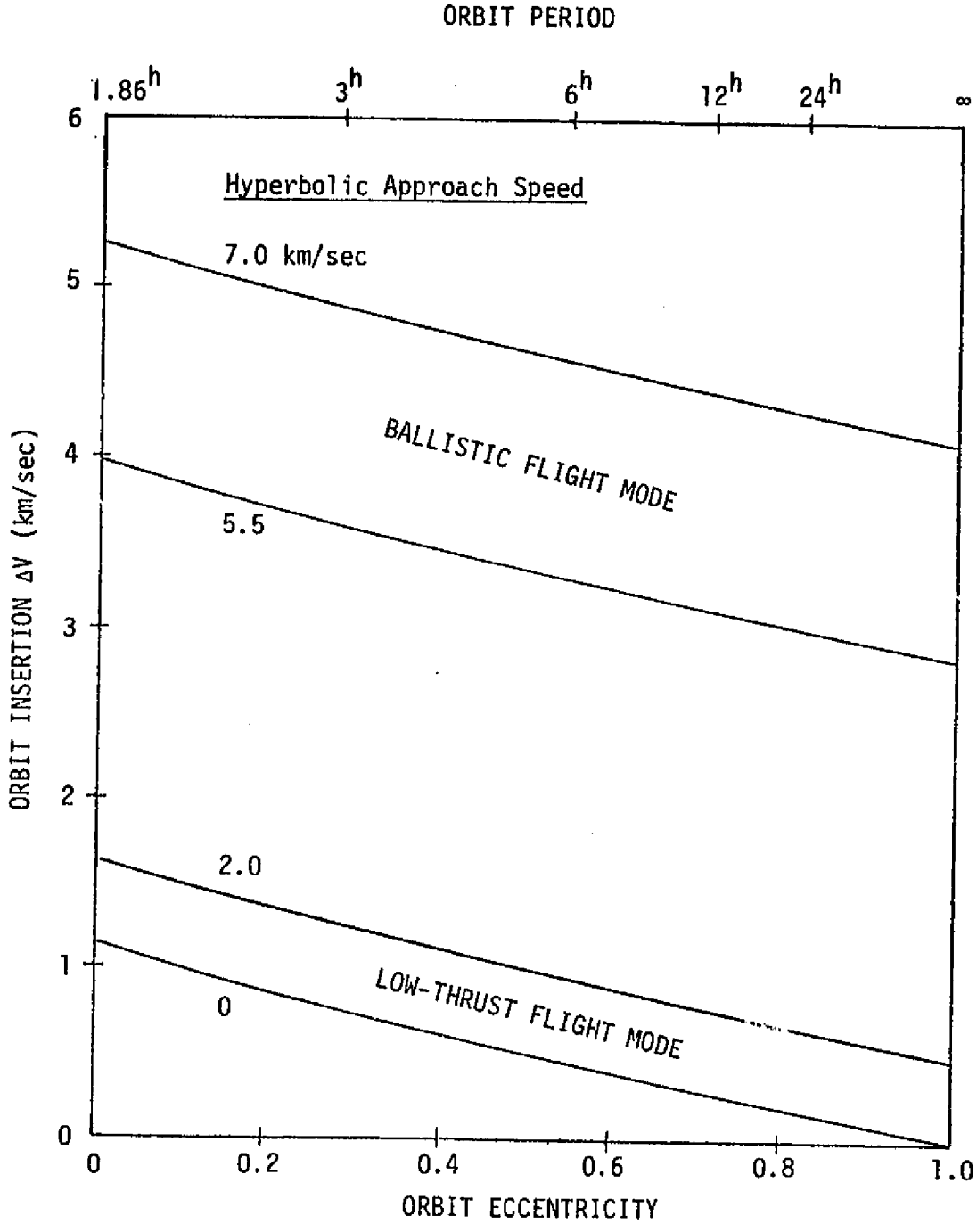

Fig. 1-1 VELOCITY IMPULSE REQUIREMENTS FOR MERCURY ORBIT INSERTION (h_p = 500 km)

Study results are intended to show the significant performance trade-offs among such key parameters as trip time, payload mass, propulsion system mass, orbit size, launch year sensitivity and relative cost-effectiveness. Handbook-type presentation formats, particularly in the case of ballistic mode data, should provide planetary program planners with an easily used source of reference information essential in the preliminary steps of mission selection and planning.

Study results are also predicated on NASA-planned launch vehicle candidates and retro propulsion systems. Table 1-2 lists the main ground rules established at the start of the study. Shuttle-launched upper stages include two configurations each of the Interim Upper Stage (IUS) and the Tug. The IUS(II)* consists of two solid motor stages (1 large, 1 small) whereas the IUS(III) is the proposed three-stage version (2 large, 1 small). The Tug(R) is recoverable in Earth orbit and therefore utilizes an additional Kick stage to achieve escape velocity. Highest injected mass performance is obtained with the expendable Tug(E) upper stage. Performance comparisons of the four launch vehicle candidates are shown in Figure 1-2.

Retro propulsion options include the solid/monopropellant and Earth-storable liquid systems, and space-storable liquid systems assumed to be available in the post-1985 time period. In the case of low-thrust applications, only Earth-storable retros are considered for Mercury orbit insertion since ΔV requirements are relatively small. Additional ground rules include provision for a 10-day launch window and a midcourse guidance budget under 250 m/sec for ballistic-swingby transfers. A standard budget of 150 m/sec for orbit trim maneuvers is allowed for all missions. Finite thrust penalties can be significant for large retro ΔV maneuvers and are therefore accounted for in all ballistic mission performance calculations. The beneficial effect of staging large retro ΔV maneuvers is also presented in the analysis.

---

*The IUS(Twin) is a more recent configuration of two large stages and would have approximately the same performance as the IUS(III) in the low C_3 region of interest.

Table 1-2

LAUNCH VEHICLE AND RETRO OPTIONS

- SHUTTLE-LAUNCHED UPPER STAGES

IUS(II)	1980 →
IUS(III)	1980 →
TUG(R)/KICK	1985 →
TUG(E)	1985 →

- RETRO PROPULSION STAGES

SOLID/MONOPROPELLANT	1980 →
EARTH-STORABLE	1980 →
SPACE-STORABLE	1985 →

- ADDITIONAL GROUNDRULES

LAUNCH WINDOW	10 DAYS
MIDCOURSE GUIDANCE	≤250 M/SEC (BALLISTIC MODE)
ORBIT TRIM MANEUVERS	150 M/SEC
FINITE THRUST EFFECT AT ORBIT INSERTION	900 LBF (LIQUID) 20,000 LBF (SOLID)
MOI STAGING EFFECT	FIRST STAGE: $\infty \rightarrow 24^H$ SECOND STAGE: $24^H \rightarrow p^H$ 1% ADAPTER MASSES

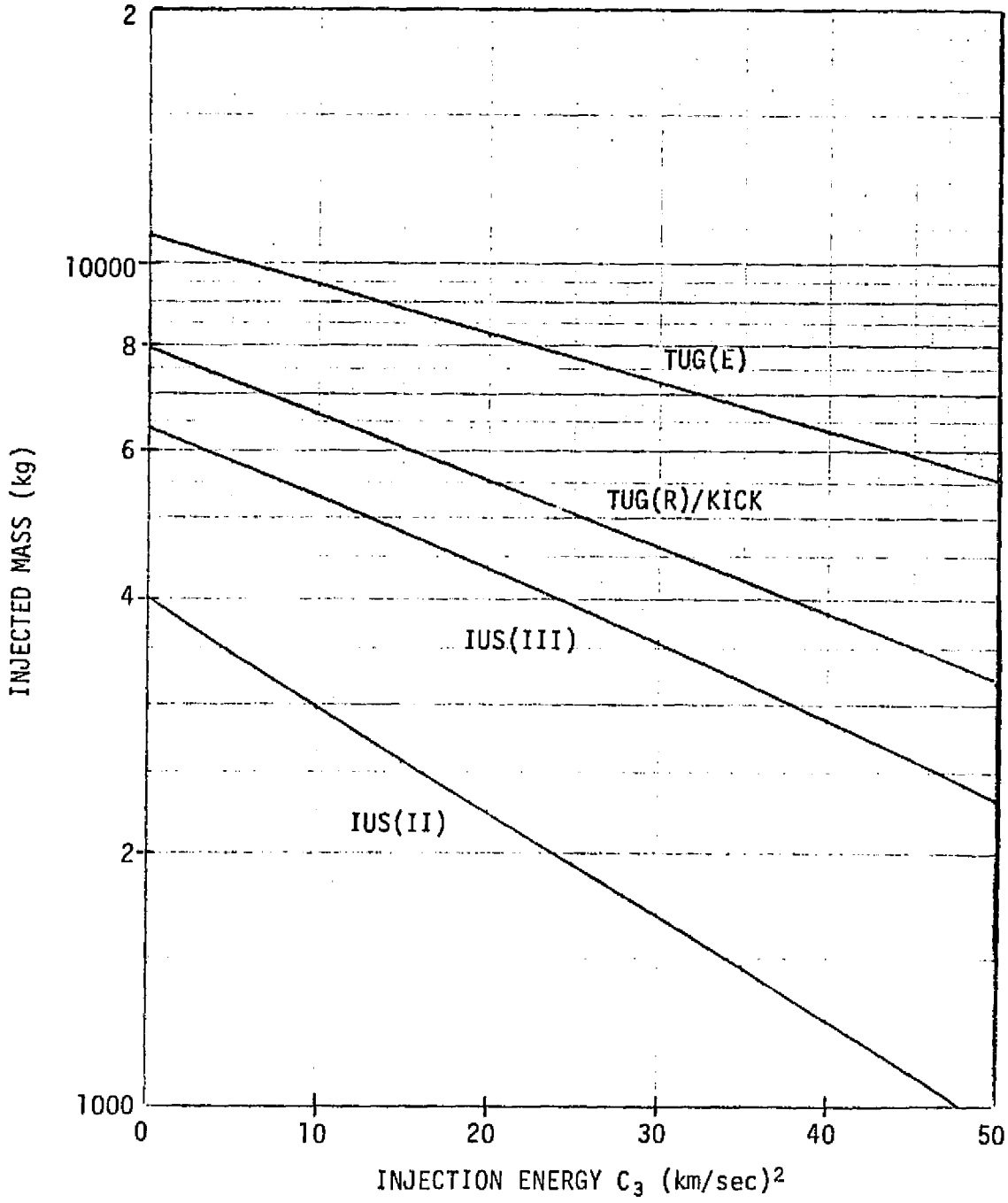

Fig. 1-2 SHUTTLE-LAUNCHED UPPER STAGE PERFORMANCE

The report is organized as follows: Section 2 discusses the ballistic and low-thrust transport modes in terms of their basic characteristics and payload capabilities. Section 3 then presents study results in a comparison format between the candidate flight modes with discussion of payload/flight time trades and cost implications. Appendix A contains all the performance graphs for ballistic launch opportunities; these are set aside in a handbook-type section for easy reference by mission analysts and planners. A summary of study results preceding this introduction section is presented for the busy reader wishing only to abstract the main results and conclusions.

2. TRANSPORT OPTION CAPABILITIES

2.1 Ballistic Mode (Venus Swingby)

The Ballistic Opportunity/Configuration Matrix shown in Table 2-1 essentially delineates the scope of the ballistic mission portion of this study. Every case examined is characterized by launch year, number of Venus swingbys, launch vehicle upper stage and retro propulsion type. The options available for any particular launch year are indicated by asterisks in the appropriate row and columns of the matrix.*

Each asterisk relating the number of Venus swingbys to a launch year represents a unique opportunity identified in prior trajectory studies performed by G. Hollenbeck, et al., at Martin-Marietta[4] and D. Bender at JPL.[5] Some of the opportunities provided by these two sources were not considered, having been eliminated because they were clearly inferior to other opportunities with similar launch dates. Note, however, that in 1981 and 1988 two asterisks appear in the V(2) column, indicating that there are two double swingby opportunities of interest in each of these years. The two 1981 opportunities are included because they represent a substantial tradeoff in flight time and payload. In the 1988 opportunities, such tradeoff possibilities are less significant; however, since neither opportunity exhibits a clear-cut performance advantage, the fact that the launches occur at different times during the year (March and July) can be important for programmatic purposes.

The remaining columns of the matrix identify candidate upper stages and retro units expected to be available in the respective launch years. These potential configurations and their anticipated IOC's have been discussed previously.

---

*Although it is not indicated by the matrix, a retro staging option has also been considered in this study (see p. 16).

Table 2-1

BALLISTIC OPPORTUNITY/CONFIGURATION MATRIX (MERCURY ORBITER)

LAUNCH YEAR	VENUS SWINGBYS				LAUNCH VEHICLE OPTIONS SHUTTLE UPPER STAGE				RETRO PROPULSION OPTIONS		
	V(1)	V(2)	V(3)	V(4)	IUS(II)	IUS(III)	TUG(R)/KICK	TUG(E)	E/S	S/S	SOLID/MONO
1980	*		*		*	*			*		*
1981		**			*	*			*		*
1983		*	*		*	*			*		*
1985	*				*	*	*	*	*	*	*
1986		*	*		*	*	*	*	*	*	*
1988		**			*	*	*	*	*	*	*
1989		*			*	*	*	*	*	*	*
1991		*			*	*	*	*	*	*	*
1994		*			*	*	*	*	*	*	*
1996			*		*	*	*	*	*	*	*
1999				*	*	*	*	*	*	*	*

Trajectory Characteristics

Table 2-2 summarizes the trajectory characteristics for all the launch opportunities considered. Listed are the flight times, injection energy C_3, planned midcourse maneuvers $\Delta V_{M/C}$, hyperbolic excess approach velocity V_{HP}, and the required velocity impulse budget ΔV_N for navigation and midcourse shaping maneuvers. Data used in constructing this table was obtained from the two aforementioned sources and augmented where needed by additional trajectory analysis using the MULIMP[6] program.

The tabulated values were derived on the basis of a 10-day launch window covering the best 10 days of each opportunity with respect to mission performance. To be conservative, the given C_3 represents the largest value over this period. The same is generally true for V_{HP} except in a small number of cases where midcourse maneuver requirements are the more critical factor. Indicated flight times are referenced to the center of the launch window.

Since the navigation and trajectory shaping requirements were available for only a few opportunities, it was necessary to develop a simple algorithm for estimating ΔV_N for the remaining cases. The alternative was to perform detailed navigation analysis for these cases, which was clearly outside the scope of this study.

The algorithm used is based on average maneuvers employed in different portions of the Earth-Venus-Mercury trajectory as derived from the data on hand. The maneuvers of interest were apportioned as shown in Table 2-3. By assuming the required number of additional solar revolutions to be equal to the number of Venus swingbys, and combining the planned midcourse maneuver with a post-Venus swingby correction, the desired algorithm can be expressed in the following equations.

Table 2-2

BALLISTIC MODE CHARACTERISTICS SUMMARY

10-Day Launch Window

LAUNCH YEAR	TRANSFER TYPE	FLIGHT TIME (DAYS)	C_3 $(km/sec)^2$	$\Delta V_{M/C}$ (km/sec)	V_{HP} (km/sec)	ΔV_N* (km/sec)
1980	V(3)	1126	30.90	0	6.070	0.263
1980	V(1)	657	34.20	0.100	6.650	0.196
1981-a	V(2)	1067	32.80	0.357	5.619	0.519
1981-b	V(2)	422	45.41	0.069	7.130	0.239
1983	V(2)	989	17.45	0.610	5.792	0.771
1983	V(3)	953	25.25	0	6.517	0.263
1985	V(1)	420	49.60	0.400	6.265	0.528
1986	V(2)	911	24.44	1.564	5.809	1.725
1986	V(3)	1247	19.17	0.054	5.645	0.291
1988-a	V(2)	741	25.80	0.200	6.160	0.364
1988-b	V(2)	621	28.05	0.574	5.995	0.735
1989	V(2)	792	43.25	0.230	5.858	0.393
1991	V(2)	1019	25.80	0	6.585	0.199
1994	V(2)	877	19.38	0.130	5.753	0.296
1996	V(3)	782	23.00	0	6.200	0.263
1999	V(4)	1177	26.35	0	6.100	0.323

*Values include $\Delta V_{M/C}$

Table 2-3

AVERAGE* NAVIGATION AND MIDCOURSE SHAPING MANEUVERS

Maneuver Function	Mean (m/sec)	S.D. (m/sec)
Removal of Launch Injection Errors	$\mu_1 = 7.46$	$\sigma_1 = 5.06$
Correction of Pre-Venus Swingby O.D. Errors	$\mu_2 = 1.04$	$\sigma_2 = 0.68$
Correction of Post-Venus Swingby Errors	$\mu_3 = 38.55$	$\sigma_3 = 25.40$
Error Correction During Non-Swingby Solar Revolutions	$\mu_4 = 0.74$	$\sigma_4 = 0.42$
Targeting Maneuvers at Mercury	$\mu_5 = 1.48$	$\sigma_5 = 1.11$

*Average based on seven trajectories derived by Martin-Marietta.[4]

$$\mu_{\Delta V} = \mu_1 + \mu_5 + N(\mu_2 + \mu_3 + \mu_4) + \left[(\Delta V_{M/C}^2 + \mu_3^2)^{\frac{1}{2}} - \mu_3\right] \quad (1)$$

$$\sigma_{\Delta V} = \left[\sigma_1^2 + \sigma_5^2 + N(\sigma_2^2 + \sigma_3^2 + \sigma_4^2)\right]^{\frac{1}{2}} \quad (2)$$

$$\Delta V_N = \mu_{\Delta V} + 3\sigma_{\Delta V} \quad (3)$$

In these equations, N represents the number of swingbys, and the various means (μ_i) and standard deviations (σ_i) are those defined in Table 2-3.

As a separate but related issue it should be noted that an additional ΔV of 150 m/sec was budgeted for each opportunity in order to carry out trim maneuvers in Mercury orbit. This value was a "best estimate" on our part, based on previous orbiter mission studies.

Finite Burn Effects

Because of its importance to Mercury orbiter missions, the effects of finite burn/gravity losses during orbit insertion must be accounted for. To incorporate these effects into this study in the simplest and most efficient manner, it was decided to model existing data by conventional curve fitting procedures. The data source for this effort was an engineering memorandum written by R. A. Wallace[7] of JPL in which he documents results obtained by using a finite burn orbit insertion simulation program (LOSS). The data, presented in graphical form, relates net spacecraft mass in orbit to the Mercury arrival mass for the following range of parameters:

(1) Orbit Period: 1.86 hours (circular) to 24 hours
(2) Orbit Periapse Altitude: 500 km (fixed)
(3) Asymptotic Approach Velocity: 5.6 km/sec to 6.4 km/sec
(4) Insertion Thrust Level:* 303.94 lbf to 20,000 lbf.

*Thrust levels and scaling laws used were based on retro systems equivalent to one, three, and ten Viking motors; and also a solid propellant system equivalent to a small shuttle IUS motor.

To isolate the effect of finite burn insertion on the net orbited payload, an equivalent data set for the case of impulsive insertion was analytically derived. A curve fitting approach was then employed to develop an approximate relationship between the payload masses obtained from the two insertion modes over the entire parameter range. The following equation is the result of this effort:

$$\frac{M_L + M_E + fM_o}{M_L' + M_E + fM_o} = \left\{[1 - e^{-3.3T/M_o}]0.0335\Delta V_I\right\} \tag{4}$$

M_L = orbited payload mass, finite burn insertion (kg)
M_L' = orbited payload mass, impulsive insertion (kg)
M_o = Mercury arrival mass (kg)
M_E = retro engine mass (kg)
f = tankage fraction
T = thrust (lbf)
ΔV_I = insertion velocity impulse (km/sec)

By use of the above and the standard payload equation,* i.e.:

$$M_L = M_o\left[(1 - f)e^{-\Delta V/C} - f\right] - M_E \tag{5}$$

C = exhaust velocity (km/sec)

a relationship could then be established between the actual and the impulsive ΔV insertion requirement. A brief explanation is given below.

Given an orbit insertion of arbitrary burn duration, where the planet arrival mass is M_o and the net orbited payload is M_L, Equation (5) specifies a corresponding equivalent velocity impulse, ΔV. Assuming that impulsive insertion into the same orbit requires a velocity impulse of magnitude ΔV_I, the payload for the same arrival mass is:

*Single-stage, rubber retro assumed.

$$M_L' = M_o\left[(1 + f)e^{-\Delta V_I/C} - f\right] - M_E \qquad (6)$$

Simple algebraic manipulation of Equations (5) and (6) leads to the following:

$$\frac{M_L + M_E + fM_o}{M_L' + M_E + fM_o} = \left[e^{-(\Delta V - \Delta V_I)/C}\right] \qquad (7)$$

Finally, substitution of the desired expression in Equation (4) and further simplification produces the desired relationship,

$$\frac{\Delta V}{\Delta V_I} = 1 - 0.0335\ C\ \ln\left[1 - e^{-3.3T/M_o}\right] \qquad (8)$$

Equation (8) has been used in plotting the two graphs shown in Figure 2-1. These graphs, based on use of an Earth-storable propellant (I_{sp} = 300 sec), are provided as an example to indicate the finite burn effect in a parameter space relevant to the cases studied. Both graphs are essentially equivalent in that they represent the loss due to finite thrust as a penalty to be added to ΔV_I. In one case this is given in terms of percentage, and in the second case, as a required velocity increment. The independent variable in both cases is the initial thrust-to-weight ratio, i.e., acceleration. It was found that over the region of interest to this study, the curve-fit model represented by Equation (8) gives a fairly accurate accounting of the actual finite thrust losses and its relative simplicity made it amenable to incorporation in the subsequent analyses.

Retro Staging Options

The upper and lower solid curves in Figure 2-2 represent the payload performance of a two-stage and one-stage retro system for the particular March 1988 launch opportunity. The two-stage curve indicates the results of an optimal staging policy, and clearly exemplifies the improved performance which could be expected over the single stage case for the range of ΔV's

Fig. 2-1

FINITE THRUST LOSSES FOR MERCURY ORBIT INSERTION

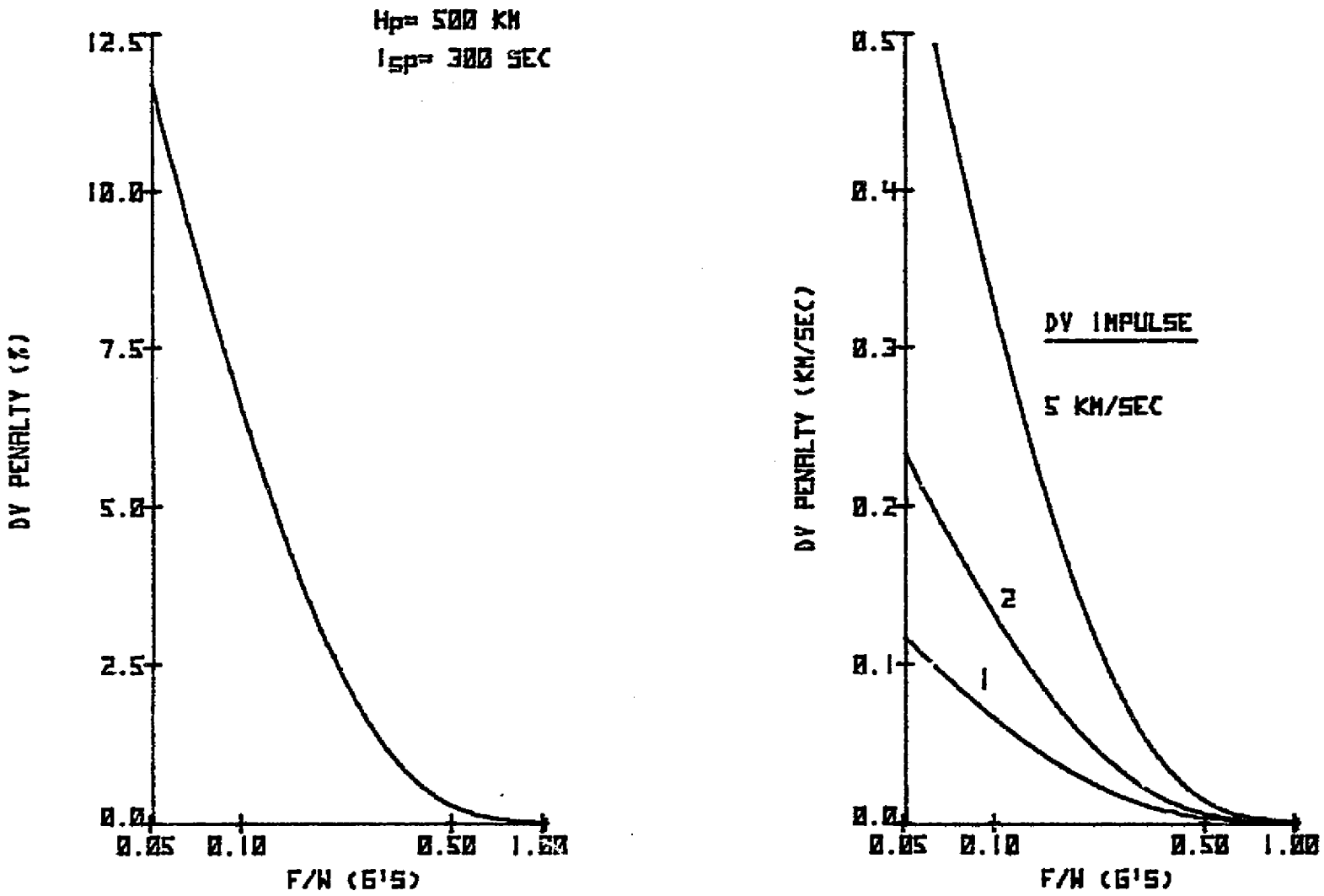

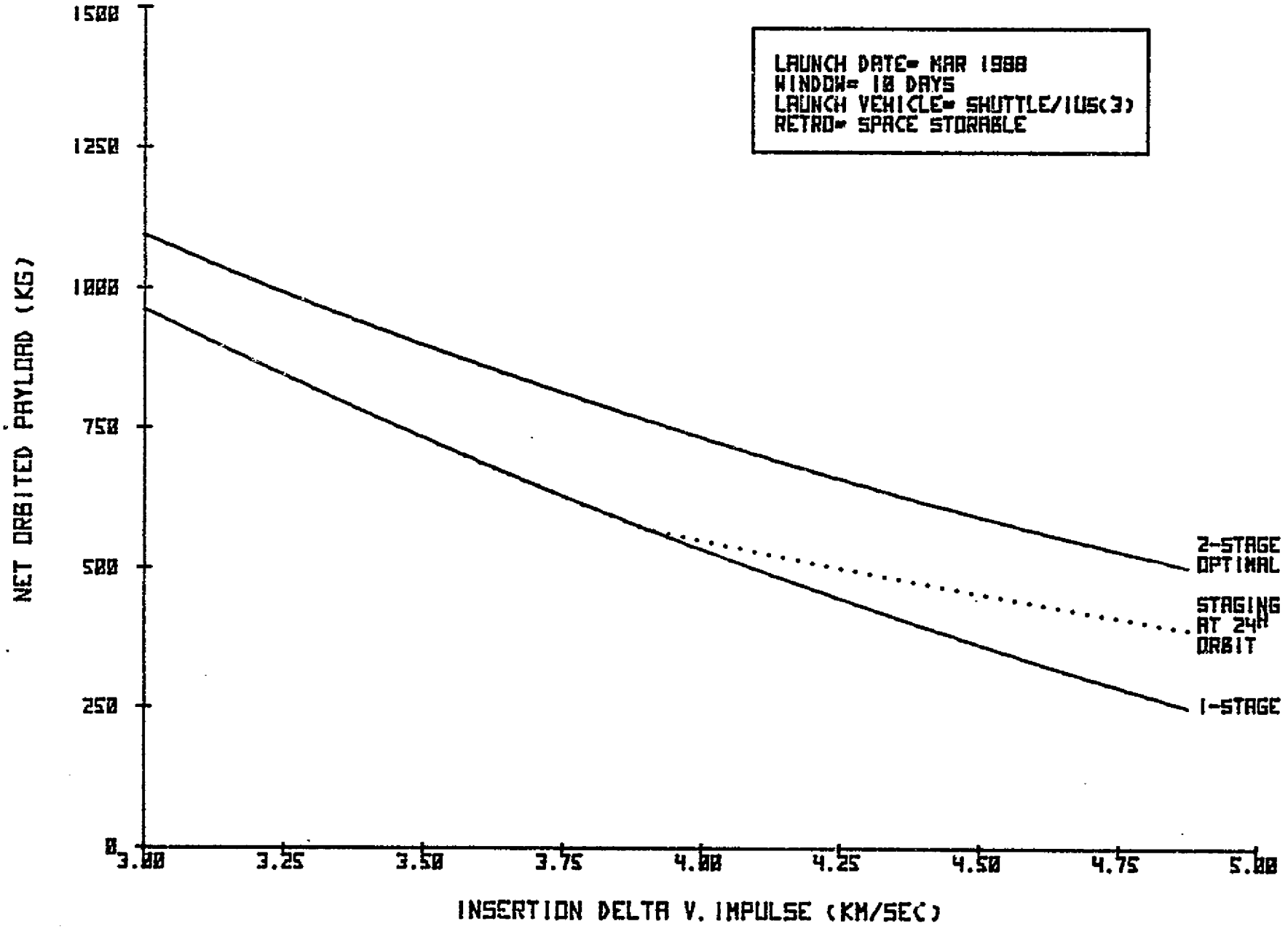

Fig. 2-2 RETRO STAGING OPTIONS-PAYLOAD EFFECTS

needed for insertion into Mercury orbits. However, use of an optimal staging policy for this application would normally require a staging maneuver prior to insertion, and because of the relatively small gravitational field of Mercury, it was felt that staging at that time would be a rather critical and risky venture. Therefore, an alternative staging policy was devised and used throughout the analyses.

The alternative staging policy assumes that the first stage is used for initial insertion into a 24-hour orbit having a periapse altitude of 500 km. The second stage would then be used for a transfer to the final orbit. The performance obtained by using this policy is indicated by the dotted curve in Figure 2-2. For the nearly circular orbits, this staging option can still provide substantial improvement over the single stage case.

A similar policy which was also examined, was one involving only a single stage, but requiring two retro burns. As in the previous policy, the first burn was again used for initial insertion into a 24-hour 500 km orbit, and the second burn used for transfer to the final orbit. The reason for investigating this strategy was the hope that splitting the total required burn into two smaller burns would result in reduced finite thrust penalties. However, it was found that the initial insertion would normally require such a large portion of the total ΔV, it would absorb most of the penalty incurred by simply proceeding with a single burn policy. Since the benefits received were not worth the additional complexity required, this strategy was dropped from further consideration.

Mercury Orbiter Performance Curves

Performance analyses of all the ballistic opportunities were performed by means of a specially written computer program whose graphical output is particularly useful for mission planning. An example of the output format is presented in Figure 2-3. In this format, payload performance curves similar to those shown in Figure 2-2 are superimposed over curves representing the orbital parameters. These latter curves are drawn as dashed lines

representing periapse altitude as a function of insertion impulse* for fixed period orbits. The curves are bounded on the right by the circular orbit limits, and on the left by the escape parabola. The solid and dotted curves are again used to represent one and two-stage payload performance respectively. In this case, such curves are drawn for four different launch vehicles.

Some simple examples will illustrate how these curves can be used. Consider first, a case where a 24-hour orbit at 500 km periapse altitude is desired. To determine the payload which could be delivered by each of the four launch vehicles, first bring a horizontal from the 500 km mark on the right-hand axis to its intersection with the dashed curve representing a 24-hour period. This intersection is indicated in Figure 2-3 by an open circle. A vertical drawn at this point will intersect the four payload curves at the points indicated by the solid circles. The net orbited payload for each launch vehicle can then be read off the left-hand axis.

As another example, suppose the desired orbit has a period of 6 hours and a periapse altitude of 1000 km. The intersection of the 6-hour curve and the 1000 km horizontal is symbolized in Figure 2-3 by an open square. A vertical drawn at this point will now intersect seven payload curves. The intersection with the four solid curves will give, as before, the net orbited payload delivered by the four different launch vehicles using single stage retros. The intersection with the three dotted curves, as represented by the solid squares, determines the payload delivered by the indicated launch vehicles and two-stage retros. The fact that the dotted and solid curves coincide at the point of intersection for IUS(2) signifies that a two-stage retro would offer no performance advantage over a single stage unit for that particular launch vehicle and orbit.

Similar performance curves for all ballistic opportunities of interest are compiled in Appendix A of this report. Three sets of curves, each representing a different retro propulsion option, are provided for each

*The values of insertion impulse do not include a finite thrust penalty. The effect of finite thrust is accounted for in the net orbited payload.

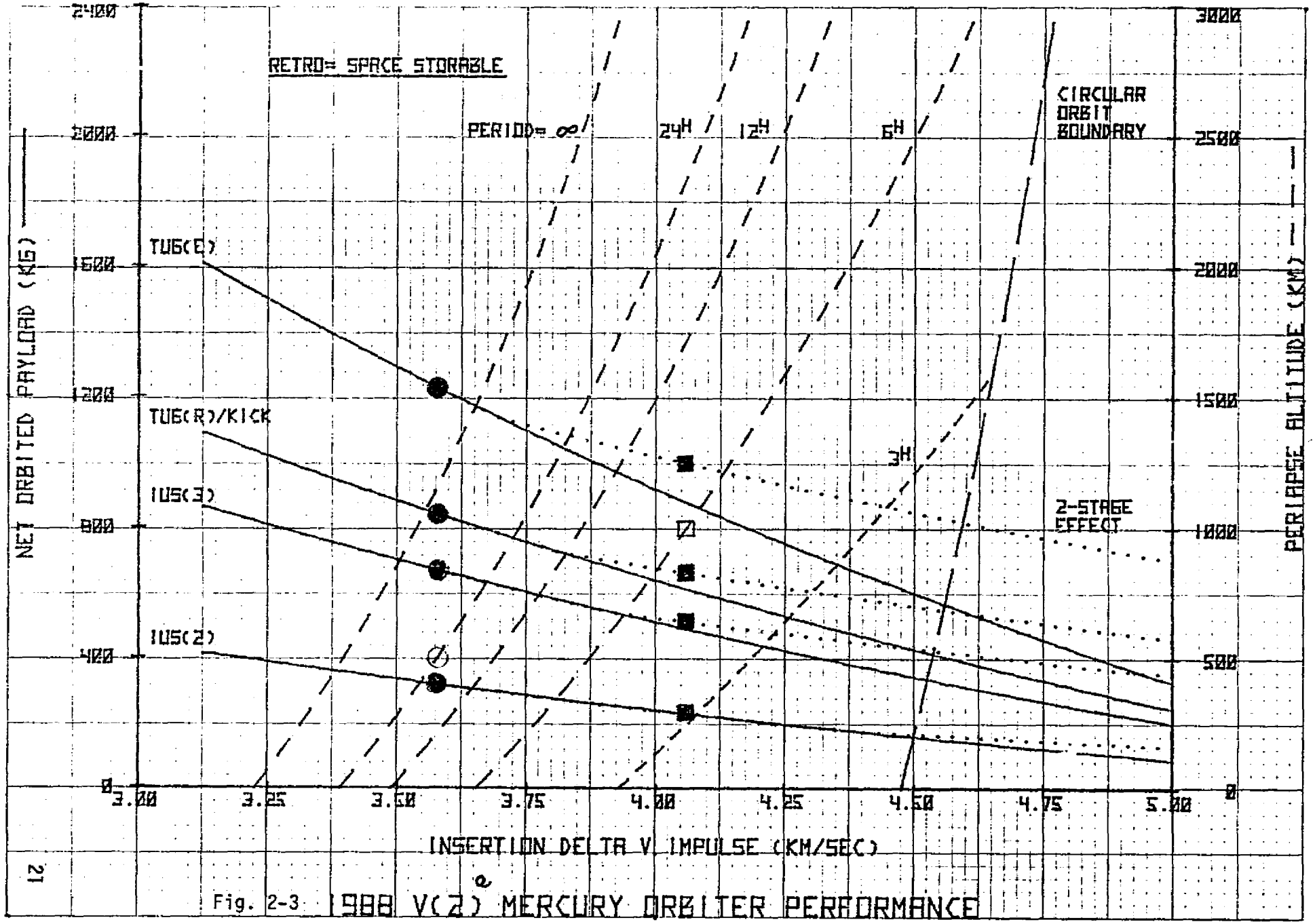

Fig. 2-3 1988 V(∞) MERCURY ORBITER PERFORMANCE

opportunity. As a matter of general interest, it was decided to include all launch vehicle and retro options for every opportunity irrespective of the availability considerations implied by the Opportunity/Configuration Matrix of Table 2-1.

2.2 Solar Electric Propulsion Mode

The SEP flight mode has long been considered a good potential candidate for Mercury orbiter missions. Technological readiness by the mid-1980's is not viewed as a problem; however, the cost of development could be relatively high (100-150 M$) and probably justifiable only if SEP is utilized over a wide range of planetary missions. Current technology and mission studies have concentrated on a SEP design in the 15-21 kw size with ion thrusters operating at 3000 sec specific impulse and an overall propulsion system efficiency of 62%. Propulsion system mass values are listed in Table 2-4. Thruster and power conditioner modules are each approximately 3 kw and two thrusters are held in standby condition in case of failure of the nominally operating thrusters.

Trajectory data for SEP transfers to Mercury were obtained from both JPL[8] and SAI sources and appropriately scaled to a common set of propulsion system parameters. An example of normalized performance data for optimal 550-day transfers to Mercury launched in 1984 is shown in Table 2-5. To illustrate how this data is used consider the case of $C_3 = 16$ $(km/sec)^2$ and $P_o = 18$ kw. The values of initial and final mass are calculated as $M_o = 18 \times 233.0 = 4194$ kg and $18 \times 144.5 = 2601$ kg. Since the injected mass capability of the IUS(III) is 4700 kg at $C_3 = 16$, this trajectory is "captured" by that launch vehicle with a margin of almost 500 kg. Somewhat better performance is thus available by increasing C_3 to match the IUS(III) capability. The interpolated result is $C_3 = 20$, $V_{HP} = 1.660$, $M_o/P_o = 239.5$, and $M_F/P_o = 151.0$. Values of initial and final mass are now 4311 kg and 2718 kg, respectively. Subtracting the SEP system mass of 942 kg from the final mass gives 1776 kg for the net mass at Mercury approach. The retro ΔV requirement for insertion into a 500 km circular orbit and orbit trim

Table 2-4

SEP SYSTEM MASS AND POWER ASSUMPTIONS

Input Power at 1 AU P_o (kw)	Number of Thrusters	Propulsion System Dry Mass M_{PS} (kg)	Effective Specific Mass $\alpha = M_{PS}/P_o$ (kg/kw)
15	8	888	59.2
18	8	942	52.3
21	10	1105	52.6

- I_{SP} = 3000 sec, η = 62%
- Solar Power Curve:

$$P/P_o = \begin{cases} \dfrac{1.4382}{R^2} - \dfrac{0.2235}{R^3} - \dfrac{0.2147}{R^4} & \text{for } R \geq 0.68 \text{ AU} \\ 1.3952 & \text{for } R < 0.68 \text{ AU} \end{cases}$$

Table 2-5

NORMALIZED SEP PERFORMANCE FOR 550[d] MERCURY TRANSFERS

Injection Energy C_3 $(km/sec)^2$	Approach Speed V_{HP} (km/sec)	Mass-to-Power Ratio* M_o/P_o (kg/kw)	Mass-to-Power Ratio* M_F/P_o (kg/kw)
6.25	1.208	213.0	124.9
9.00	1.242	219.2	130.9
12.25	1.348	226.1	137.7
16.00	1.493	233.0	144.5
20.25	1.668	240.0	151.4
25.00	1.863	246.8	158.2
30.25	2.067	253.5	164.9
36.00	2.268	259.9	171.3

*M_o is initial mass at injection.
M_F is final mass at Mercury approach.
$(M_o - M_F)$ is propellant expenditure.

maneuvers is 1.478 + 0.15 = 1.628 km/sec. Finally, assuming an Earth-storable system, the retro mass is calculated at 928 kg leaving 848 kg available as net orbited payload.

A graphical illustration of the payload calculation is shown in Figure 2-4 which plots net spacecraft mass in a 500 km circular orbit as a function of injection energy for SEP power ratings of 15, 18 and 21 kw. The three dashed curves indicate the limiting capability of the IUS(II), IUS(III) and Tug(R)/Kick; i.e., the region to the left of these curves is captured by the respective launch vehicles. SEP performance with the IUS(II) requires low injection energy ($C_3 < 8$) and delivers 500-600 kg to a circular orbit about Mercury. Use of the IUS(III) raises the payload range to 680-935 kg with required injection energy between 15 and 28 km^2/sec^2. In the latter case, increasing the power from 15 to 18 kw results in a 170 kg payload gain, and a further increase to 21 kw gains an additional 85 kg. Availability of the Tug(R)/Kick launch vehicle offers a modest improvement in payload delivery performance. For example, at P_r = 21 kw the net orbited mass is 1030 kg which is 10% higher than the IUS(III) capability.

Payload variation with flight time to Mercury is shown in Figure 2-5 (a) and (b). The short transfer class, between 1.5 and 2.5 solar revolutions, requires flight times between 250 and 350 days. Since the payload delivered to circular orbit is typically less than 400 kg, the short transfers would restrict science payload capability or require elliptical orbits to regain payload margin. As the flight time increases above 350 days the payload curve tends to flatten out until intersection with the 2.5-3.5 revolution class transfers, at which point the payload then increases quite sharply. The long transfer class missions have flight times between 450 and 600 days and payload capability between 300 and 1600 kg depending upon the orbit size and SEP power rating. For example, at TF = 600 days and P_o = 21 kw, payloads of 1560 kg can be transported to a 24-hour elliptical orbit and 1035 kg to a circular orbit. Payloads in this range would allow comprehensive orbit mapping plus one or more small lander deployments.

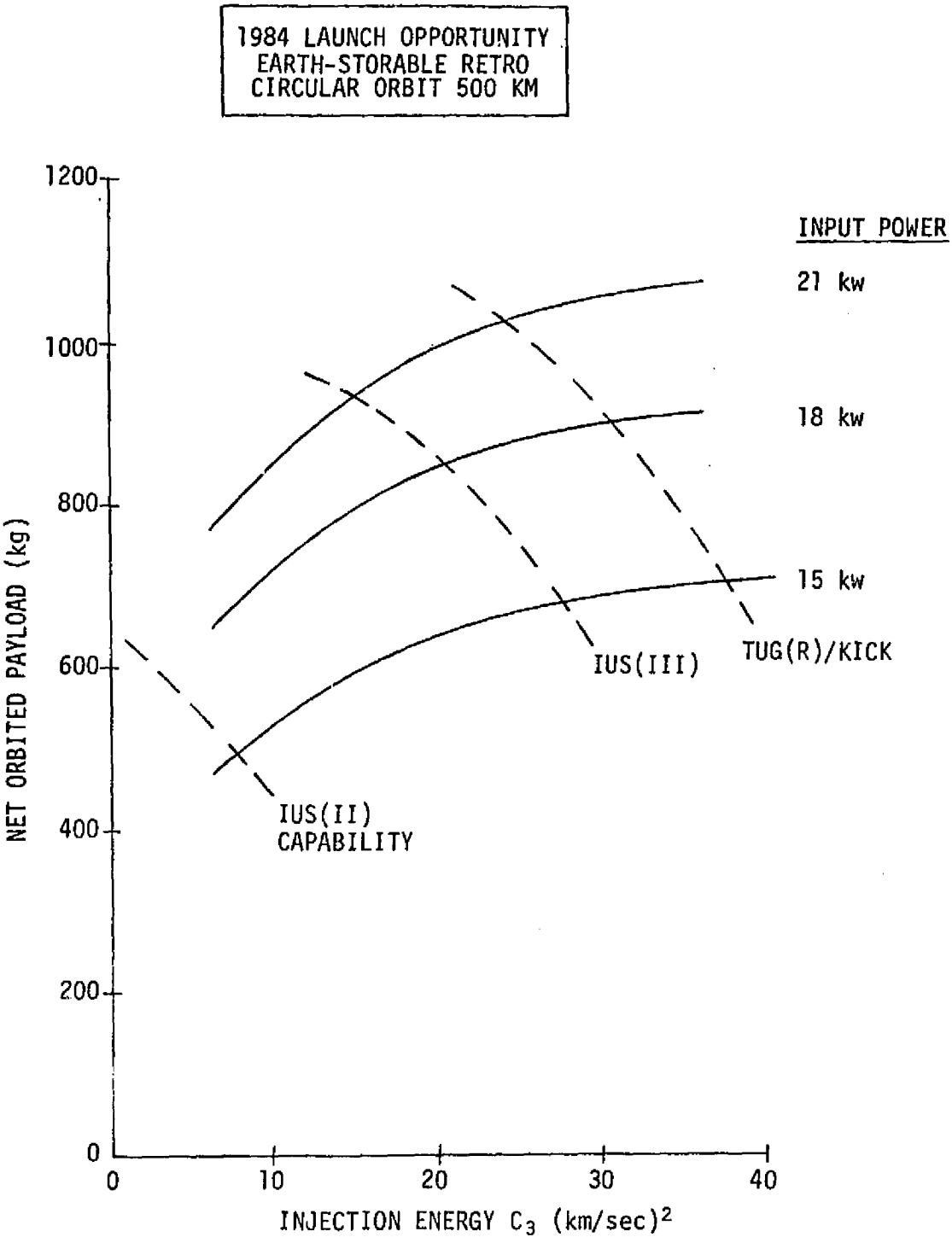

Fig. 2-4 SEP PAYLOAD CHARACTERISTICS FOR 550[d] MERCURY ORBITER

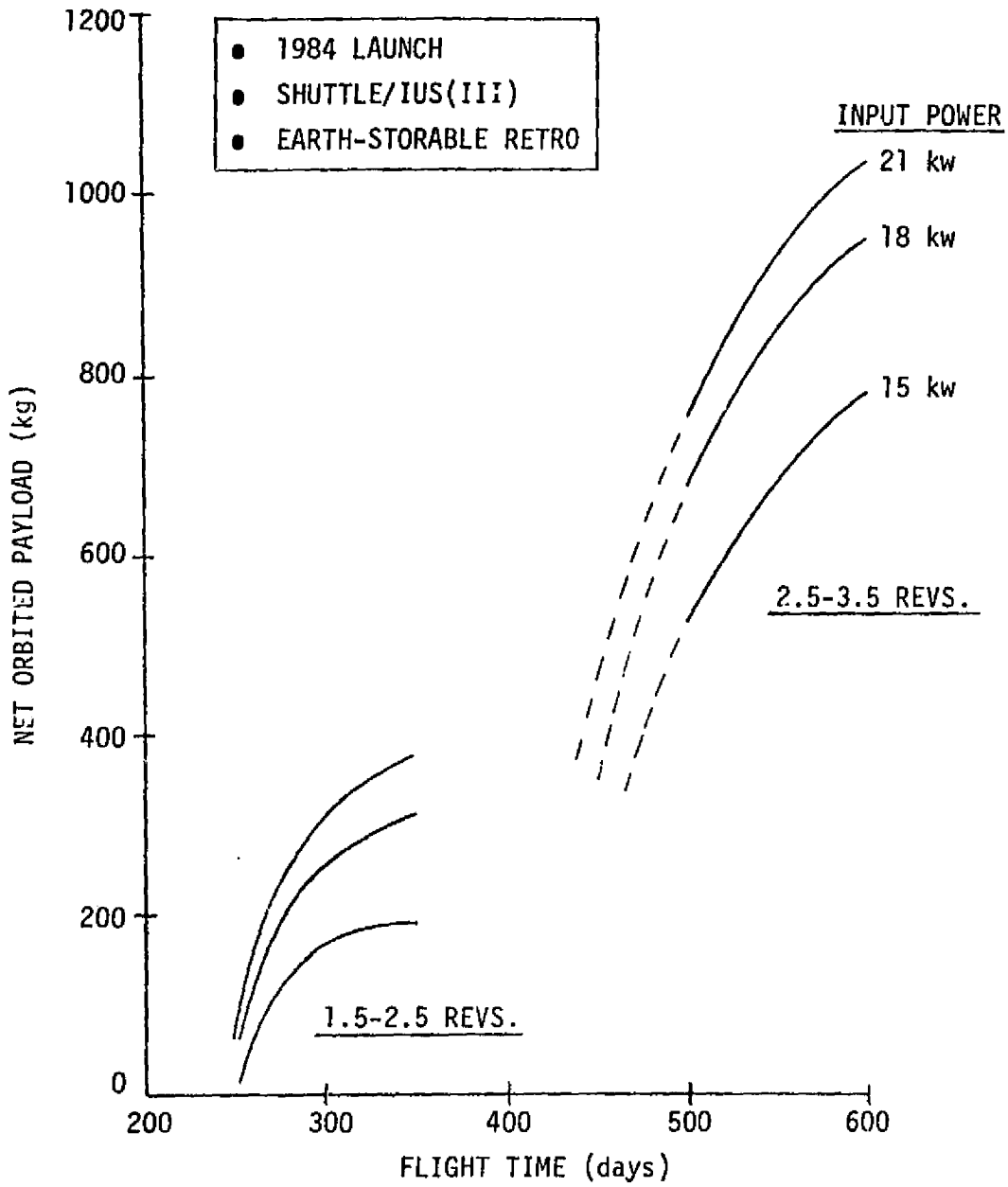

Fig. 2-5 SEP PERFORMANCE FOR MERCURY ORBITER MISSION, a) 500 KM CIRCULAR ORBIT

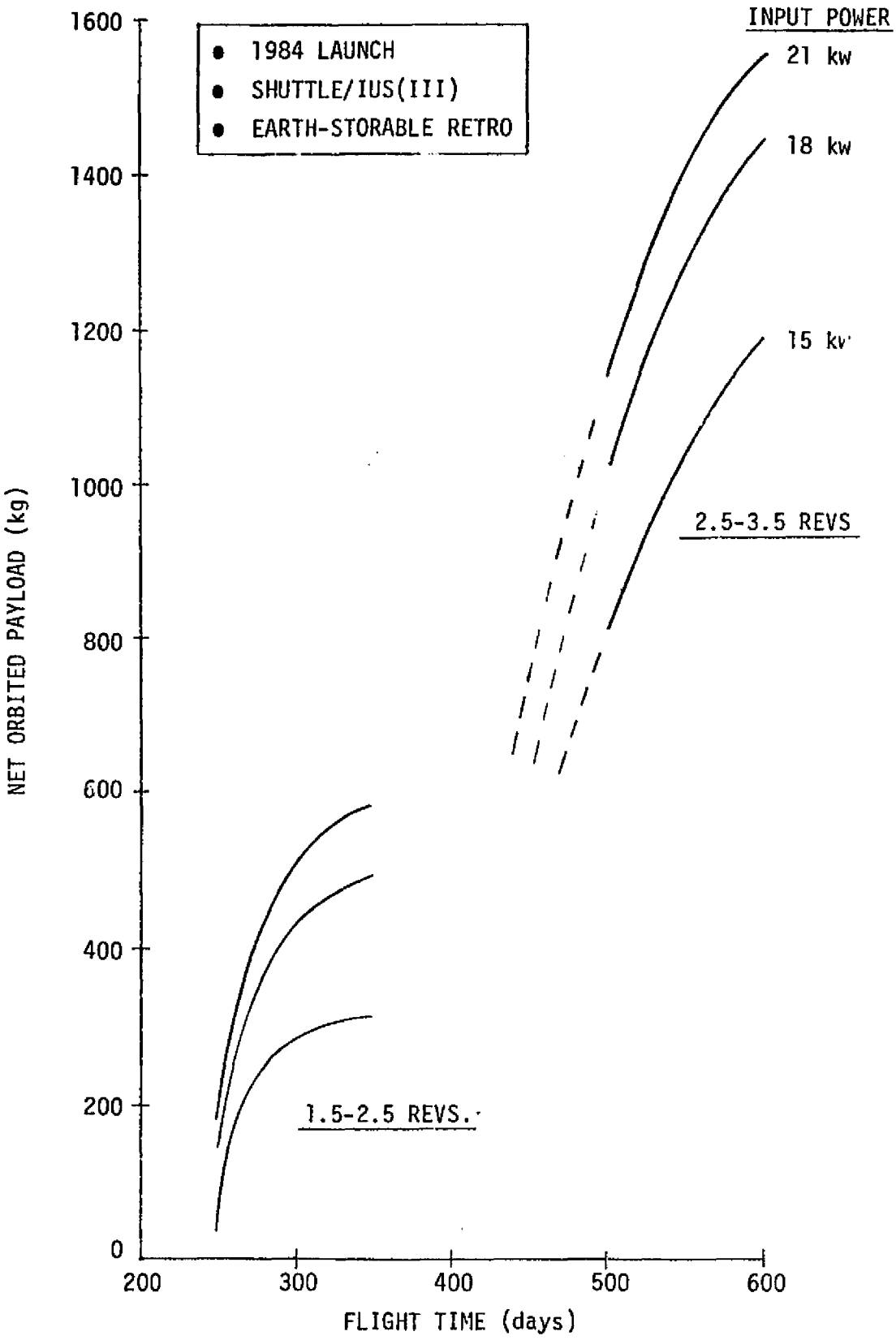

Fig. 2-5 SEP PERFORMANCE FOR MERCURY ORBITER MISSION, b) ELLIPTICAL ORBIT, h_p = 500 km, p = 24^h

The data presented so far was for the 1984 launch opportunity. This opportunity has slightly below average capability as can be seen from the launch year sensitivity graph of Figure 2-6. The best opportunities in the next decade are 1980 and 1986. Although the Earth-Mercury synodic period cycle is 13 years, there exists a near-resonance period of 6 years. This explains the fact that performance data tends to repeat closely every 6 years. The amplitude characteristics are such that the average performance is only 8% down from the maximum and the minimum performance launch year suffers an 18% penalty.

2.3 Solar Sailing Mode

The concept of solar sailing appeared in the literature as early as 1936, was studied more intensively during 1958-1962 after the advent of the space program, but then went into hibernation in lieu of other propulsion system developments. The main drawbacks had to do with assembly and deployment of very large sails, structural dynamics and attitude control, and sail material lifetime. With the anticipated new technology of large-scale in-orbit assembly in the post-Shuttle era, the potential of solar sail vehicles has received renewed attention, most recently by Battelle Memorial Institute.[9]

Thrust acceleration developed by the sail results from the reaction force of solar radiation pressure acting on a large surface area. The solar pressure at a distance of 1 AU is approximately 9×10^{-6} newton/m^2 (0.2×10^{-6} lb/ft^2). Characteristic acceleration a_o is defined as the effective thrust acceleration at 1 AU acting on a planar sail oriented normal to the sunline

$$a_o = 9 \times 10^{-6} \eta \frac{A}{M_o} \tag{9}$$

where η is the sail reflectance efficiency, A is the sail area, and M_o is the total mass of the sail vehicle including payload. If the sail normal is set to an angle θ off the sunline, then the magnitude of the acceleration at any distance r is given by the expression

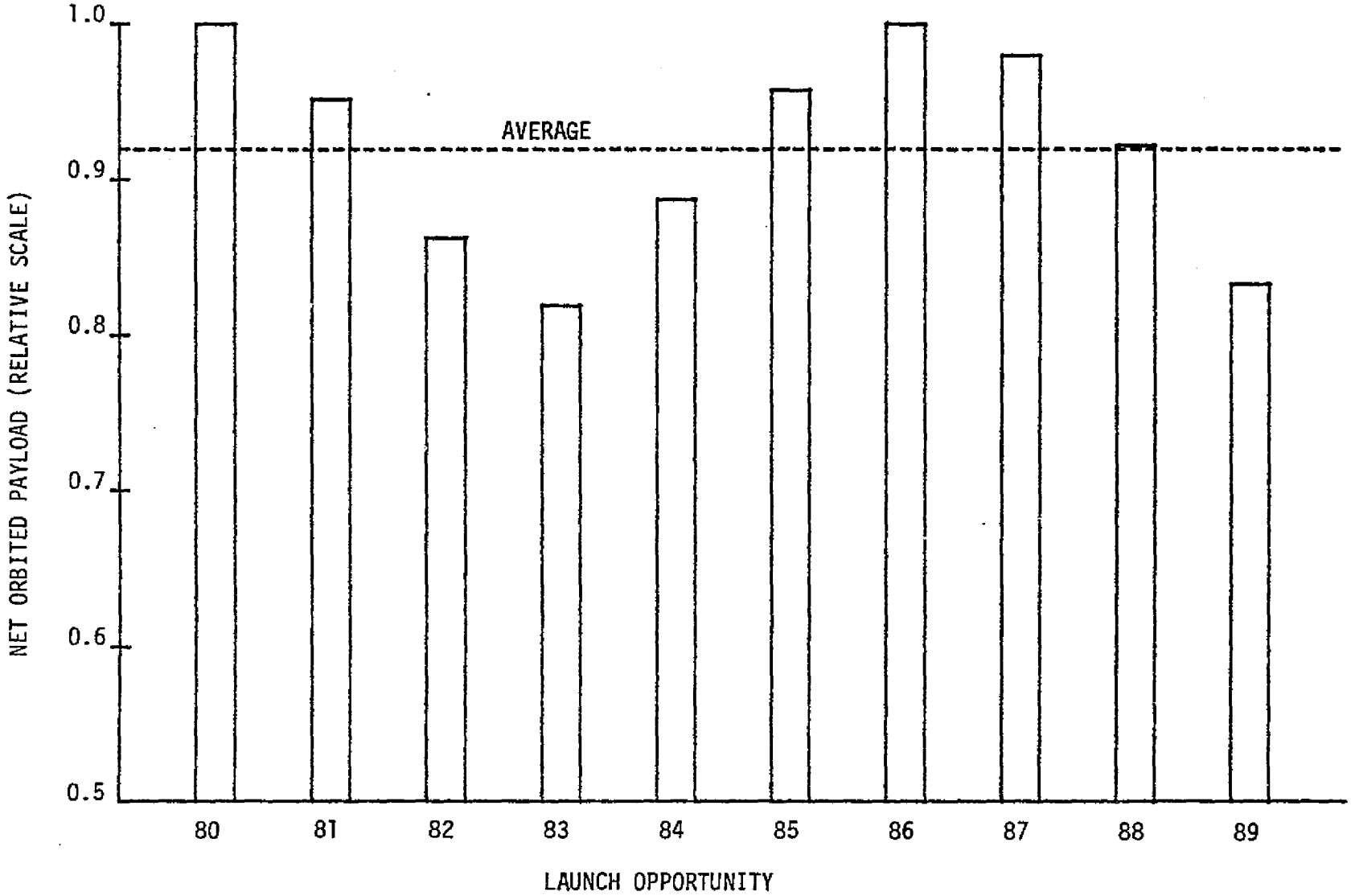

Fig. 2-6 LAUNCH OPPORTUNITY EFFECT FOR MERCURY ORBITERS - SEP TRANSPORT MODE

$$a = a_o \cos^2\theta / r^2 \qquad (10)$$

and the radially outward and circumferential components are a cos θ and a sin θ, respectively. Trajectory control is obtained by the sail angle program θ(t) which typically lies in the range $-60° \leq \theta \leq 60°$. Outward motion occurs for positive θ and inward motion for negative θ. In the case of Mercury transfers, the optimal angle setting is near -35° throughout most of the flight. At Mercury's distance ($r \approx 0.388$ AU) the acceleration available is thus 4.46 a_o. Because of the $1/r^2$ effect, it is readily appreciated why the sail can be so effective at close solar distances.

To illustrate payload and sail size characteristics, consider that the total vehicle mass is made up of sail vehicle and payload, i.e., $M_o = M_{SV} + M_{PL}$. The component M_{SV} is comprised of sail material and structure. For the sake of simplicity, assume that the structure component is proportional to the sail sheet mass so that

$$M_{SV} = \sigma A \qquad (11)$$

where $\sigma = (1 + k)\sigma_s$ is the effective density or loading of the sail vehicle. The payload* fraction may then be written as

$$\frac{M_{PL}}{M_o} = 1 - \frac{\sigma A}{M_o}$$

$$= 1 - \frac{\sigma a_o}{9 \times 10^{-6}\ \eta} \qquad (12)$$

Generalized performance parameters of a sail vehicle are graphed in Figure 2-7 as a function of the characteristic acceleration. An efficiency of 85% is assumed to account for non-ideal reflection of incident light and also

*This includes any chemical retro system needed for orbit insertion. Hence, for Mercury missions M_{PL} represents the net mass on approach to Mercury.

Fig. 2-7 SOLAR SAIL PERFORMANCE CHARACTERISTICS

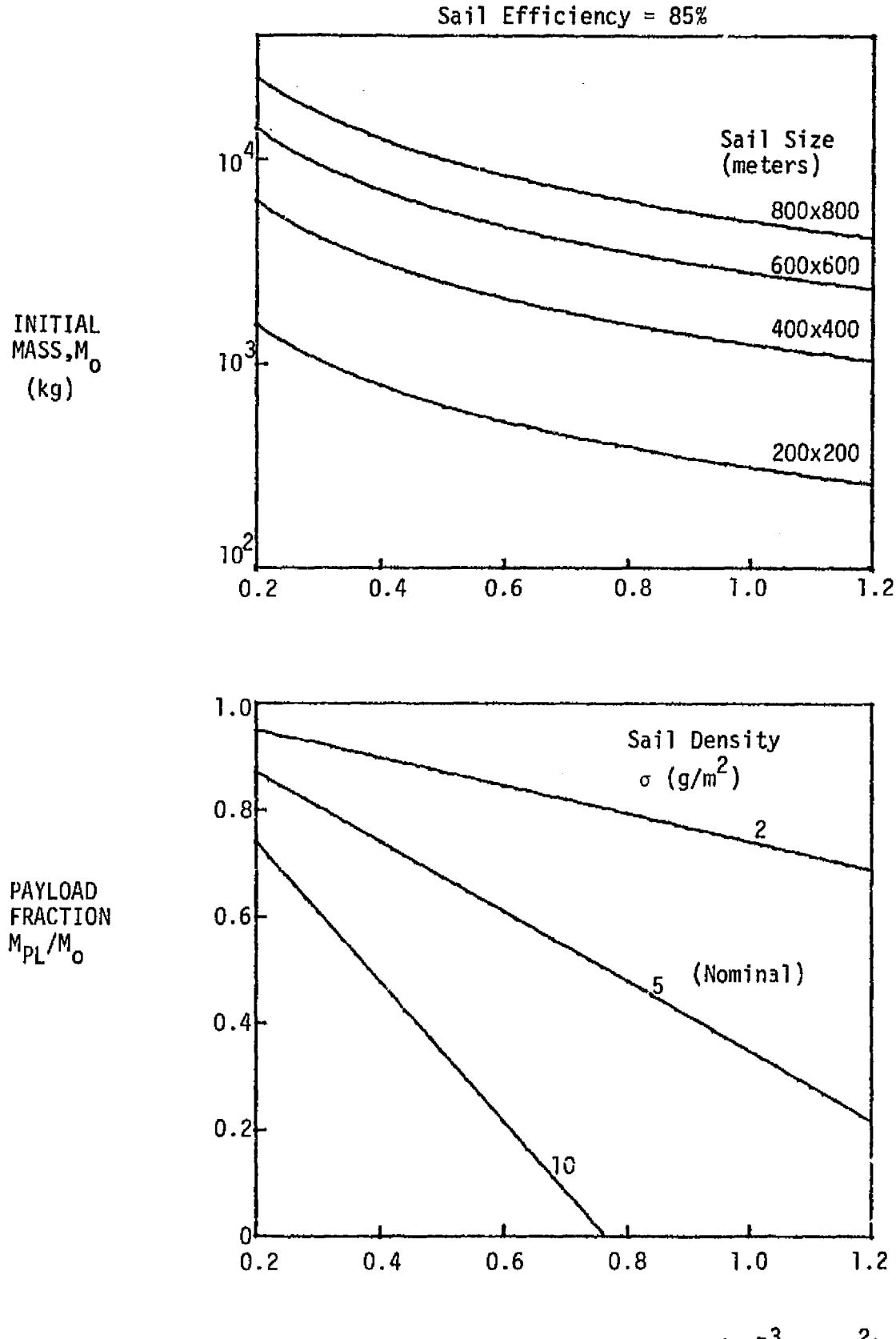

deflection or warping of the sail under pressure. A sail vehicle density of 5 g/m^2 is considered to be achievable with state-of-the-art materials and technology. Note that the payload fraction can be above 90% at low acceleration levels. The upper graph in Figure 2-7 is plotted from Equation (9) assuming a square sail configuration. Initial mass is inversely proportional to acceleration and linearly dependent on the sail area.

Mission payload and trajectory requirements are related through the flight time necessary to achieve the terminal boundary conditions at a given value of characteristic acceleration. Data for Mercury transfers obtained from Carl Sauer[8] of JPL is graphed as T_F vs. a_o in Figure 2-8. A 200-day trip requires a characteristic acceleration of 0.7×10^{-3} m/sec^2 and yields an approach payload fraction of 0.54 for $\sigma = 5$ g/m^2 (see Figure 2-7). Corresponding data for a 1000-day trip is a characteristic acceleration of 0.125×10^{-3} m/sec^2 and a payload fraction of 0.92.

The above sail characteristics are translated into specific performance for Mercury orbiter missions as shown in Figures 2-9(a) and (b). Curves of net orbited payload as a function of flight time are presented for both a circular orbit and a 24^h period orbit. The solid, straight line curves depict performance for fixed square sail sizes of 200, 300 and 400 meters; this data is launch vehicle independent. The broken line curves show the maximum capability for launches off the IUS(II), IUS(III) and Tug(R)/Kick vehicles. As an example, consider insertion into a 500 km circular orbit and a 300-day transfer to Mercury. Launches off the above-mentioned vehicles require sail sizes of 331, 471 and 533 meters, and deliver payloads of 765, 1626, and 2100 kg, respectively. Alternatively, suppose that the sail size is fixed at 300 meters. The flight time/payload performance is 365 days and 825 kg for the IUS(II), 720 days and 2020 kg for the IUS(III), and 915 days and 2680 kg for the Tug(R)/Kick.

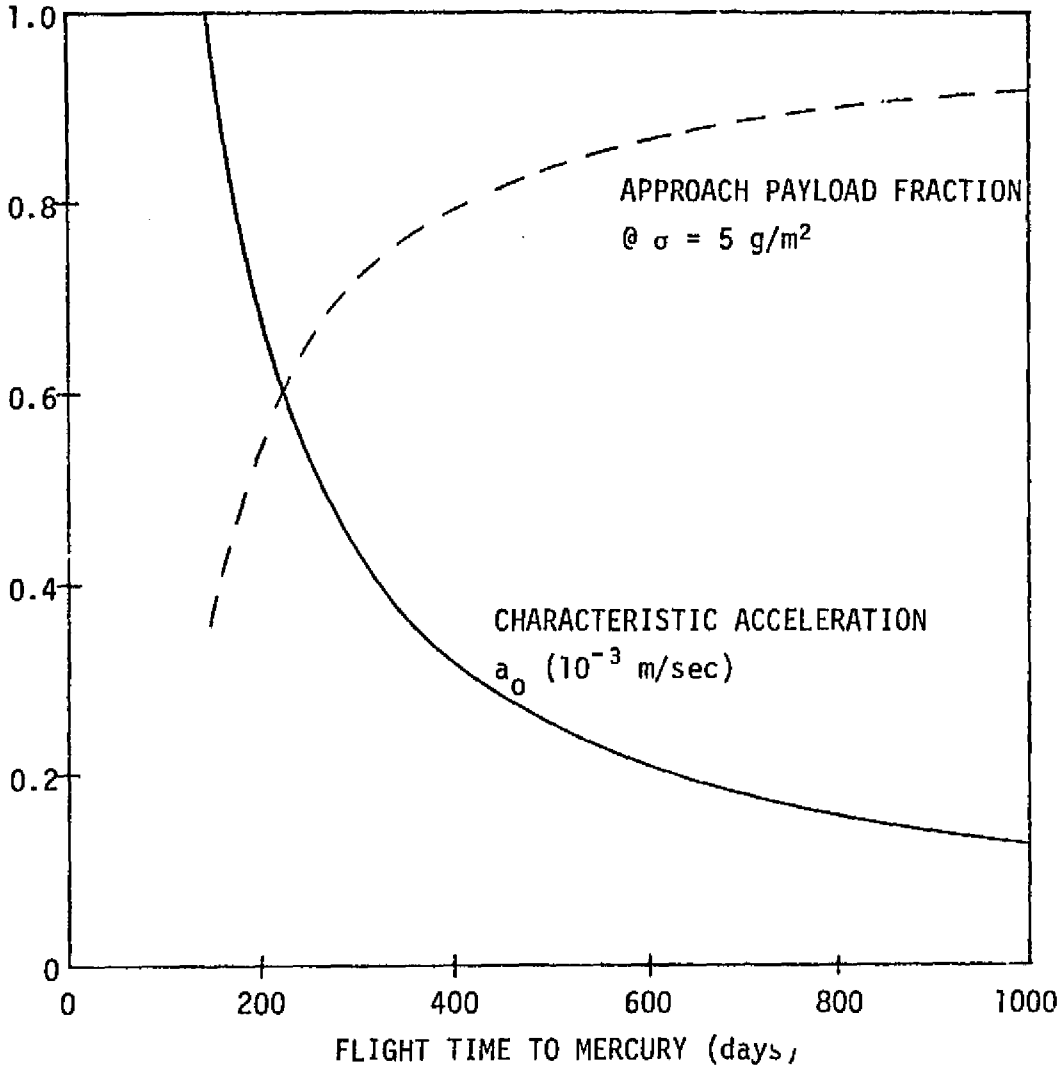

Fig. 2-8 CHARACTERISTIC ACCELERATION AND PAYLOAD FRACTION FOR SOLAR SAIL TRANSFERS TO MERCURY

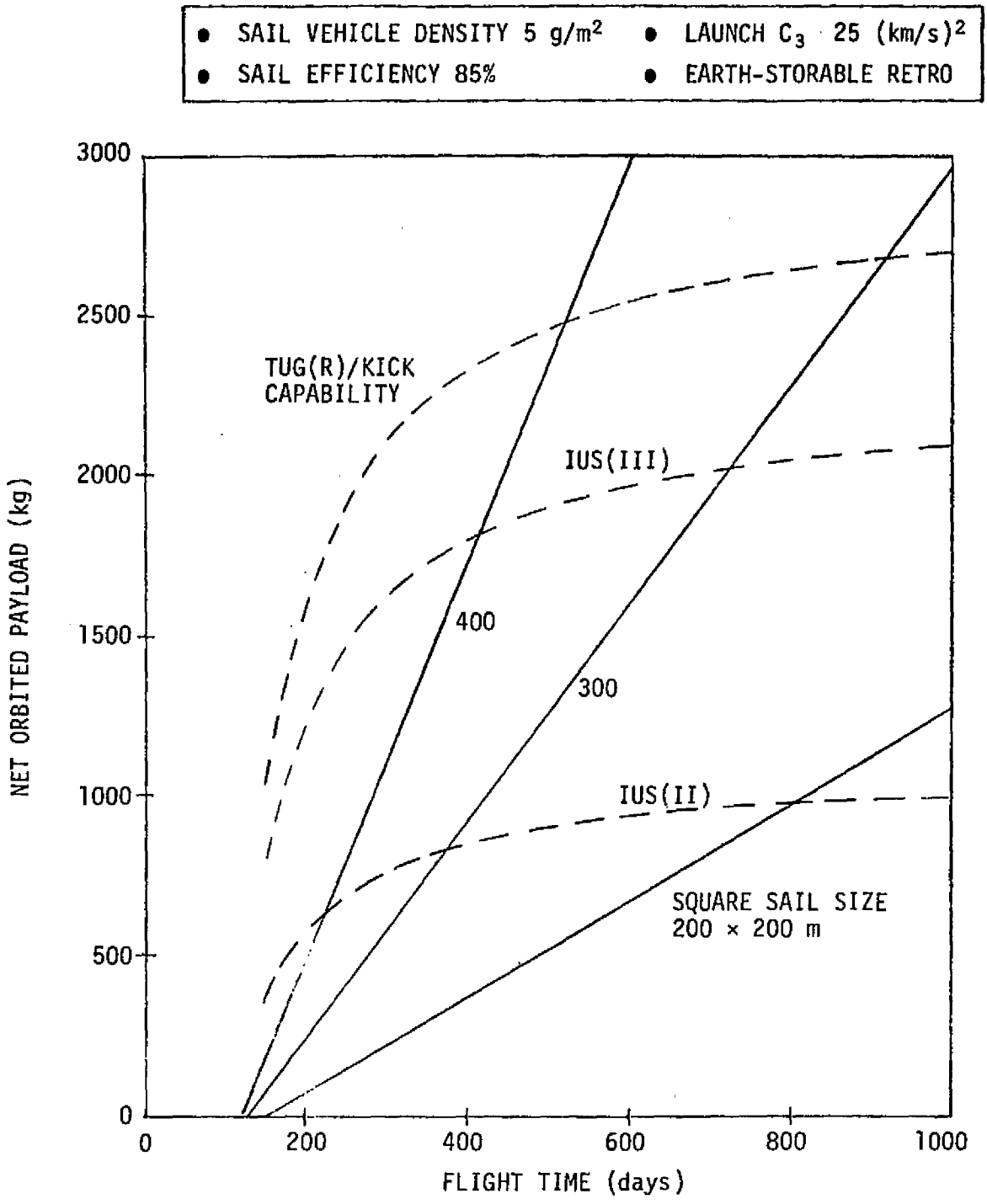

Fig. 2-9 SOLAR SAIL PERFORMANCE FOR MERCURY ORBITER MISSION, a) 500 km CIRCULAR ORBIT

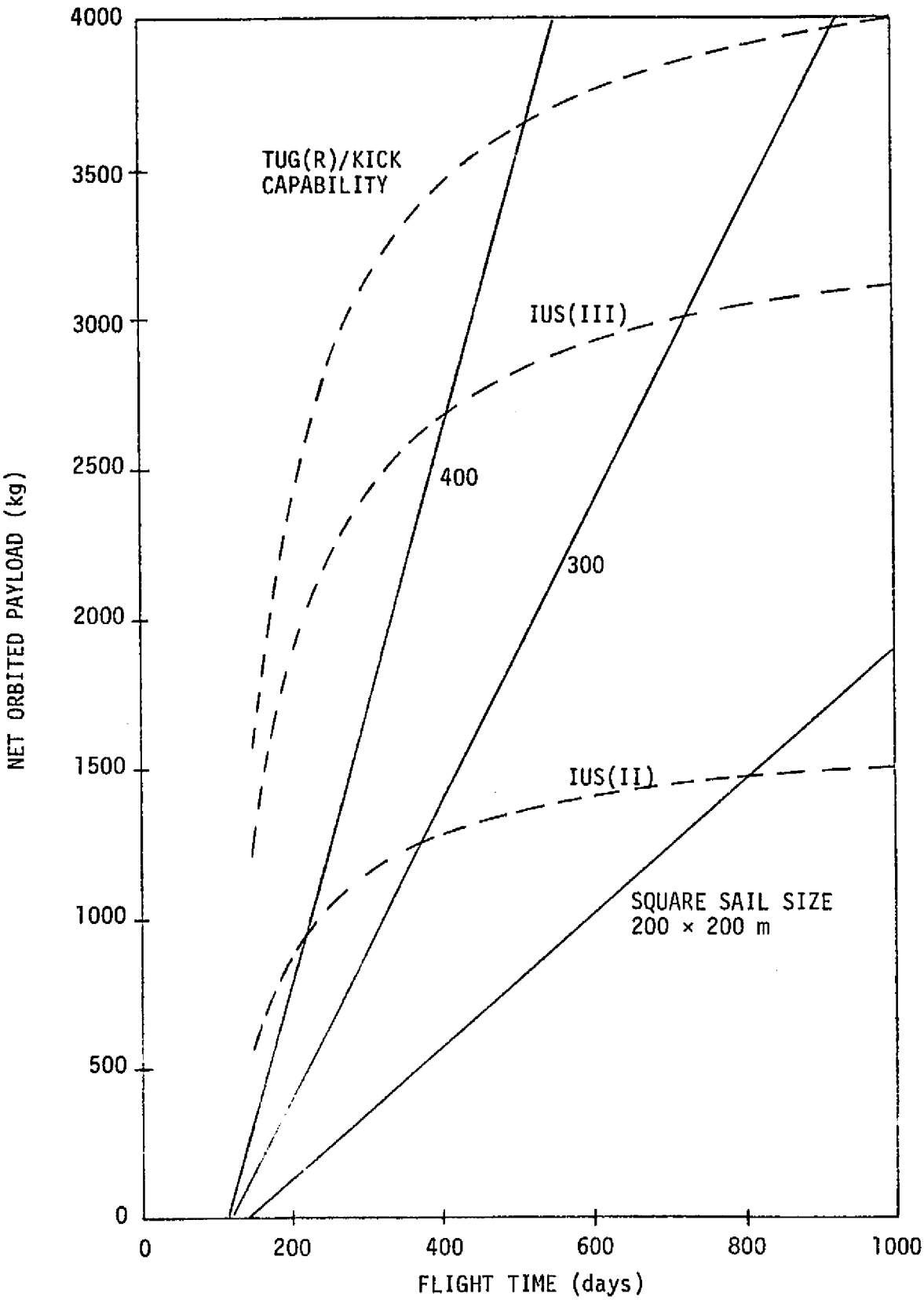

Fig. 2-9 SOLAR SAIL PERFORMANCE FOR MERCURY ORBITER MISSION, b) ELLIPTICAL ORBIT, h_p = 500 km, p = 24^h

The following observations may be discerned from the performance data:

(1) Solar sailing is an extremely effective propulsion concept for transporting payloads to Mercury;

(2) For modest sized payloads (<1000 kg) and sail sizes (<400 meters), short trip times under one year are possible;

(3) Substantially larger payloads can be delivered at the expense of longer trip times, with the point of diminishing return occurring at about 2 years. The IUS(III) capability is about double that of the IUS(II), and the Tug(R)/Kick provides an additional 30% performance above the IUS(III). The payload range extends to nearly 4 metric tons for high eccentricity orbits and 2.5 metric tons for close circular orbits.

These performance results assumed a sail vehicle mass density of 5 g/m^2. The sensitivity to this parameter is such that even if σ is underestimated by 50% the payload capability is reduced only 16% for 1-year trips and 7% for 2-year trips.

3. PERFORMANCE COMPARISON

Performance data generated for the ballistic, SEP and solar sail flight modes are collated in this section for purposes of direct comparison. Payload/flight time formats are presented first and then followed by propulsion system cost comparisons.

3.1 Payload and Flight Time Trades

Figure 3-1 compares payload/flight time performance of the three flight modes for achieving a 500 km circular orbit at Mercury. Use of the Shuttle/IUS(III) launch vehicle is assumed. The six sample ballistic opportunities shown on the graph span the range of ballistic mission performance, i.e., flight times between 750 and 1250 days and orbited payloads between 250 and 650 kg. Retro system capability, in order of increasing performance, is Earth-storable, solid/monopropellant and space-storable. Solar electric propulsion offers a considerable improvement in terms of reduced flight time (500-600 days) and payload increases to the level 500-1000 kg. This potential of low-thrust transport is further enhanced by the solar sailing concept which could deliver sufficient payload, up to 2000 kg, for multiple surface lander deployment missions.

Similar comparison data is presented in Figure 3-2, but now use of the Shuttle/Tug(E) and space-storable retro propulsion is assumed for the ballistic mode missions. This represents the best performance that may be expected for ballistic transport to Mercury through the remainder of the present century. Also indicated on the figure is the range of payload between a 24^h elliptical orbit and a circular orbit. Consider the 1988 ballistic launch opportunity, which has the shortest trip time ($\sim$2 years) relative to low-thrust flight. A payload of 1240 kg can be inserted into a 24^h orbit or 840 kg into a circular orbit. This capability is still less than the SEP performance which assumes an IUS(III) launch and Earth-storable retro, and far short of the solar sail performance. The 1994 ballistic opportunity is considerably better than 1988, and provides more nearly comparable performance to low-thrust capability.

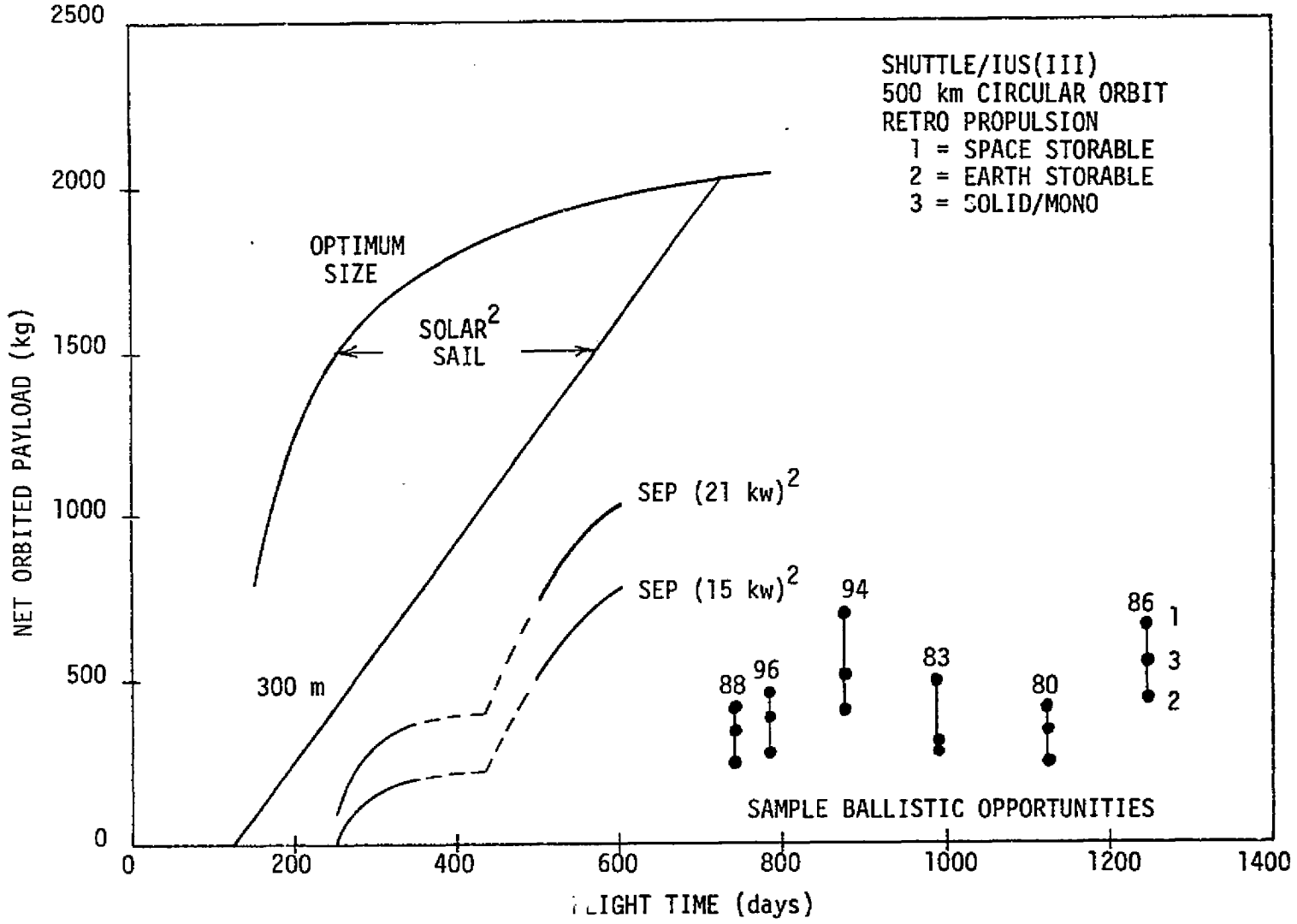

Fig. 3-1 PAYLOAD PERFORMANCE COMPARISON FOR MERCURY ORBITER MISSIONS

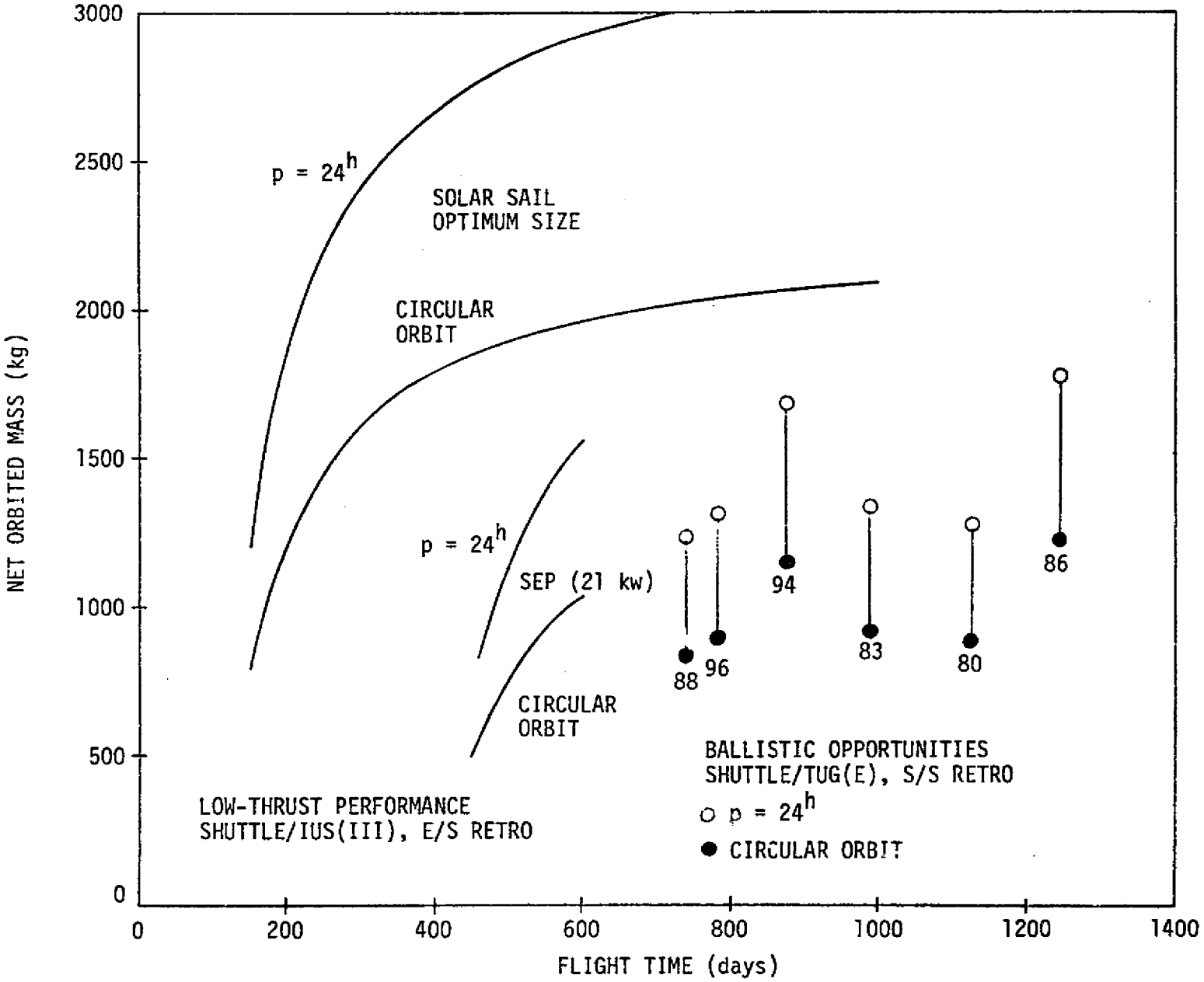

Fig. 3-2 MERCURY ORBITER PERFORMANCE WITH TUG-LAUNCHED BALLISTIC MISSIONS

Another interesting basis of comparison is the size of the retro system needed for Mercury orbit insertion. The retro weights listed in Table 3-1 include both inerts and propellant loading. A 600-day transfer and Earth-storable retro is assumed for the low-thrust flights, while the ballistic data assumes an 877-day flight (1994 launch) and space-storable retro.

Table 3-1

COMPARISON OF RETRO SIZE[a]

	SEP (21 kw)	Sail (300 m)	Ballistic (1994)
Retro Mass (kg)	996	1209	3770
Orbited Mass (kg)	1035	1619	630
M_{retro}/M_{orb}	0.96	0.75	5.98

[a]Shuttle/IUS(III) launch, 500 km circular orbit.

The ballistic mode retro mass is more than three times larger than that required for low-thrust transport. Note also that the ratio of retro to orbited mass is almost 6 for the ballistic mode.

3.2 Cost Implications

In evaluating the relative merits of propulsion options, the program planner is concerned with cost as well as mission performance trades. Estimates were made of the propulsion system cost for each flight mode. Figure 3-3 shows the total (development plus recurring) cost of chemical retro systems as a function of retro inert weight as predicted by the SAI planetary mission cost model.[10] Historical experience shows that the recurring component is approximately 15% of the propulsion system development cost, and would most likely not exceed 5 M$. However, for the present application, total cost seems a more relevant index since the retro system is not likely to be an "off-the-shelf" item, but rather a unique design match to Mercury

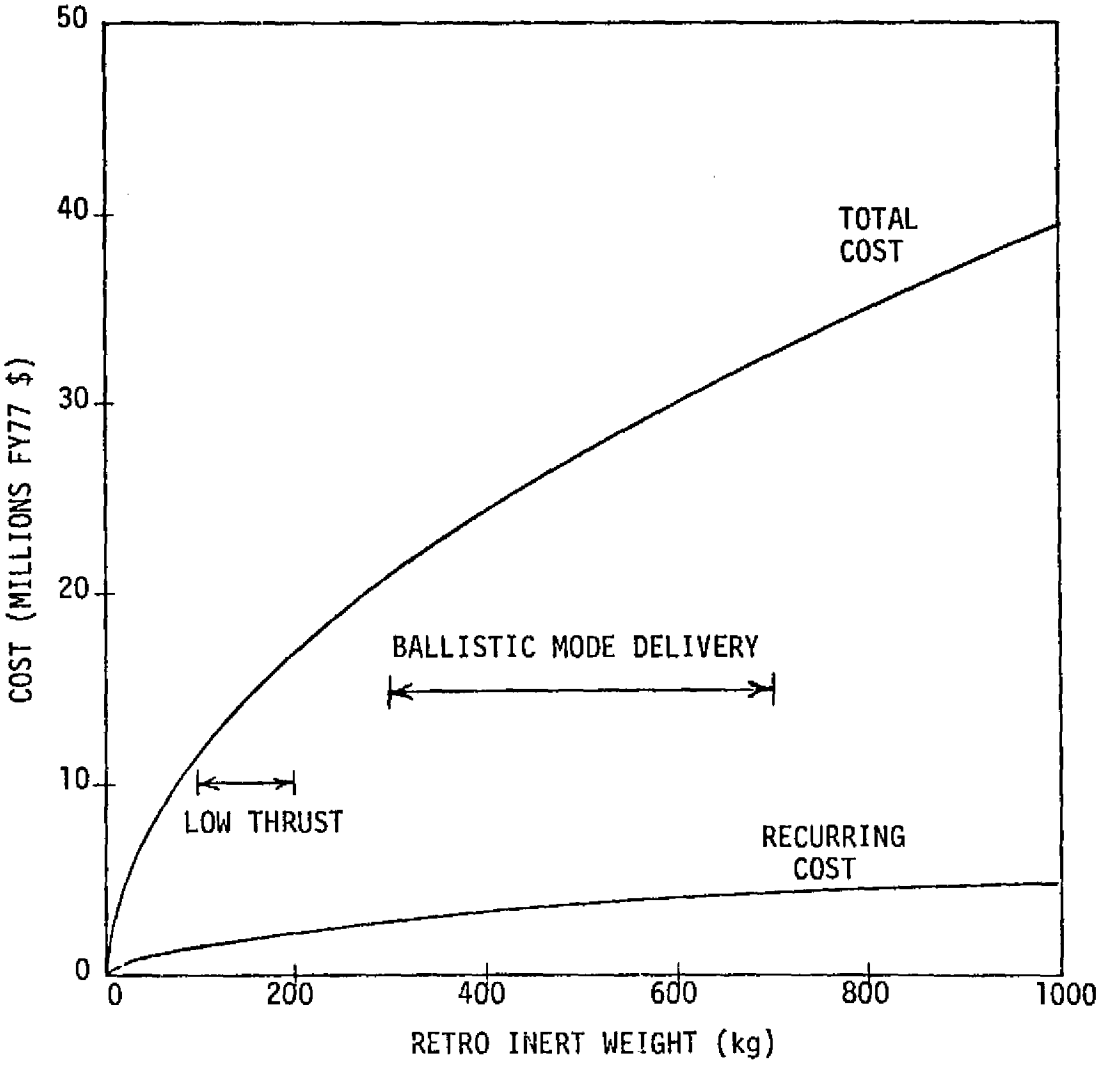

Fig. 3-3 ESTIMATED COST OF CHEMICAL RETRO SYSTEMS FOR MERCURY ORBIT CAPTURE APPLICATIONS

mission requirements. The smaller retro systems for low-thrust flight are estimated to incur a total cost in the range 12-17 M$ (fiscal year 1977 dollars are used for all cost). Significantly higher cost in the range 21-32 M$ is estimated for ballistic mission applications.

It seems reasonable to assume that low-thrust propulsion (SEP or sail) would only be developed if applied to a wide base of planetary missions. We will therefore ignore the initial development cost and use only the recurring component in the present cost comparison. Updating earlier SEP cost estimates to FY'77 dollars, the recurring costs of 15, 18 and 21 kw systems are taken to be 20, 22 and 24 M$, respectively. The recurring cost of a 300 × 300 meter solar sail is taken as 6 M$ which is 15% of an estimated 40 M$ development cost.* We stress the uncertainty in the sail cost--it could easily double under closer scrutiny.

Propulsion cost comparisons of the three flight modes are shown in Figure 3-4. These results are calculated for a Shuttle/IUS(III) launch and a 500 km circular orbit of Mercury. SEP transport costs are the highest at 35-40 M$, and solar sail costs the lowest at 17-23 M$. Retro propulsion costs for ballistic missions are 21-32 M$ with the solid/monopropellant systems being least expensive and space-storable systems being most expensive.

Figure 3-5 compares the three flight modes in terms of a specific cost index, i.e., propulsion system cost per kilogram of delivered payload. Since low specific cost and short flight times are most desirable, it is seen that solar sailing provides the best performance, followed by SEP and then ballistic mode transport. In the ballistic case, the most cost-effective retro propulsion is generally the combined solid/monopropellant system, followed closely by space-storable, with Earth-storable systems being least cost-effective.

In making the above comparison between SEP and solar sailing, the basic assumption used was a SEP recurring cost of 20-24 M$ and a considerably lower sail recurring cost of 6 M$. Furthermore, the payload performance stated for SEP was based on current technology parameters. Since these

*Personal communication with Jerry Wright, JPL.

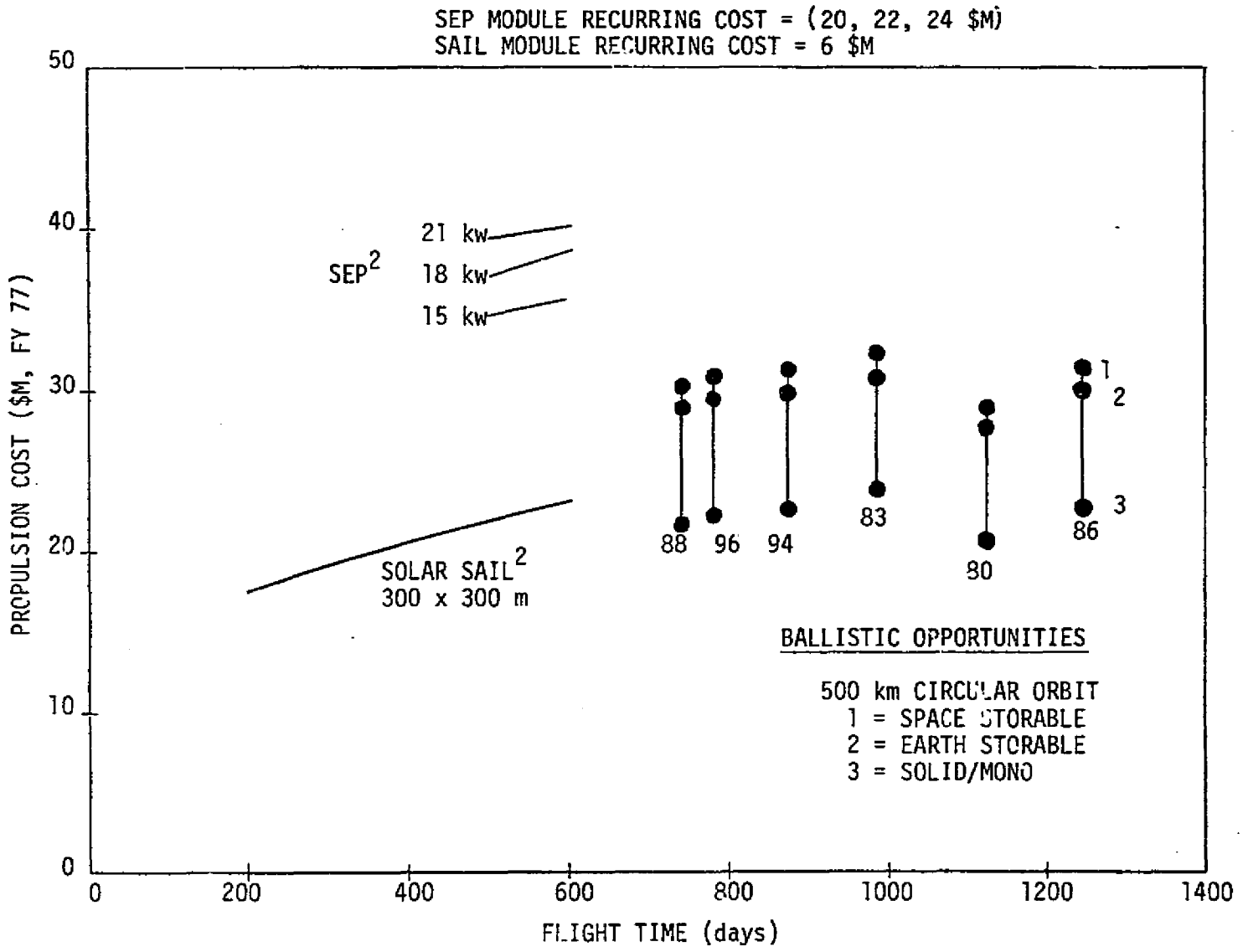

Fig. 3-4 PROPULSION SYSTEM COST COMPARISON FOR MERCURY ORBITER MISSIONS

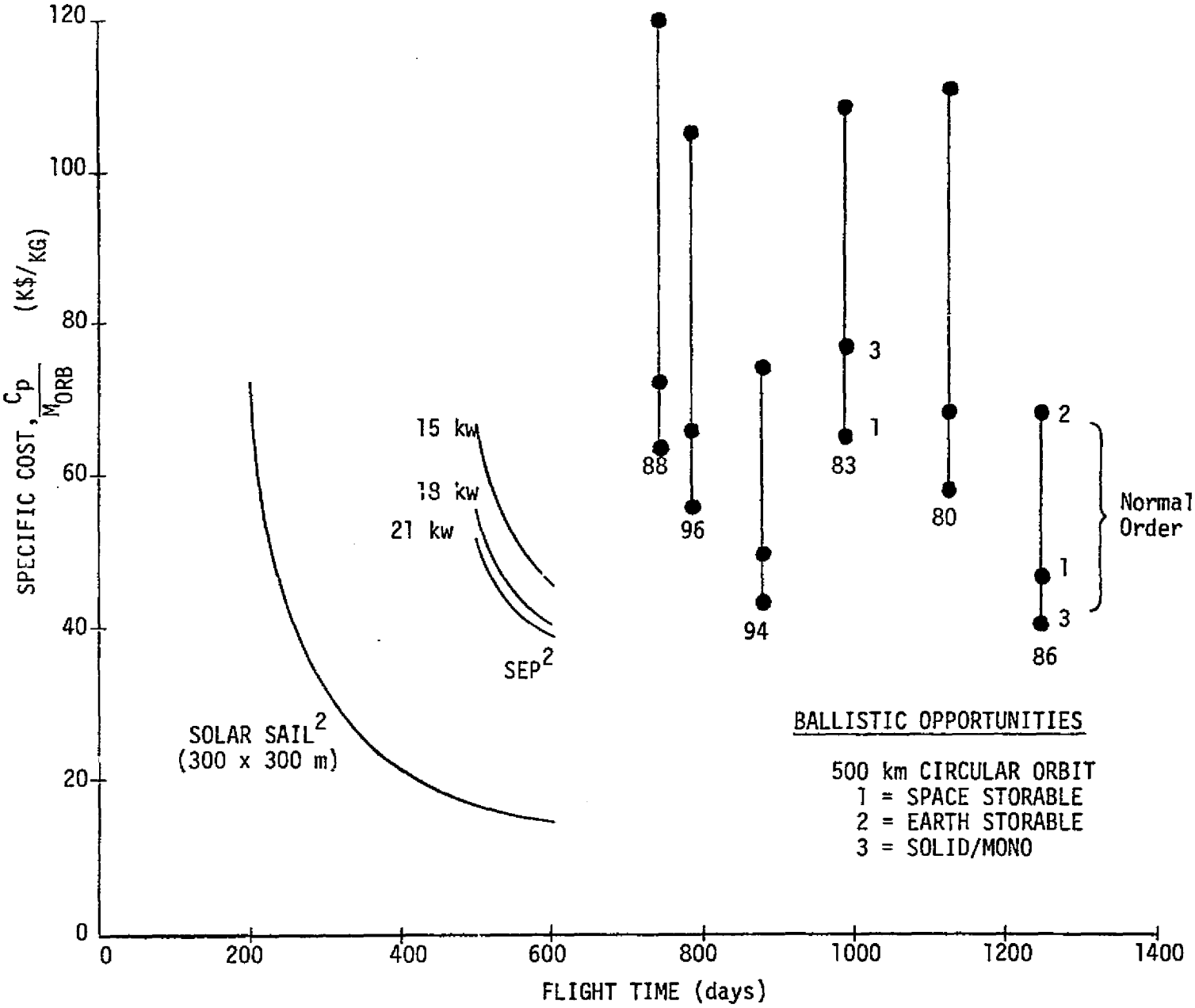

Fig. 3-5 PROPULSION SYSTEM SPECIFIC COST COMPARISON FOR MERCURY ORBITER MISSIONS

assumptions are certainly subject to question, a sensitivity analysis was performed and the comparative results are shown in Figure 3-6. One may conclude, for example, that a SEP vehicle of advanced design is more nearly comparable with a solar sail vehicle in terms of cost-effectiveness.

In summary, the results of this study have shown that low-thrust propulsion is far superior to the ballistic flight mode in transporting appreciable payloads to Mercury orbit. It also appears to be more cost-effective, provided that low-thrust systems are developed for and used across a wide spectrum of planetary mission applications. Solar sail vehicles have a performance advantage over SEP for Mercury missions. This might not be the case for other planetary targets beyond 1 AU distance. Although "conventional" ballistic missions can be flown to Mercury, the flight time tends to be quite long and the payload delivery marginal with IUS launches. Large payload delivery requires the equivalent of a Tug(E) launch vehicle and a very large retro propulsion system carried to Mercury. Also, good ballistic launch opportunities occur infrequently (only twice between 1985-2000 with circular orbit payloads > 500 kg) compared to annual low-thrust opportunities.

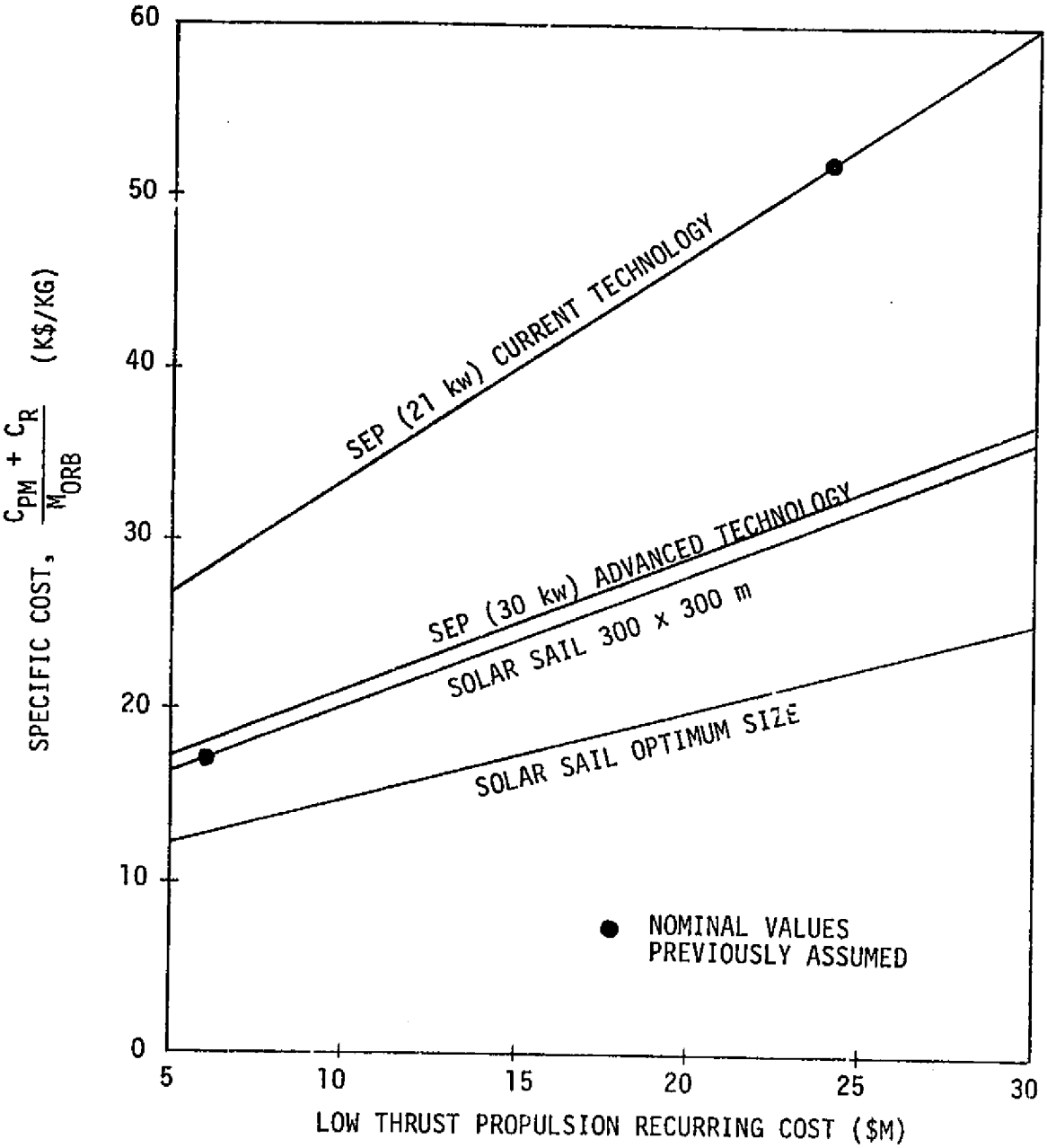

Fig. 3-6 PARAMETRIC COST COMPARISON OF SEP AND SOLAR SAIL FOR MERCURY ORBITER MISSION
TF = 500 days; 500 km CIRCULAR ORBIT
EARTH-STORABLE RETRO

REFERENCES

1. "Lunar and Planetary Missions Handbook, Vol. IV, Mission Descriptions," prepared for NASA by Jet Propulsion Laboratory, April 1977.

2. Friedlander, A. L. and Davis, D. R., "Penetrator Mission Concepts for Mercury and the Galilean Satellites," Report No. SAI 1-120-399-M5, Science Applications, Inc., February 1976.

3. French, J. R., "Alternate Planetary Lander Study Report," JPL 760-149, Jet Propulsion Laboratory, July 1976.

4. Hollenbeck, G., et al., "Study of Ballistic Mode Mercury Orbiter Missions," Report Series NASA CR-2298, CR-114618, Martin-Marietta Corporation, July 1973.

5. Bender, D. F., "Ballistic Trajectories for Mercury Orbiter Missions Using Optimal Venus Flybys, A Systematic Search," AIAA Paper No. 76-796, presented at the AIAA/AAS Astrodynamics Conference, San Diego, California, August 18-20, 1976.

6. Friedlander, A. L., "(MULIMP) Multi-Impulse Trajectory and Mass Optimization Program," Report No. SAI 1-120-383-T4, Science Applications, Inc., April 1975.

7. Wallace, R. A., "Net Spacecraft Mass in Orbit About Mars, Venus, Mercury, and the Moon," JPL Engineering Memorandum 392-204, Jet Propulsion Laboratory, February 1976.

8. Sauer, C., communication of unpublished data, Jet Propulsion Laboratory, 1976.

9. Wright, J. L., "Solar Sailing: Evaluation of Concept and Potential," Report No. BMI-NLVP-TM-74-3, Battelle Memorial Institute, November 1974.

10. Kitchen, L. D., "Manpower/Cost Estimation Model--Automated Planetary Projects," Report No. SAI 1-120-194-C1, Science Applications, Inc., March 1975.

Appendix A

PERFORMANCE CURVES FOR BALLISTIC OPPORTUNITIES

Computer-generated plots of Mercury orbiter payload are included for each of 16 launch opportunities covering the period 1980-2000 for the Venus swingby ballistic transfer mode. There are five cases of two launch opportunities in a single calendar year; both are included but one usually has superior performance and would be a clear-cut choice. The graphs are ordered chronologically, in sets of three. Each set contains separate graphs for Earth storable, solid/monopropellant and space-storable retros, presented in that order. Interpretation and use of the graphs has been explained in Section 2.1 of this report. Table A which follows presents a brief comparative summary of trajectory and payload characteristics for the 16 opportunities. The Shuttle/IUS(III) launch vehicle, a space-storable retro, and a 500 km circular orbit are assumed for this purpose.

Table A

COMPARATIVE SUMMARY OF BALLISTIC MODE MERCURY ORBITERS

Launch Date	Transfer Type	Flight Time (days)	C_3 $(km/sec)^2$	Retro* Mass (kg)	Orbited* Payload (kg)
2/26/80	V(3)	1126	30.90	3095	425
6/26/80	V(1)	657	34.20	2965	285
7/9/81	V(2)-a	1067	32.80	2930	450
10/22/81	V(2)-b	422	45.41	2425	125
3/6/83	V(2)	989	17.45	4075	500
7/8/83	V(3)	953	25.25	3550	350
6/24/85	V(1)	420	49.60	2150	190
7/18/86	V(2)	911	24.44	3790	200
7/29/86	V(3)	1247	19.17	3750	670
3/19/88	V(2)-a	741	25.80	3460	420
7/10/88	V(2)-b	621	28.05	3345	355
7/2/89	V(2)	792	43.25	2370	320
7/13/91	V(2)	1019	25.80	3505	365
7/25/94	V(2)	877	19.38	3770	630
2/9/96	V(3)	782	23.00	3630	470
7/13/99	V(4)	1177	26.35	3380	445

*Shuttle/IUS(III), space-storable retro (two stages), 500 km circular orbit.

1980 V(3) OPPORTUNITY

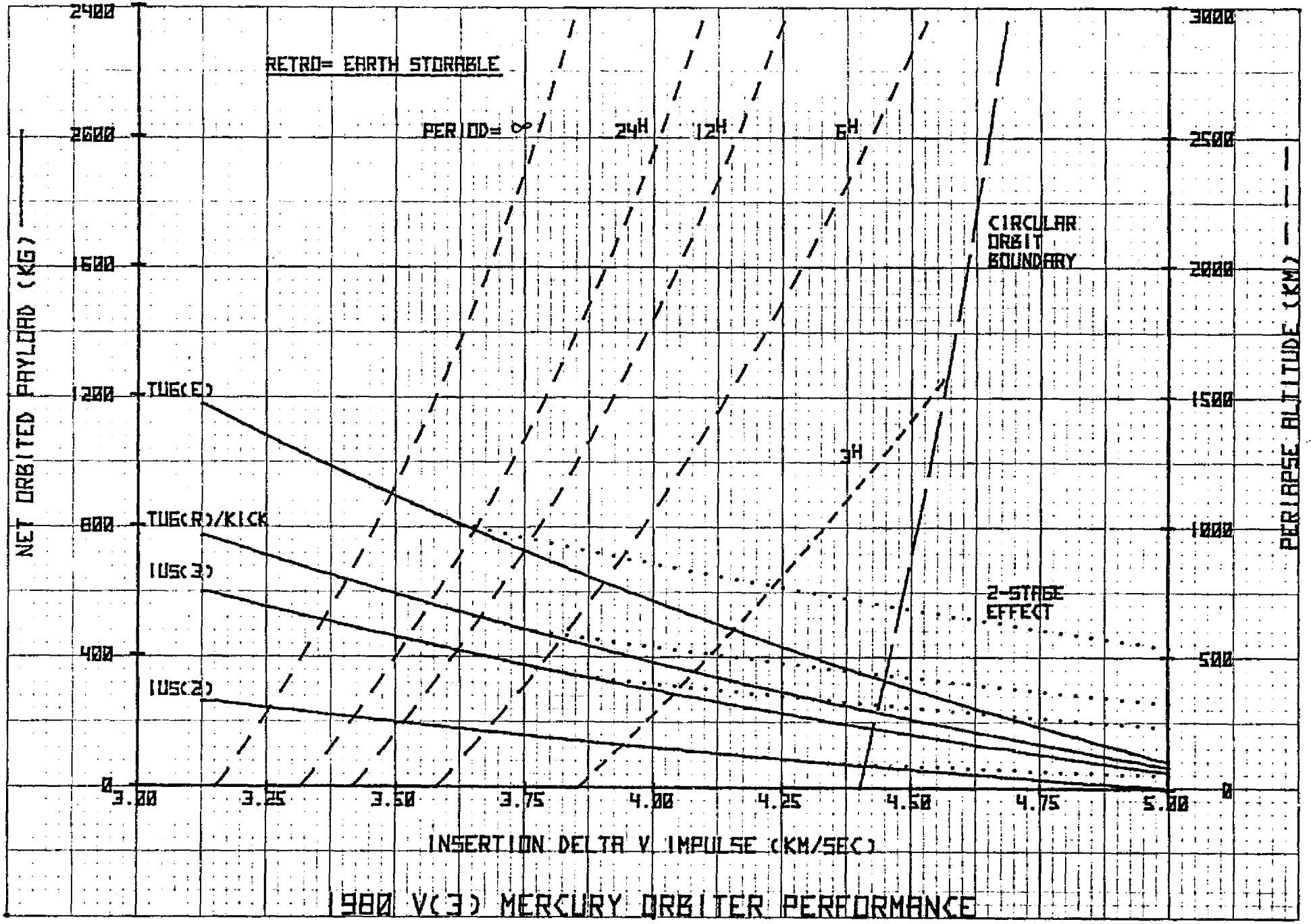

1980 V(3) MERCURY ORBITER PERFORMANCE

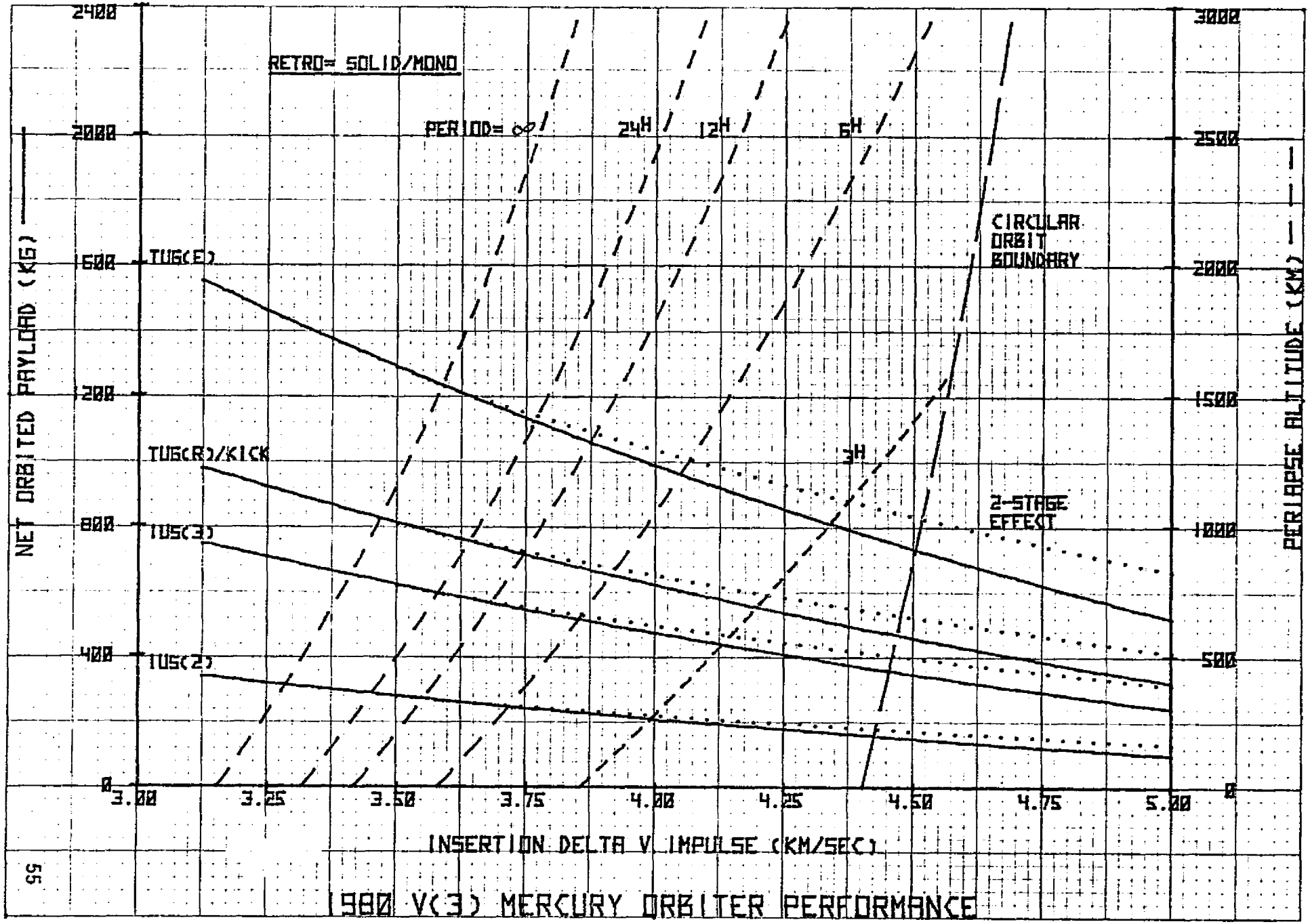

55

1980 V(3) MERCURY ORBITER PERFORMANCE

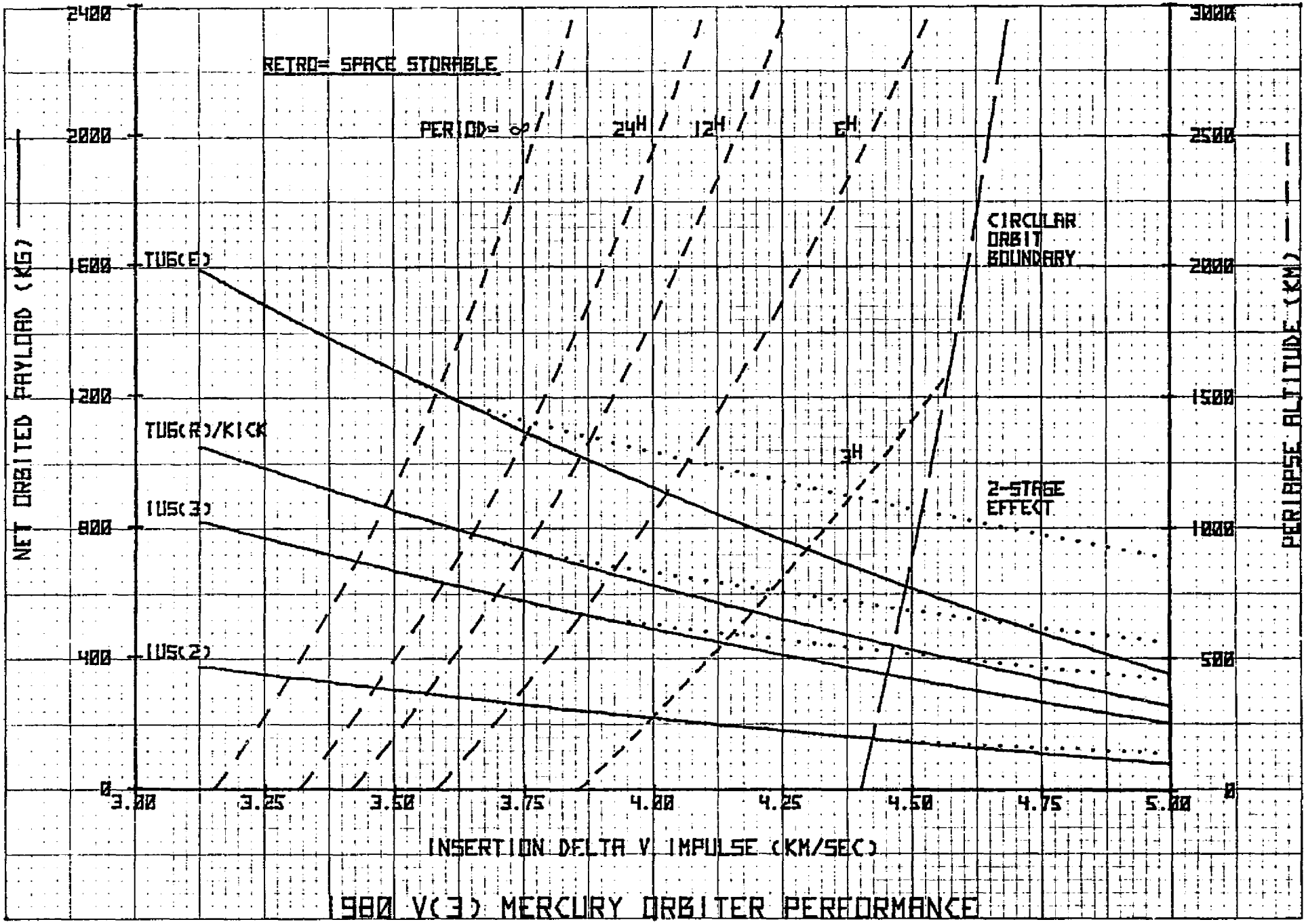

1980 V(3) MERCURY ORBITER PERFORMANCE

1980 V(1) OPPORTUNITY

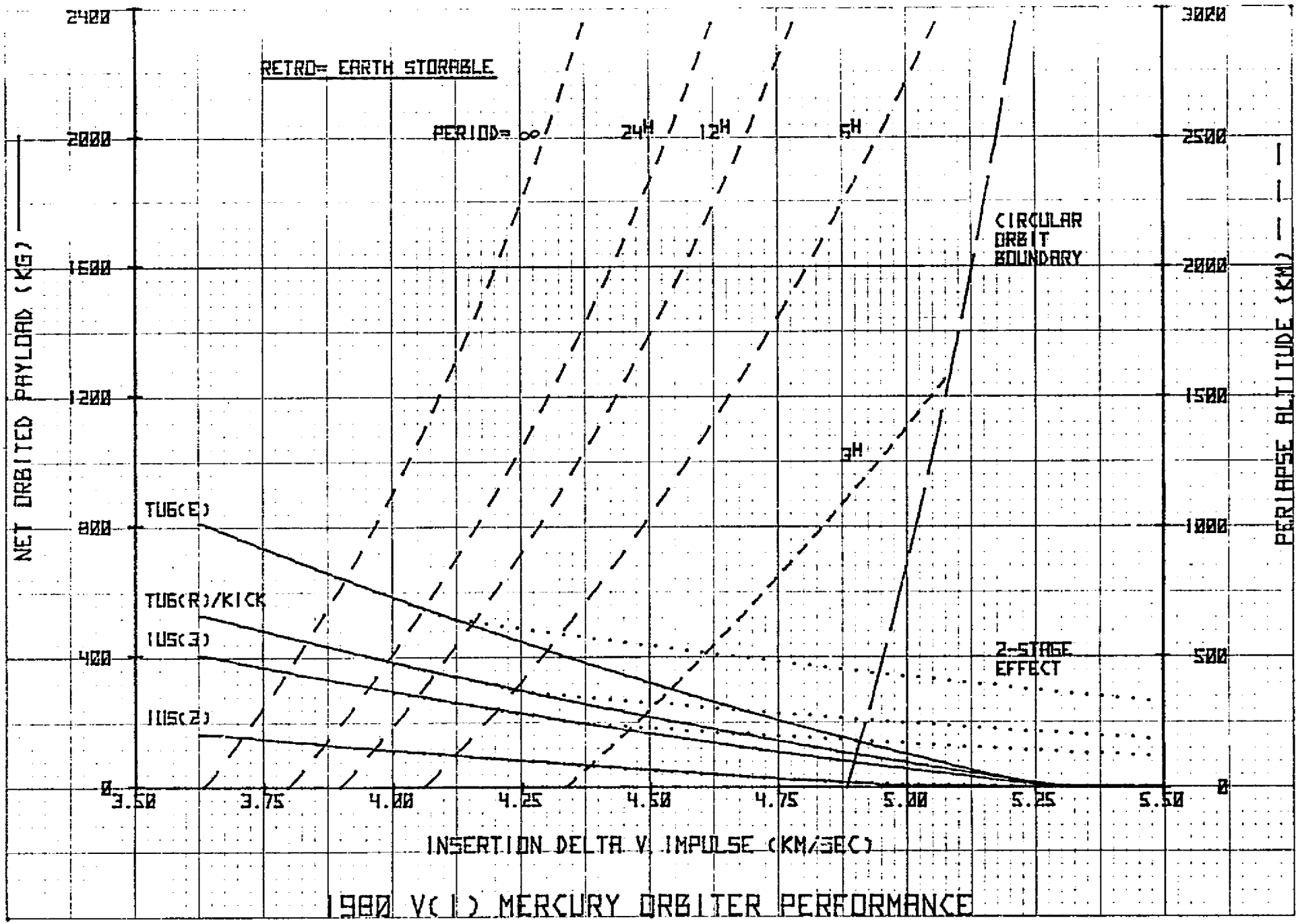

1980 V(I) MERCURY ORBITER PERFORMANCE

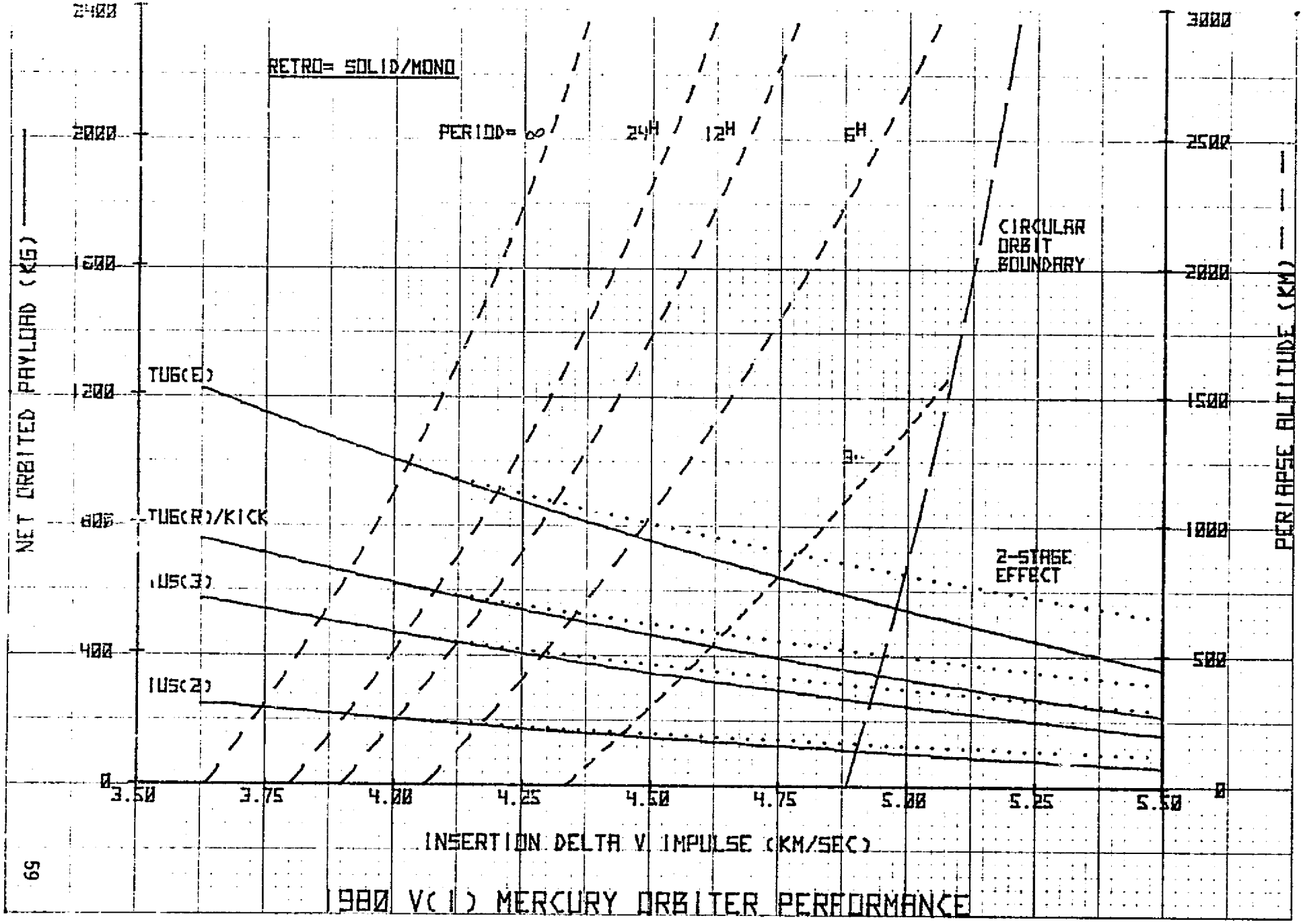

69

1980 V(I) MERCURY ORBITER PERFORMANCE

09

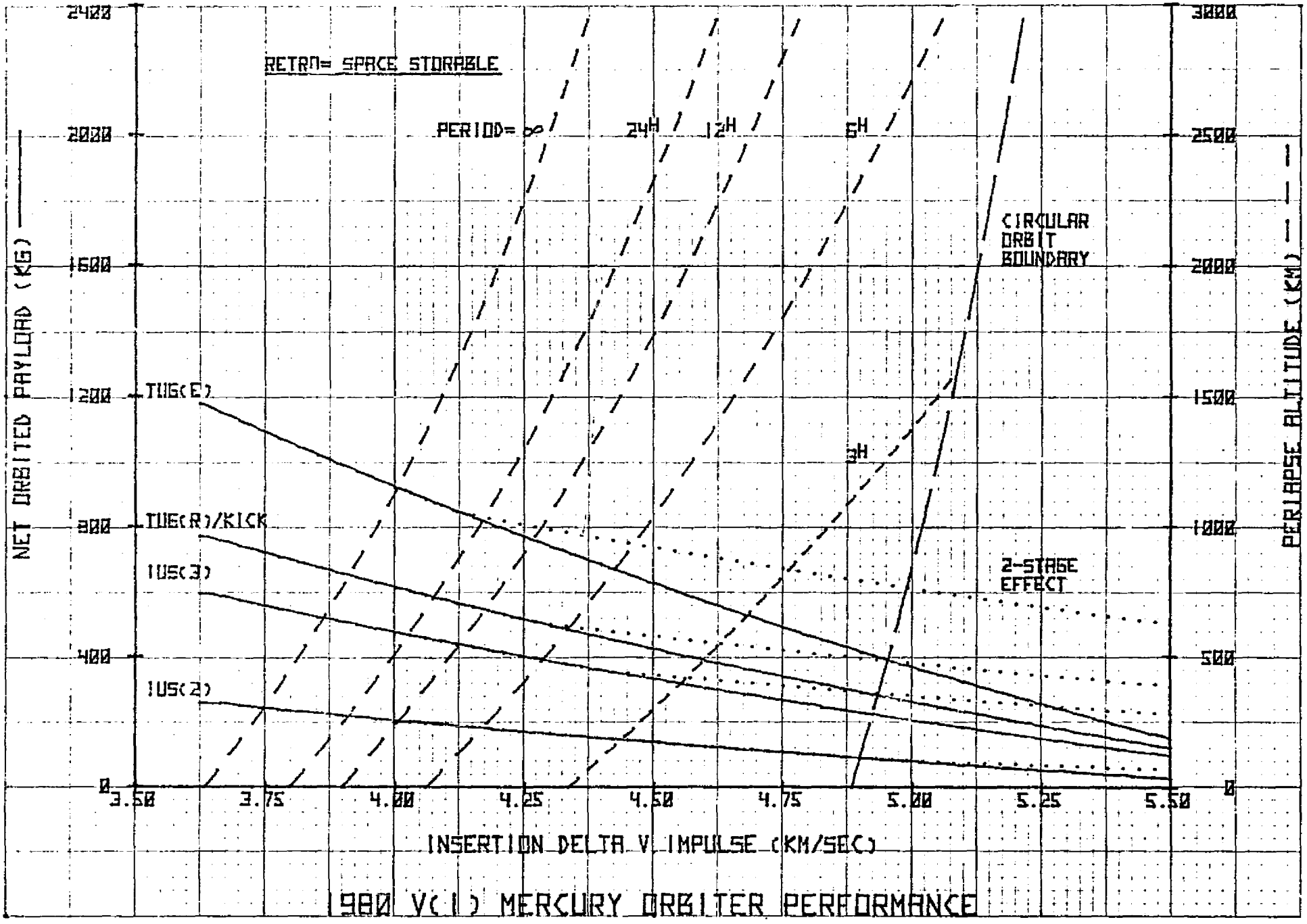

1980 V(I) MERCURY ORBITER PERFORMANCE

1981 V(2)-a OPPORTUNITY

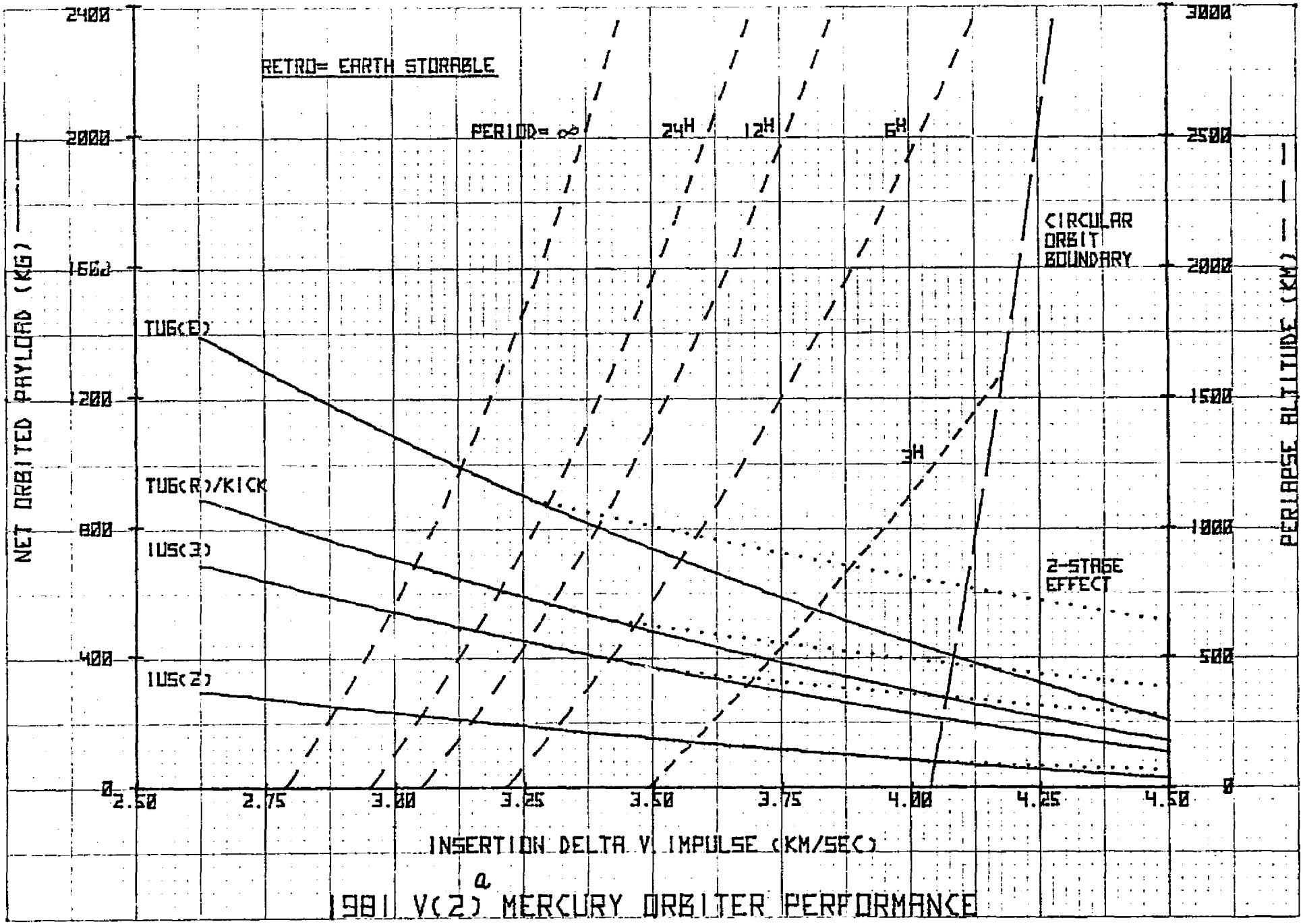

a

1981 V(2) MERCURY ORBITER PERFORMANCE

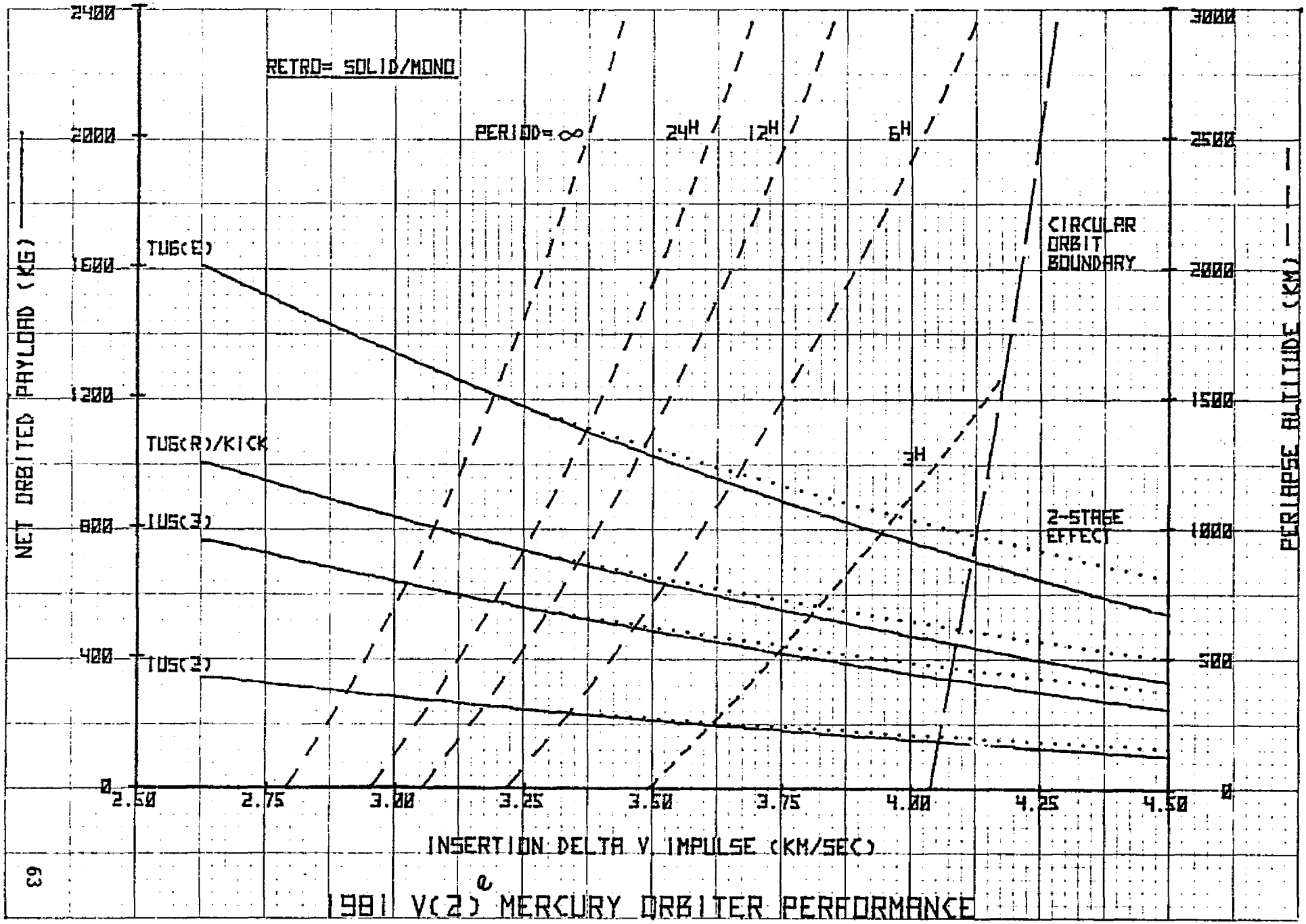

63

1981 V(2) MERCURY ORBITER PERFORMANCE

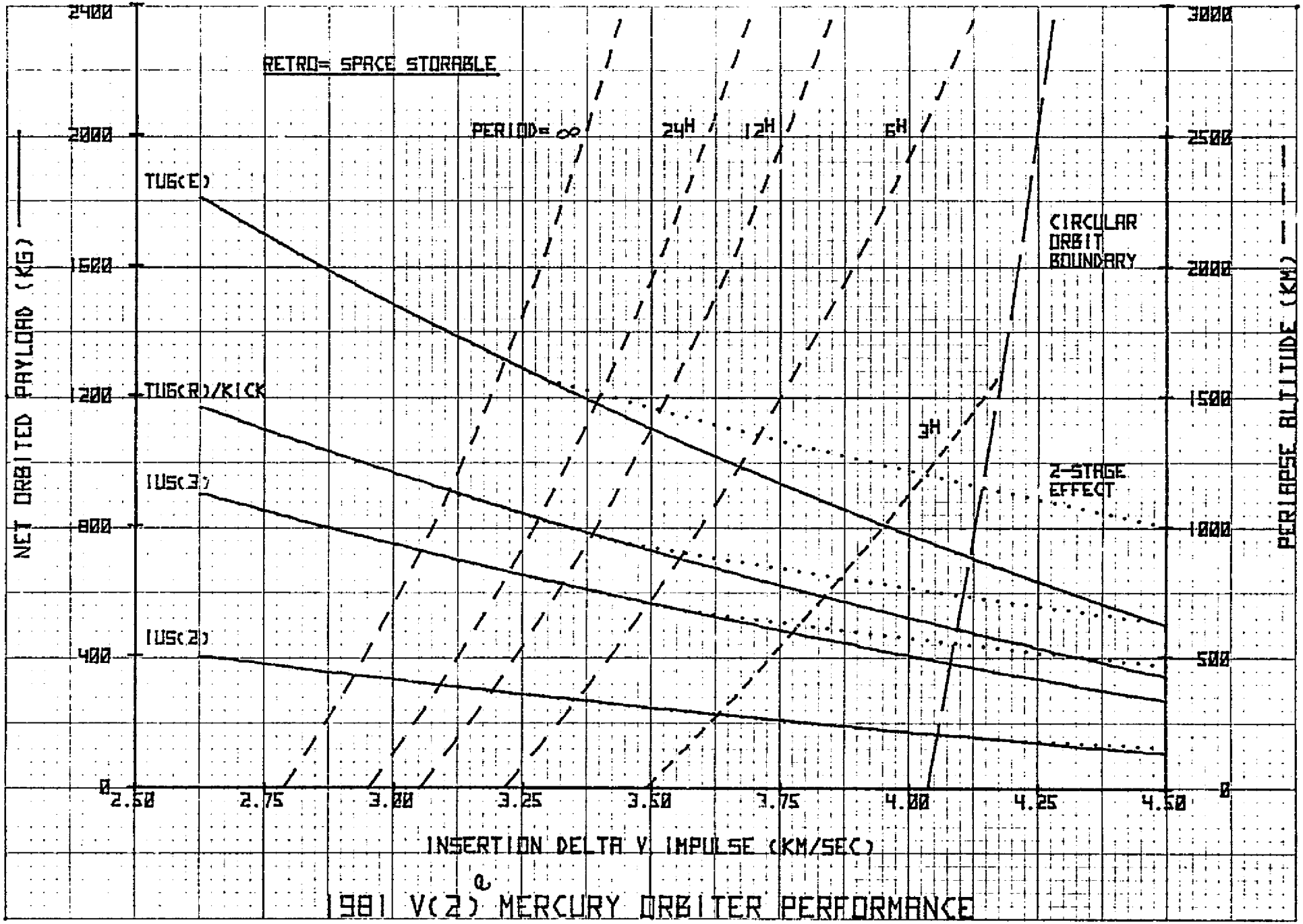

1981 V(2) MERCURY ORBITER PERFORMANCE

1981 V(2)-b OPPORTUNITY

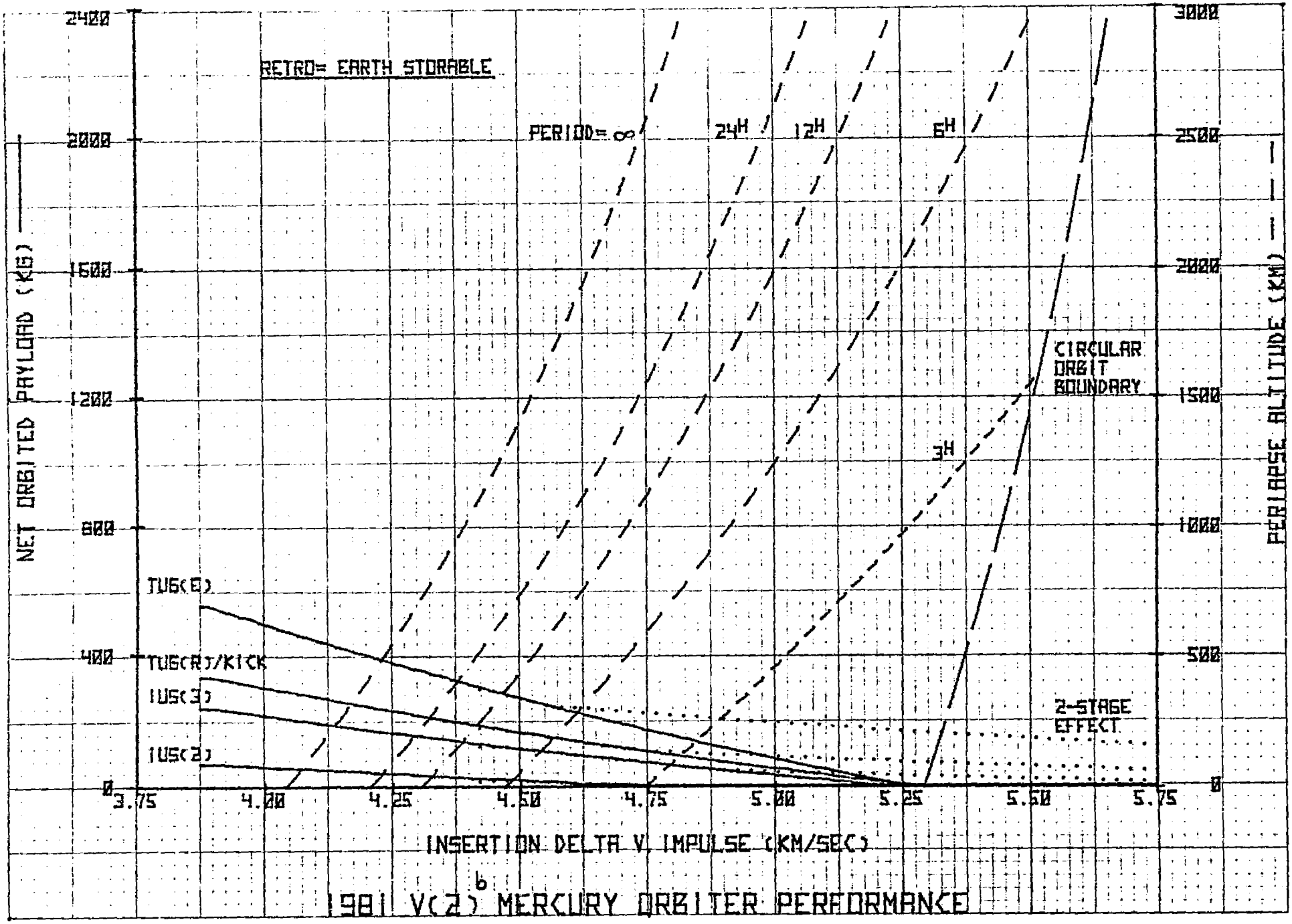

b

1981 V(2) MERCURY ORBITER PERFORMANCE

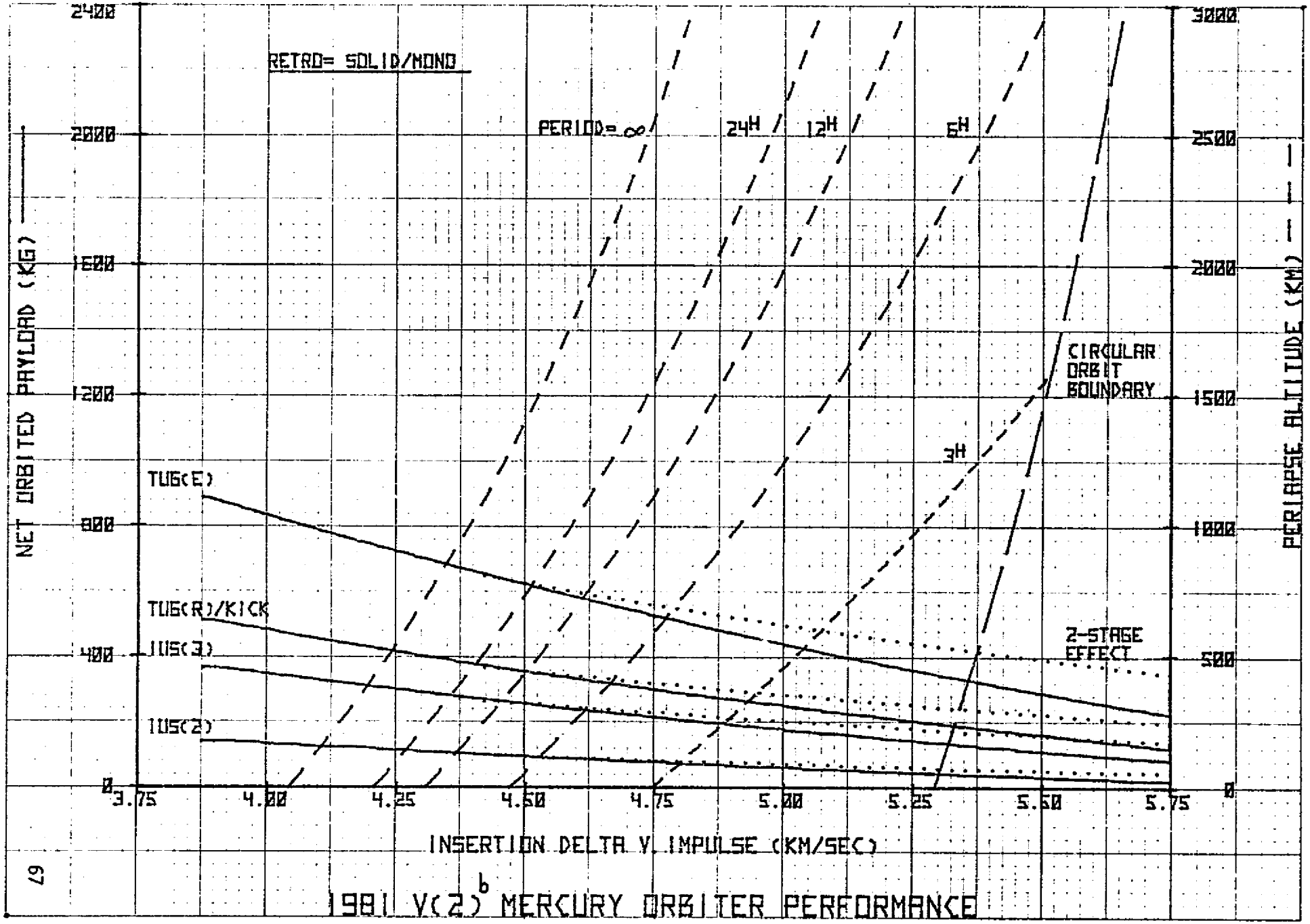

1981 V(2)^{b} MERCURY ORBITER PERFORMANCE

67

09

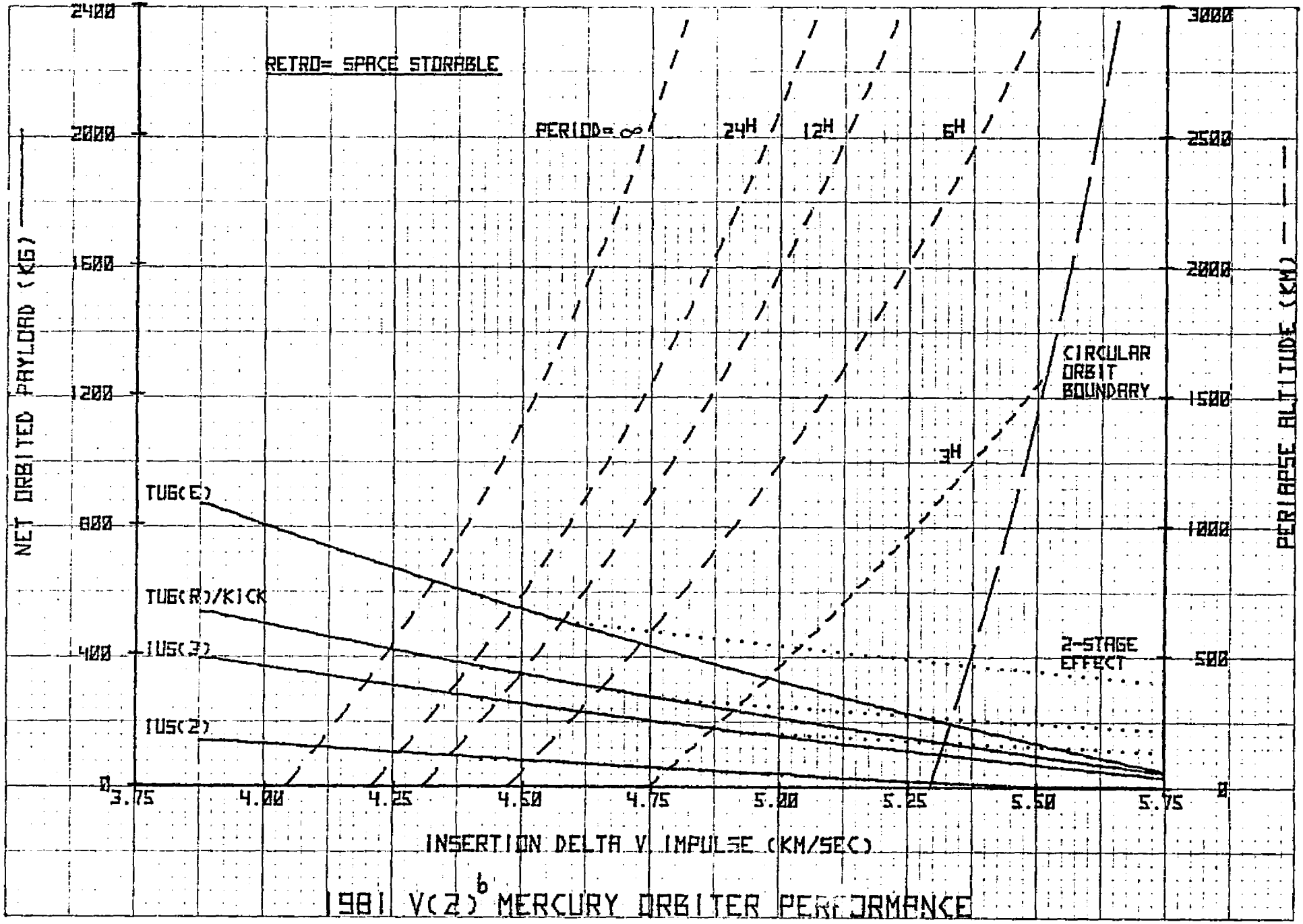

1981 V(2)[b] MERCURY ORBITER PERFORMANCE

1983 V(2) OPPORTUNITY

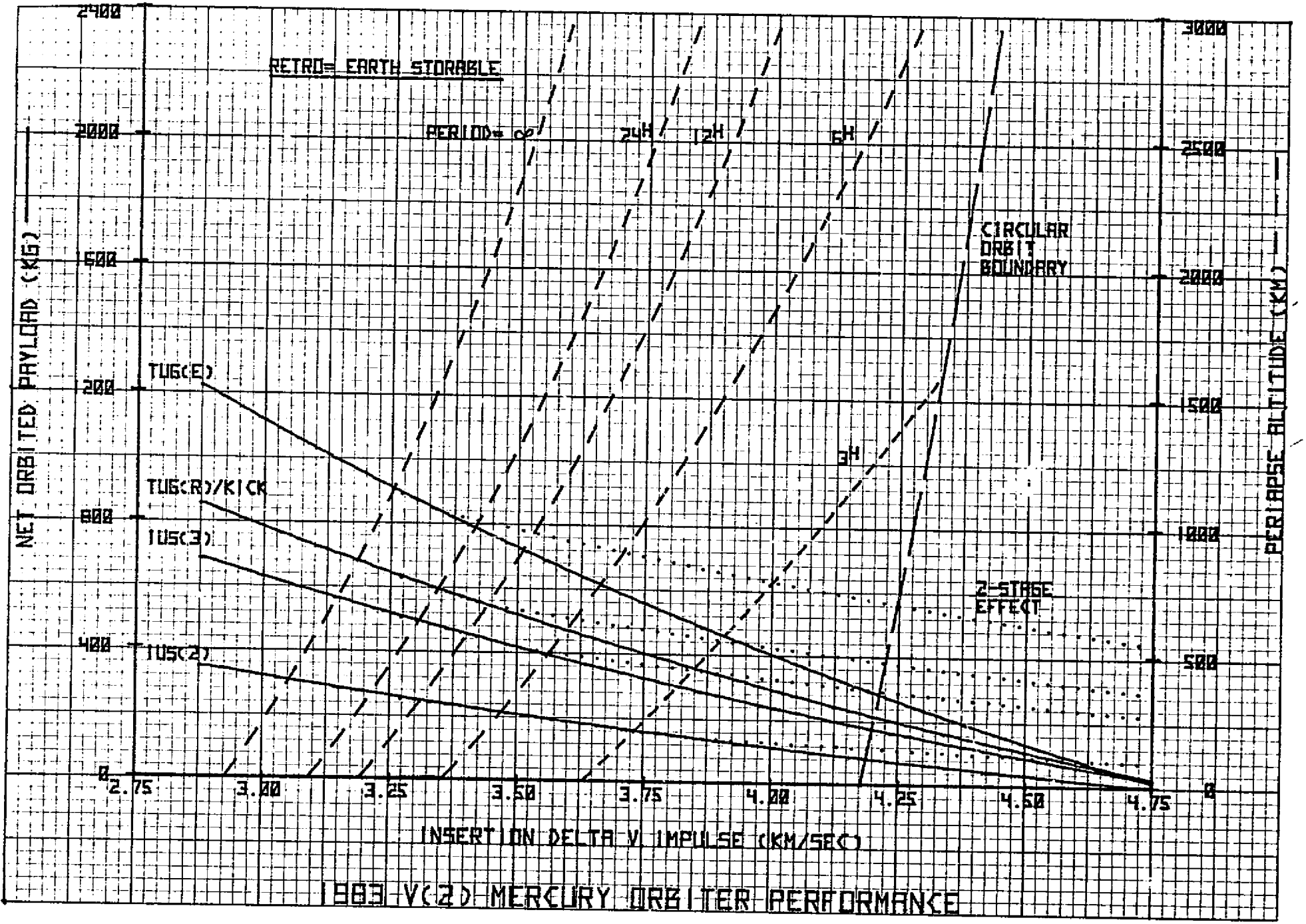

1983 V(2) MERCURY ORBITER PERFORMANCE

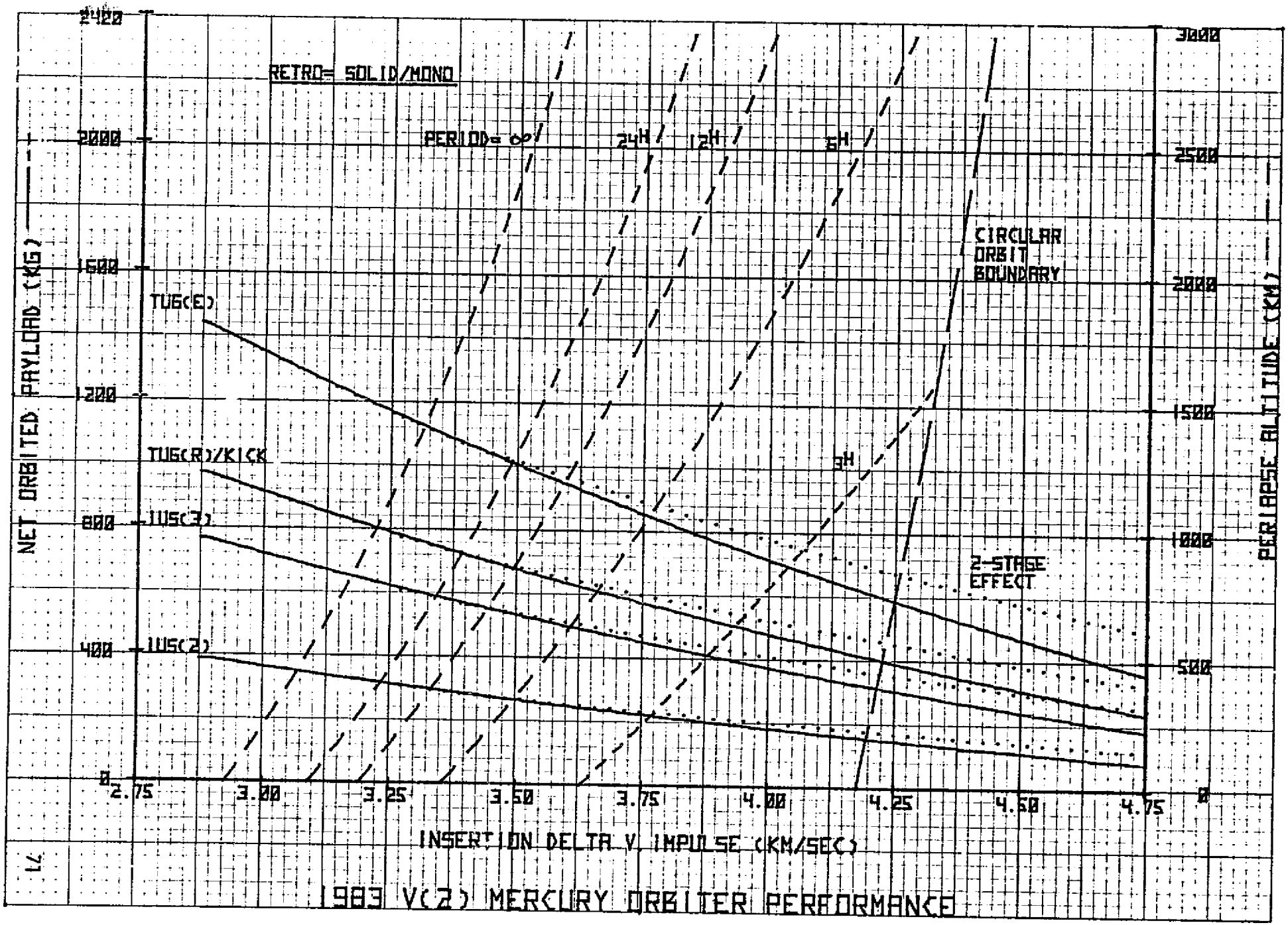

1983 V(2) MERCURY ORBITER PERFORMANCE

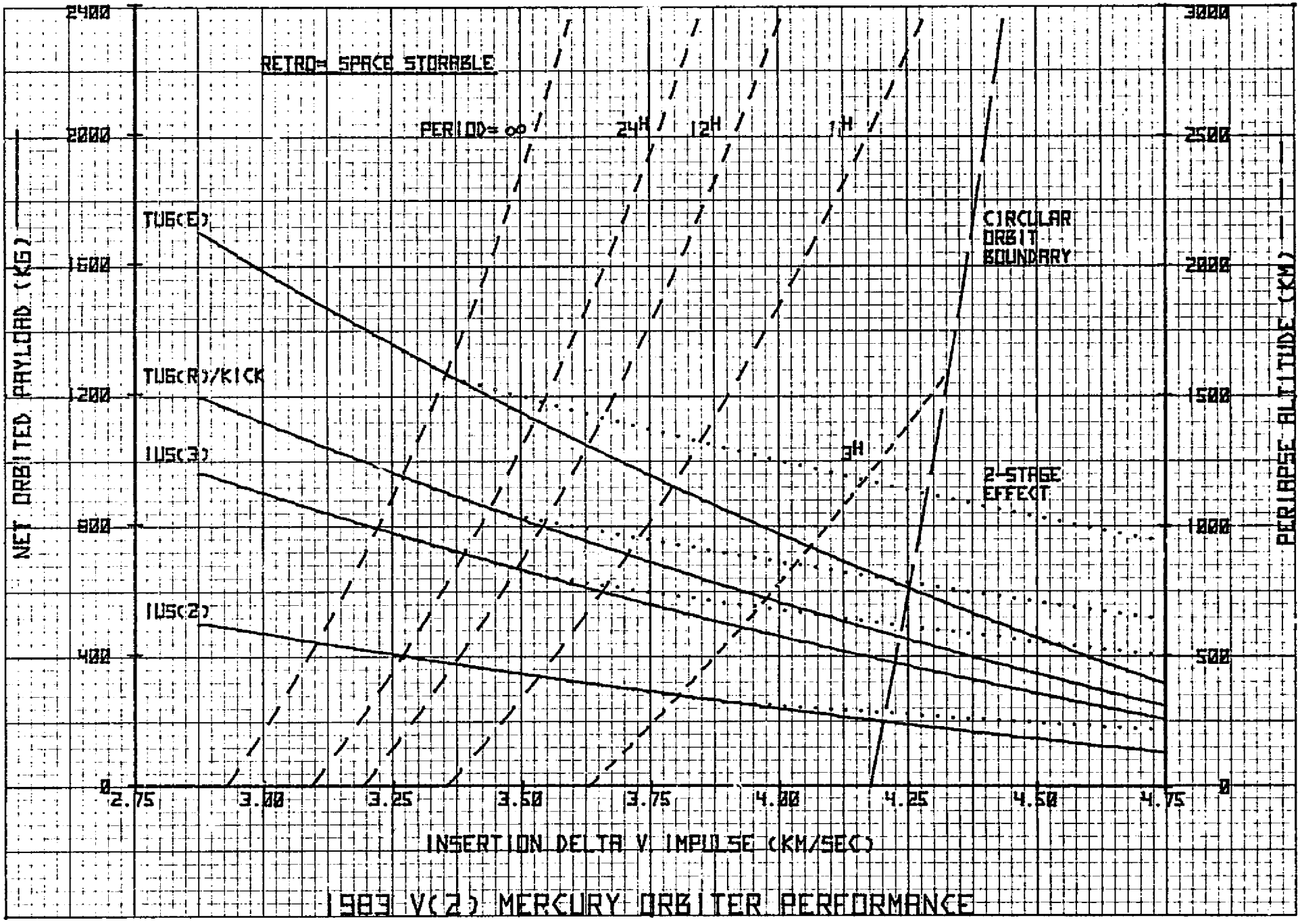

1983 V(2) MERCURY ORBITER PERFORMANCE

1983 V(3) OPPORTUNITY

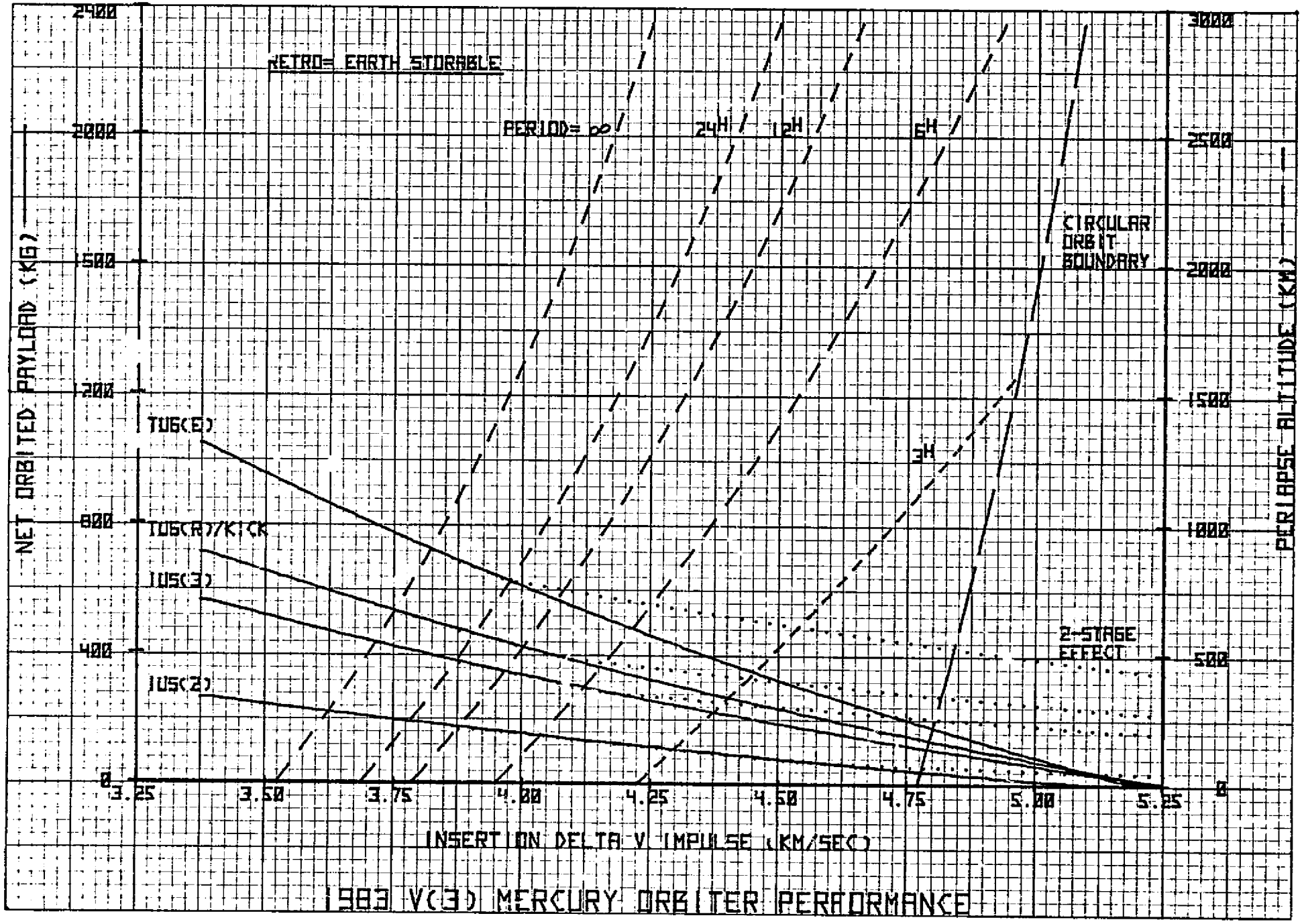

1983 V(3) MERCURY ORBITER PERFORMANCE

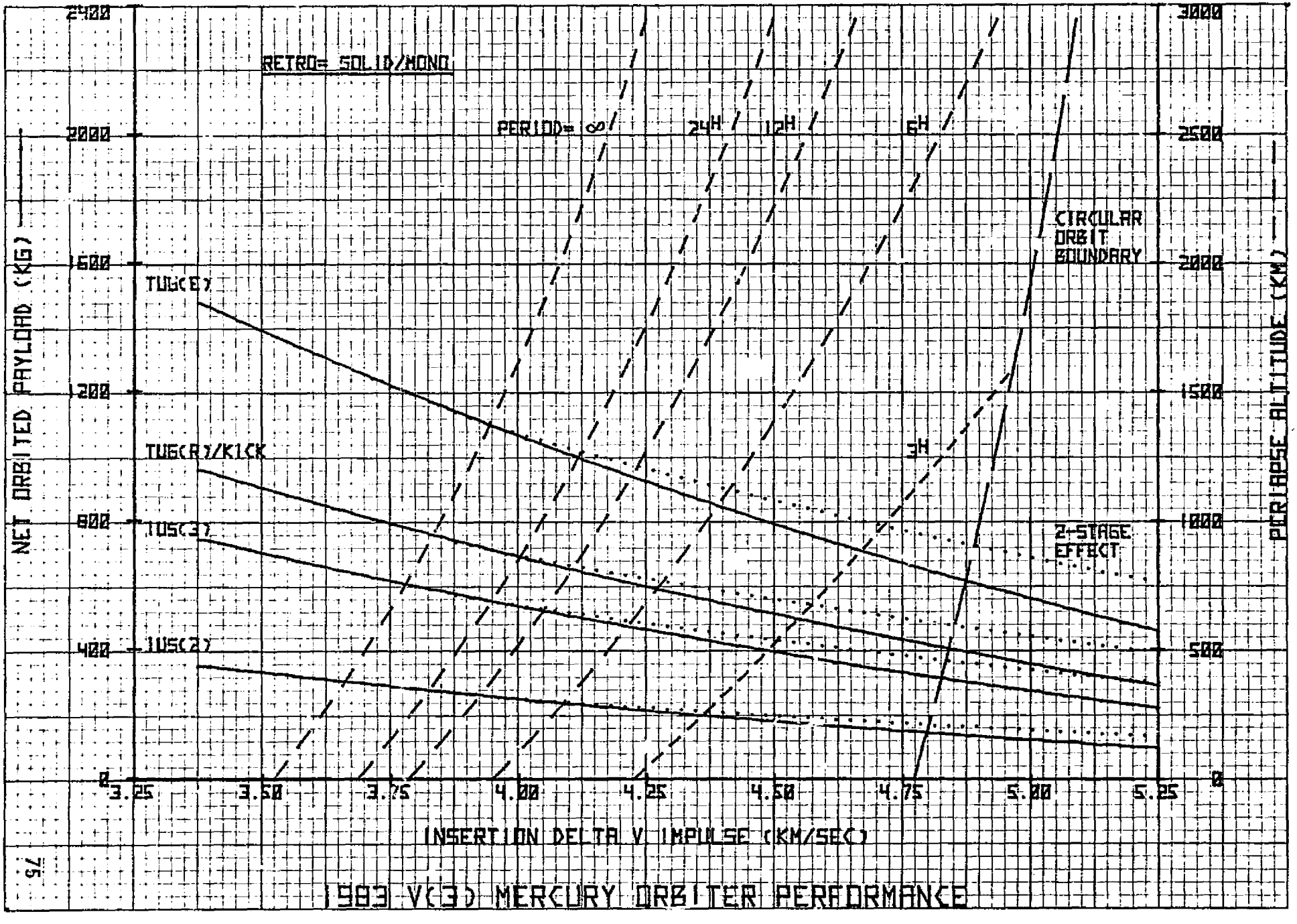
RETRO= SOLID/MONO
PERIOD= ∞
24H
12H
6H
3H
CIRCULAR ORBIT BOUNDARY
2-STAGE EFFECT
TUG(E)
TUG(R)/KICK
IUS(3)
IUS(2)
NET ORBITED PAYLOAD (KG)
PERIAPSE ALTITUDE (KM)
2400
2000
1600
1200
800
400
0
3000
2500
2000
1500
1000
500
0
3.25
3.50
3.75
4.00
4.25
4.50
4.75
5.00
5.25
INSERTION DELTA V IMPULSE (KM/SEC)
1983 V(3) MERCURY ORBITER PERFORMANCE

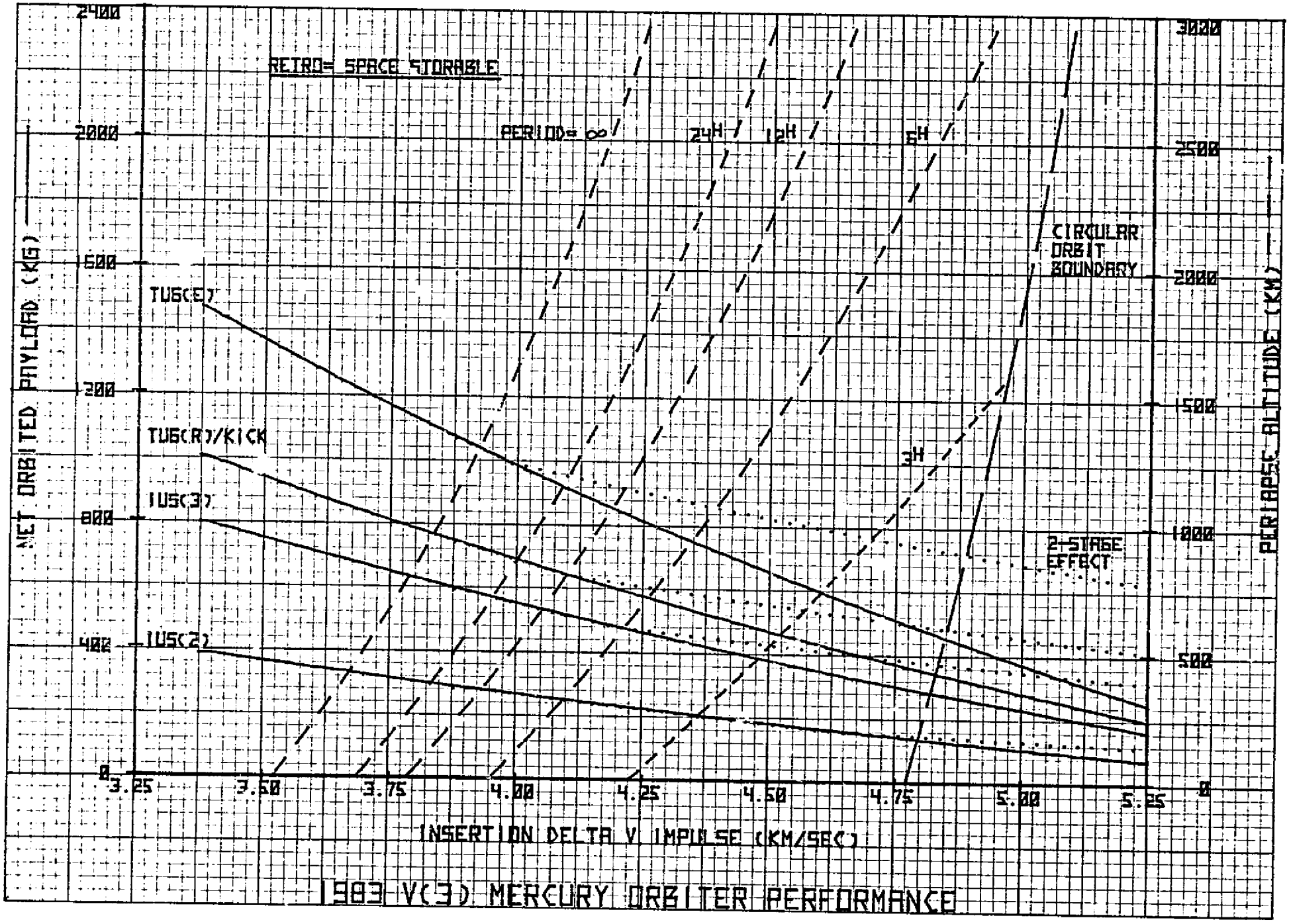

1983 V(3) MERCURY ORBITER PERFORMANCE

1985 V(1) OPPORTUNITY

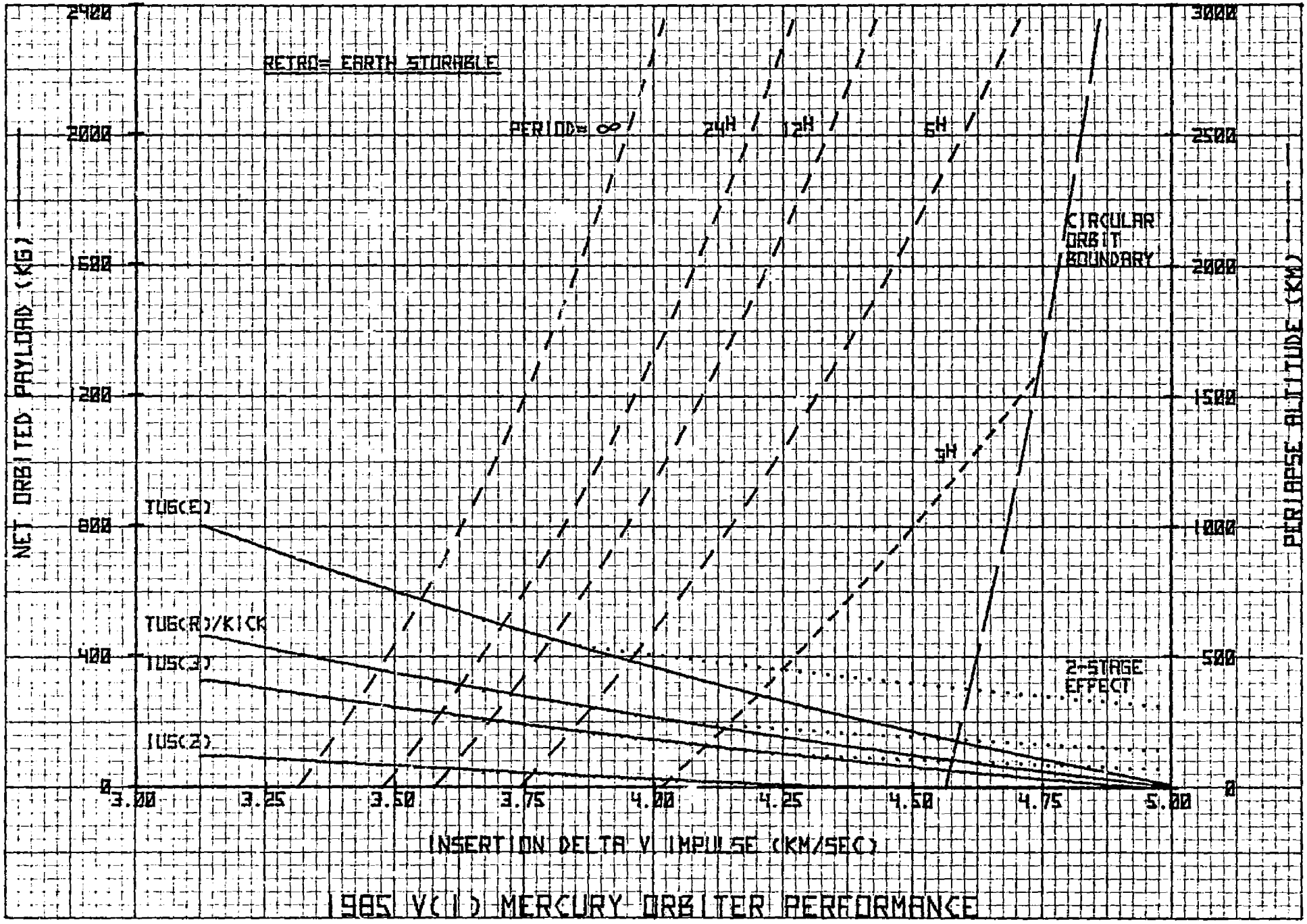

1985 V(I) MERCURY ORBITER PERFORMANCE

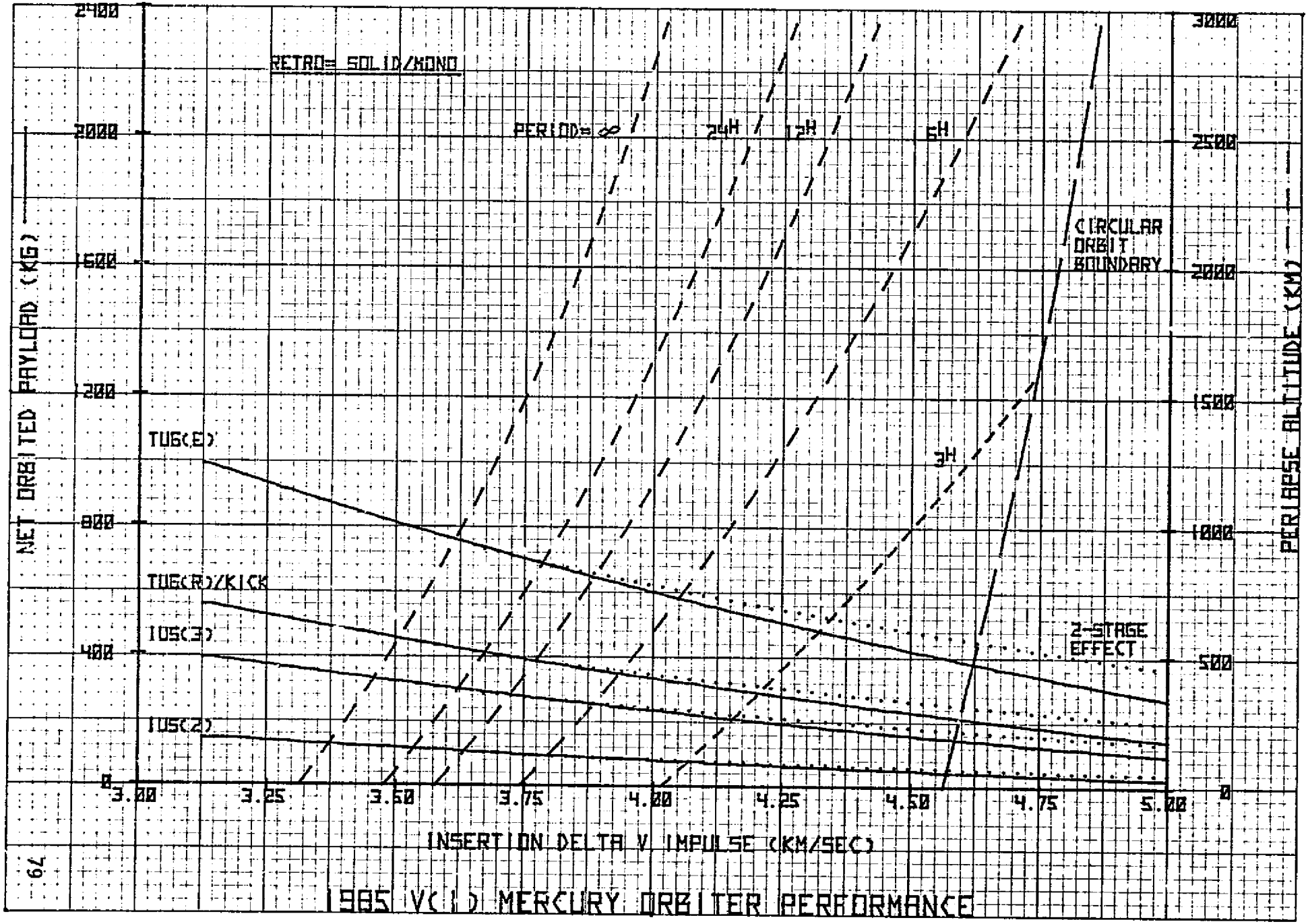

1985 V(1) MERCURY ORBITER PERFORMANCE

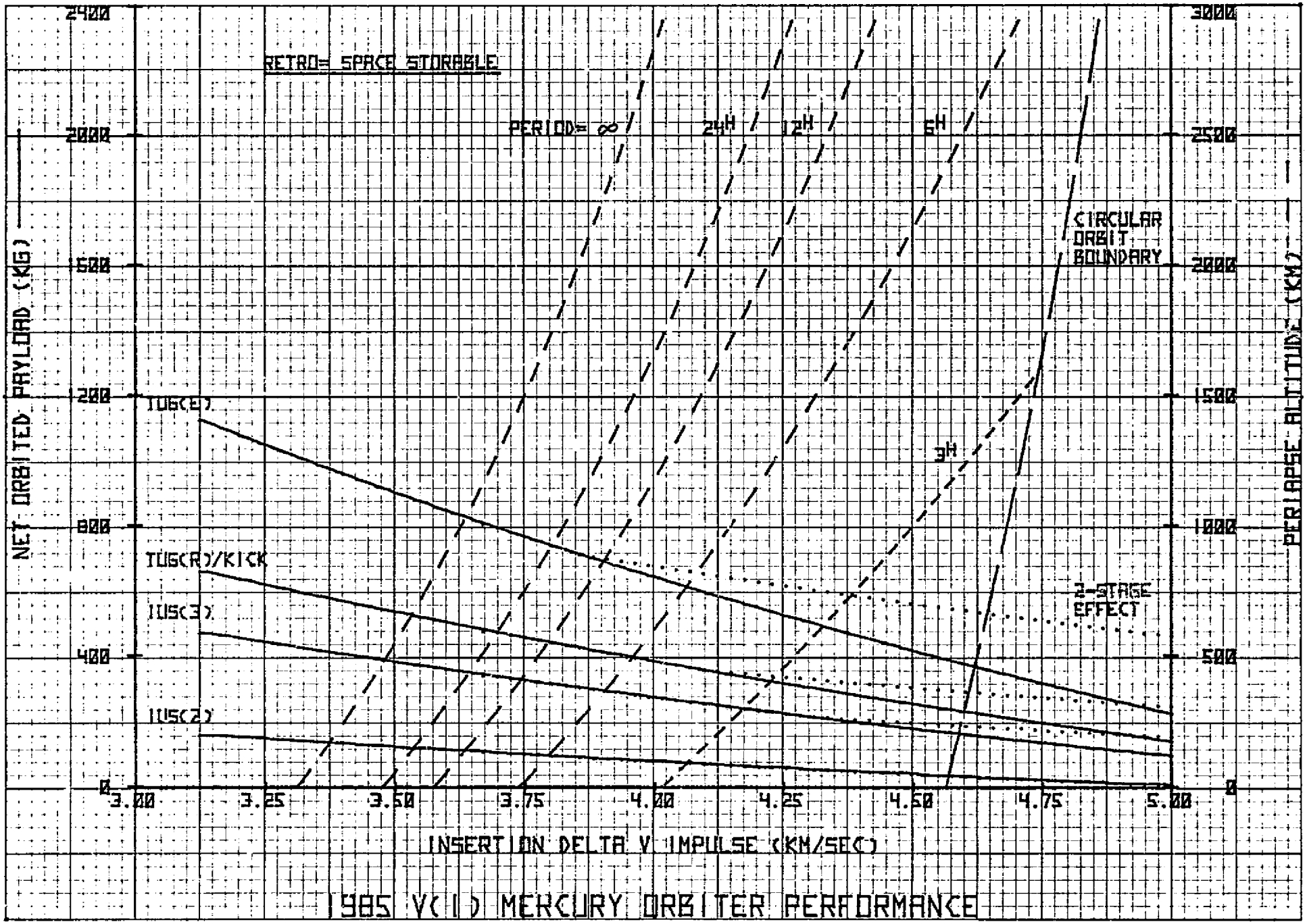

1985 VCID MERCURY ORBITER PERFORMANCE

1986 V(2) OPPORTUNITY

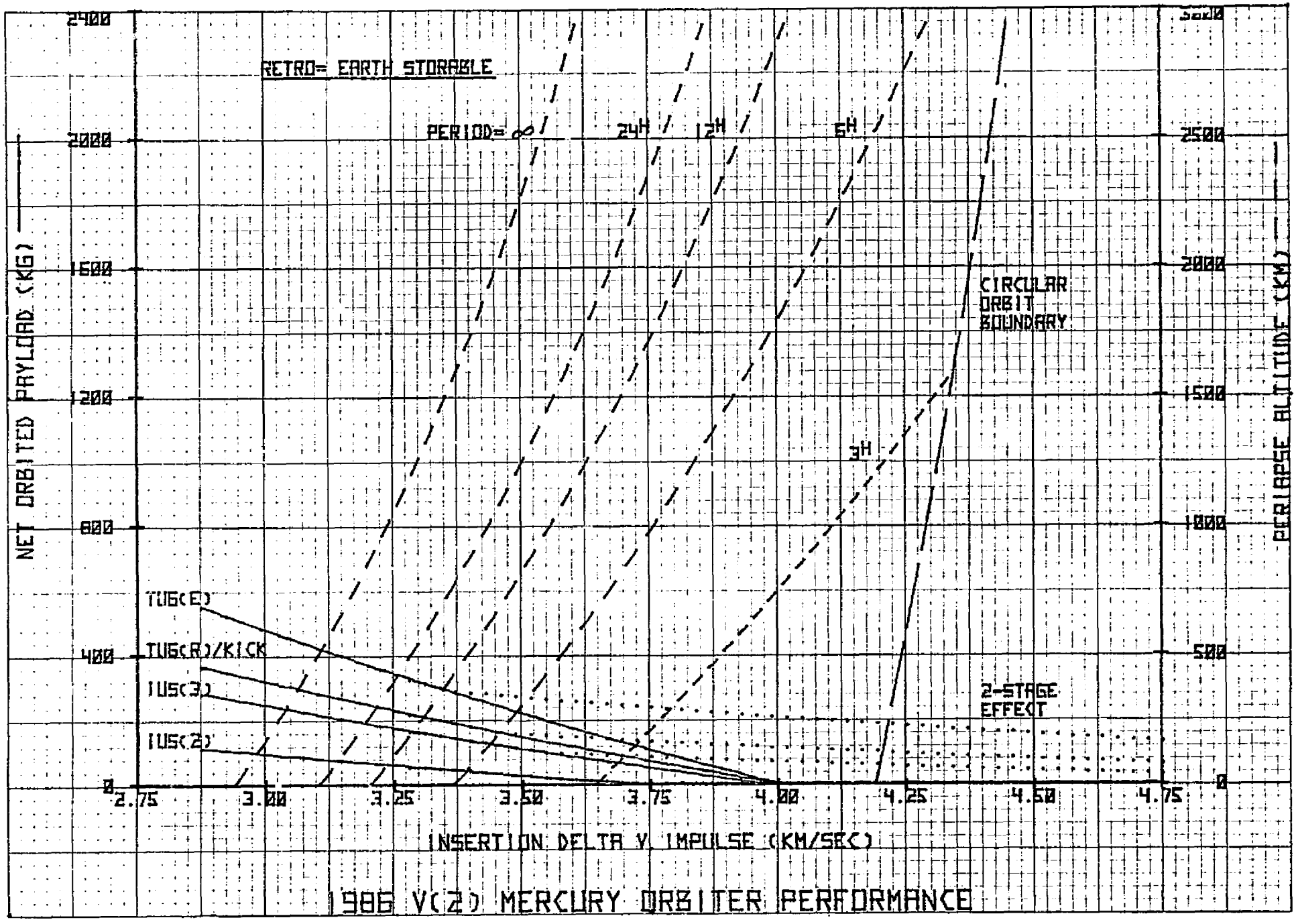

1986 V(2) MERCURY ORBITER PERFORMANCE

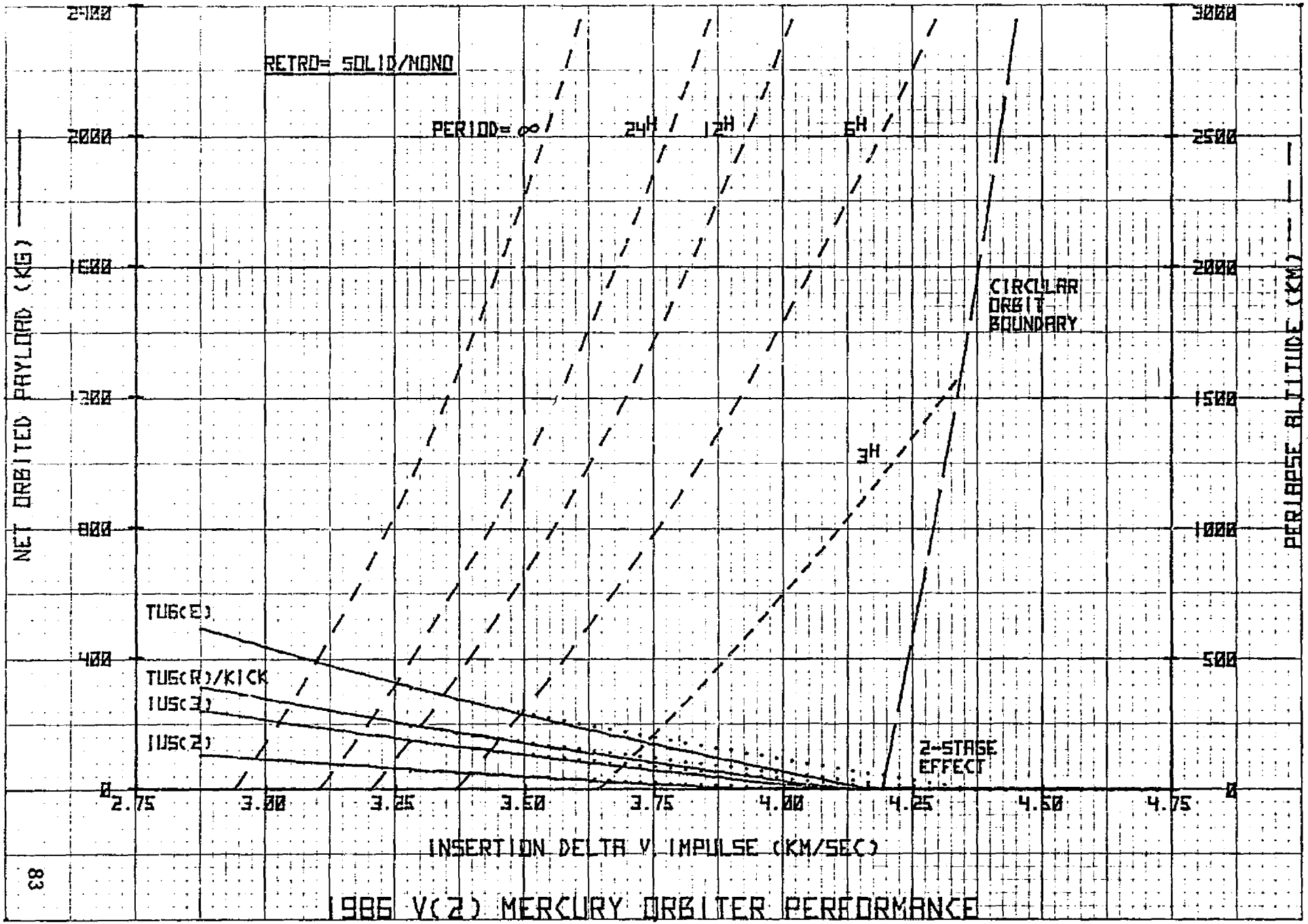

1986 V(2) MERCURY ORBITER PERFORMANCE

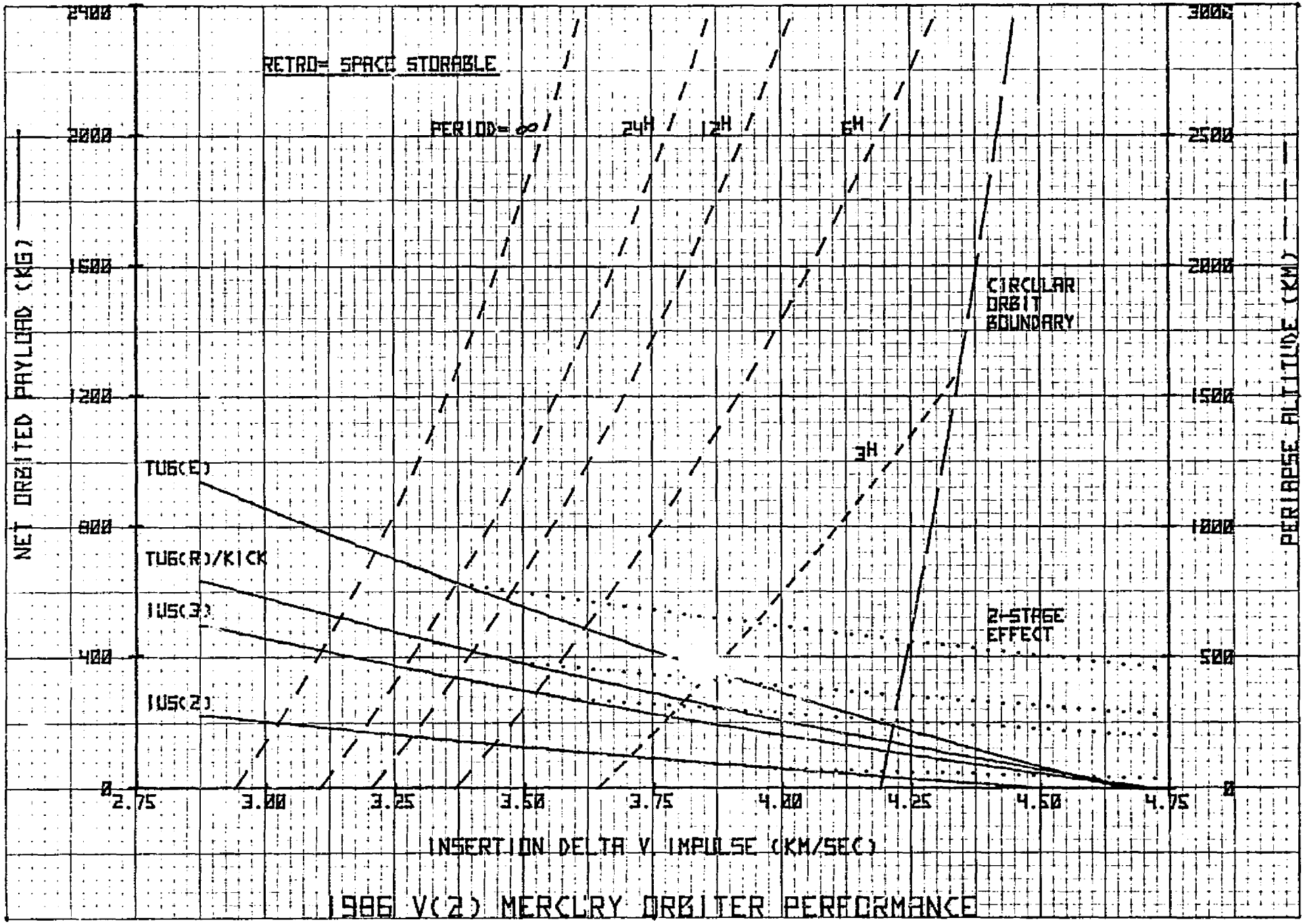

1986 V(2) MERCURY ORBITER PERFORMANCE

1986 V(3) OPPORTUNITY

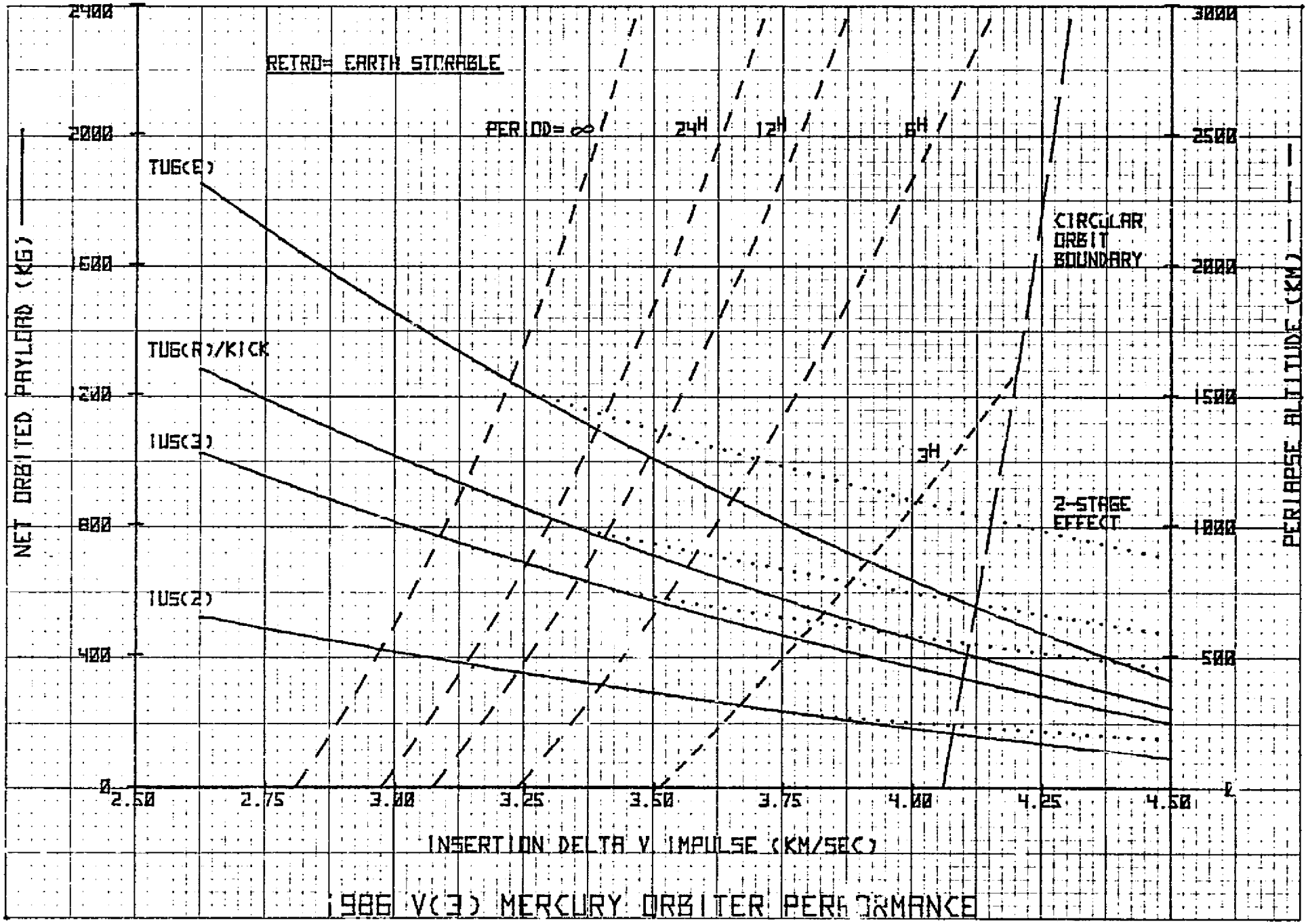

1986 V(3) MERCURY ORBITER PERFORMANCE

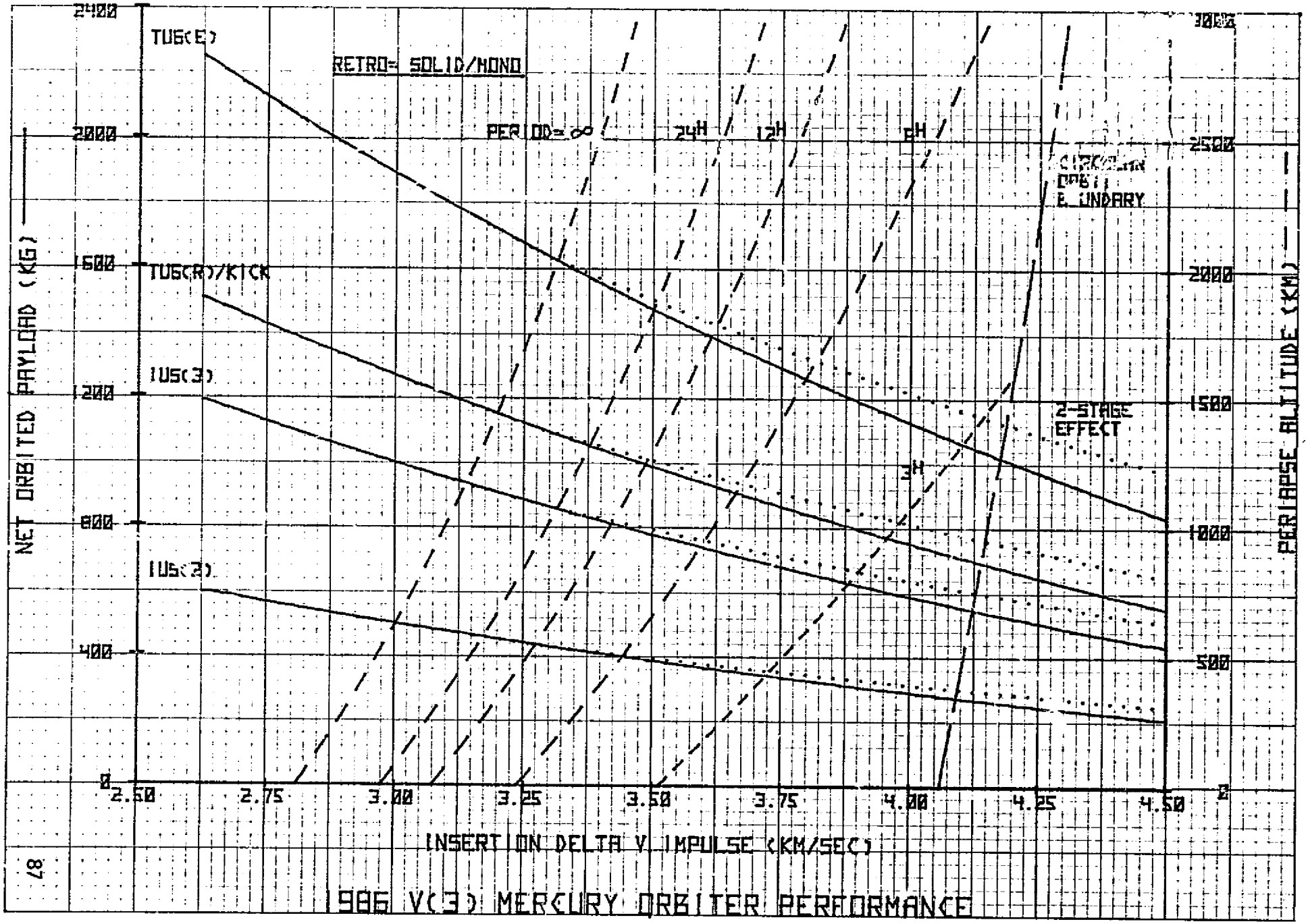

1986 V(3) MERCURY ORBITER PERFORMANCE

48

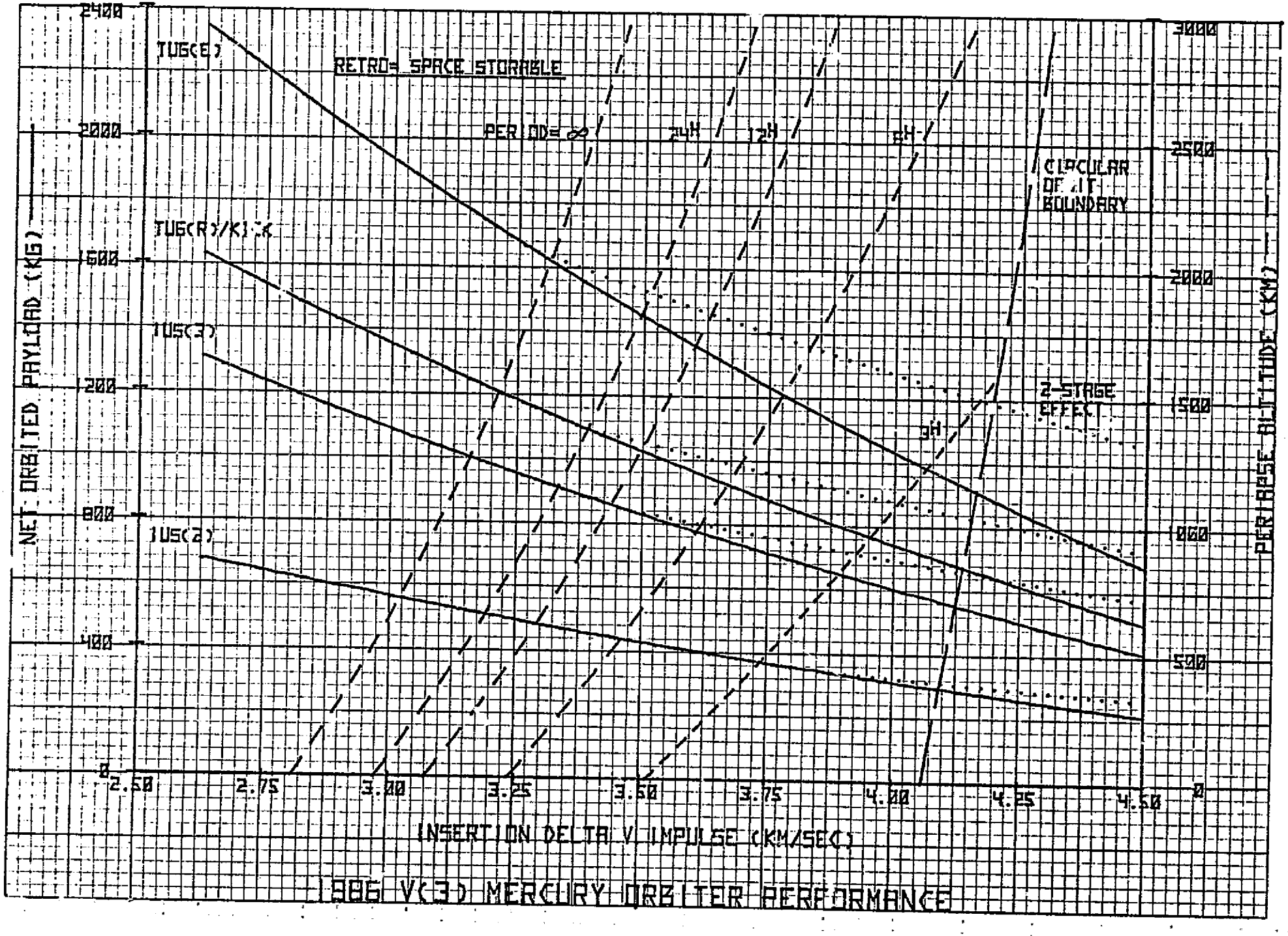
TUG(E)
RETRO= SPACE STORABLE
PERIOD= ∞
24H
12H
8H
3H
CIRCULAR
DE-ORBIT
BOUNDARY
TUG(R)/K1.2K
TUS(3)
TUS(2)
2-STAGE
EFFECT
NET ORBITED PAYLOAD (KG)
PERIAPSE ALTITUDE (KM)
2400
2000
1600
1200
800
400
0
3000
2500
2000
1500
1000
500
0
2.50
2.75
3.00
3.25
3.50
3.75
4.00
4.25
4.50
INSERTION DELTA V IMPULSE (KM/SEC)
A86 V(3) MERCURY ORBITER PERFORMANCE

1988 V(2)-a OPPORTUNITY

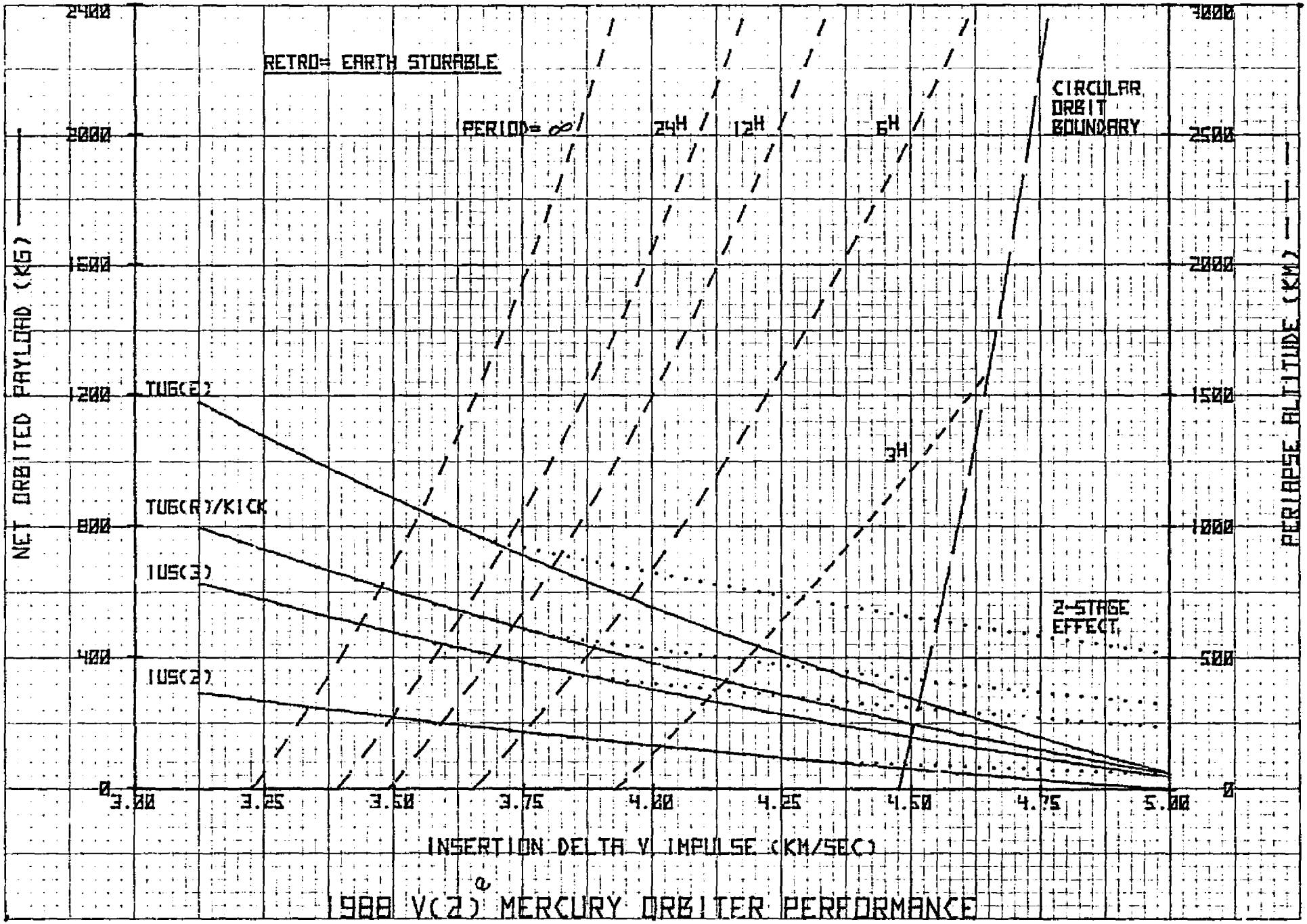

1988 V(2) MERCURY ORBITER PERFORMANCE

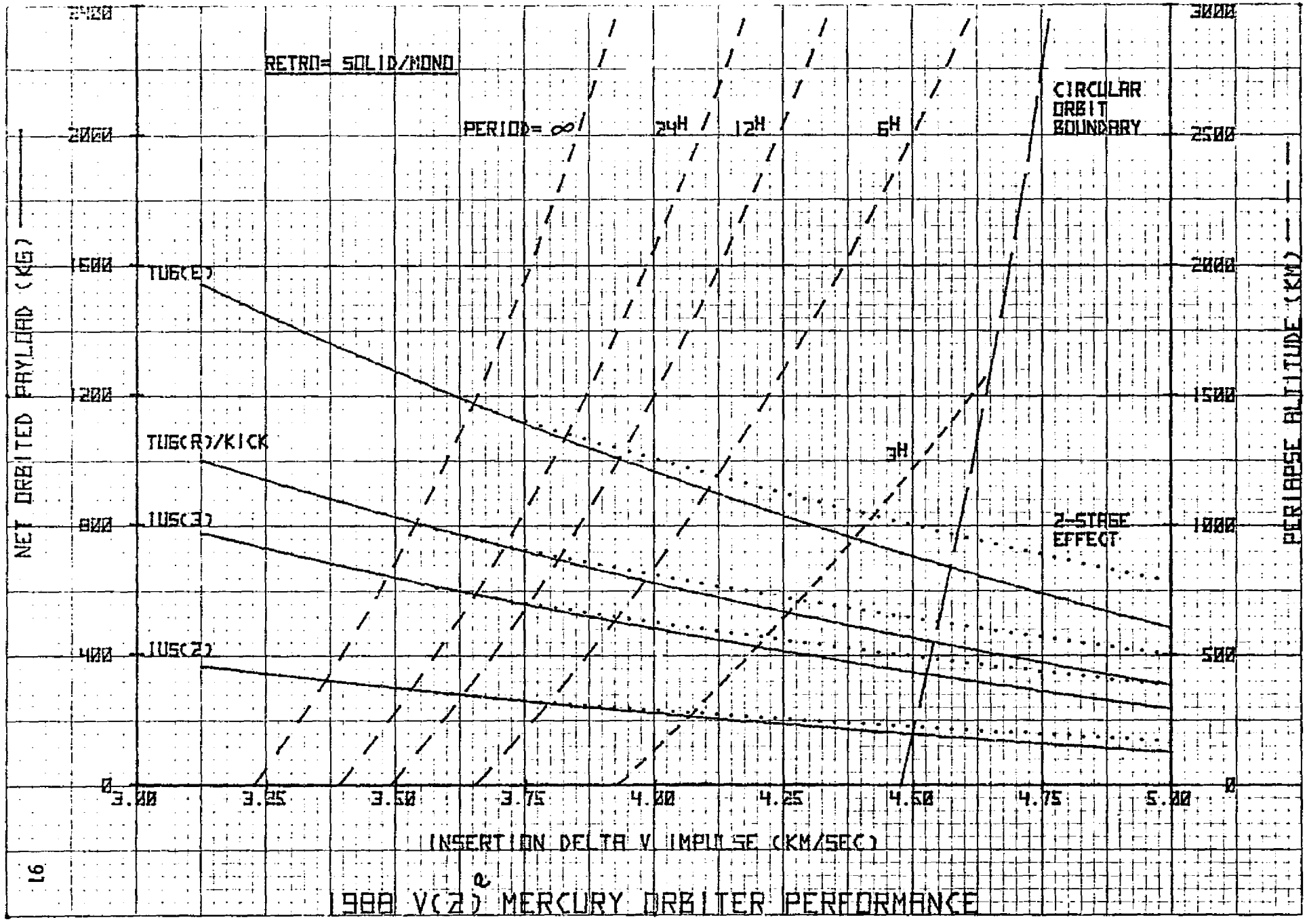

1988 V(2) MERCURY ORBITER PERFORMANCE

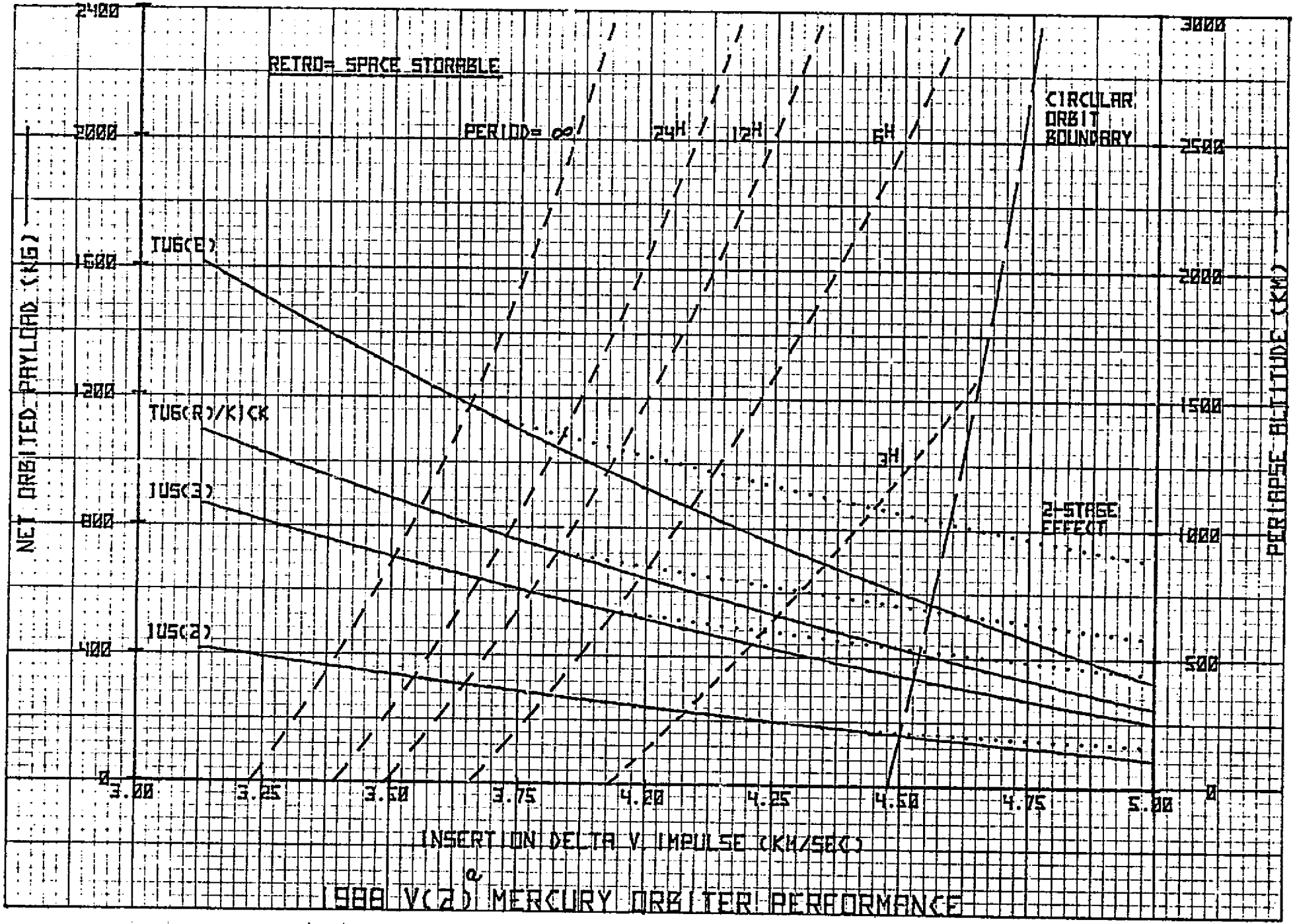

1988 V(2) MERCURY ORBITER PERFORMANCE

1988 V(2)-b OPPORTUNITY

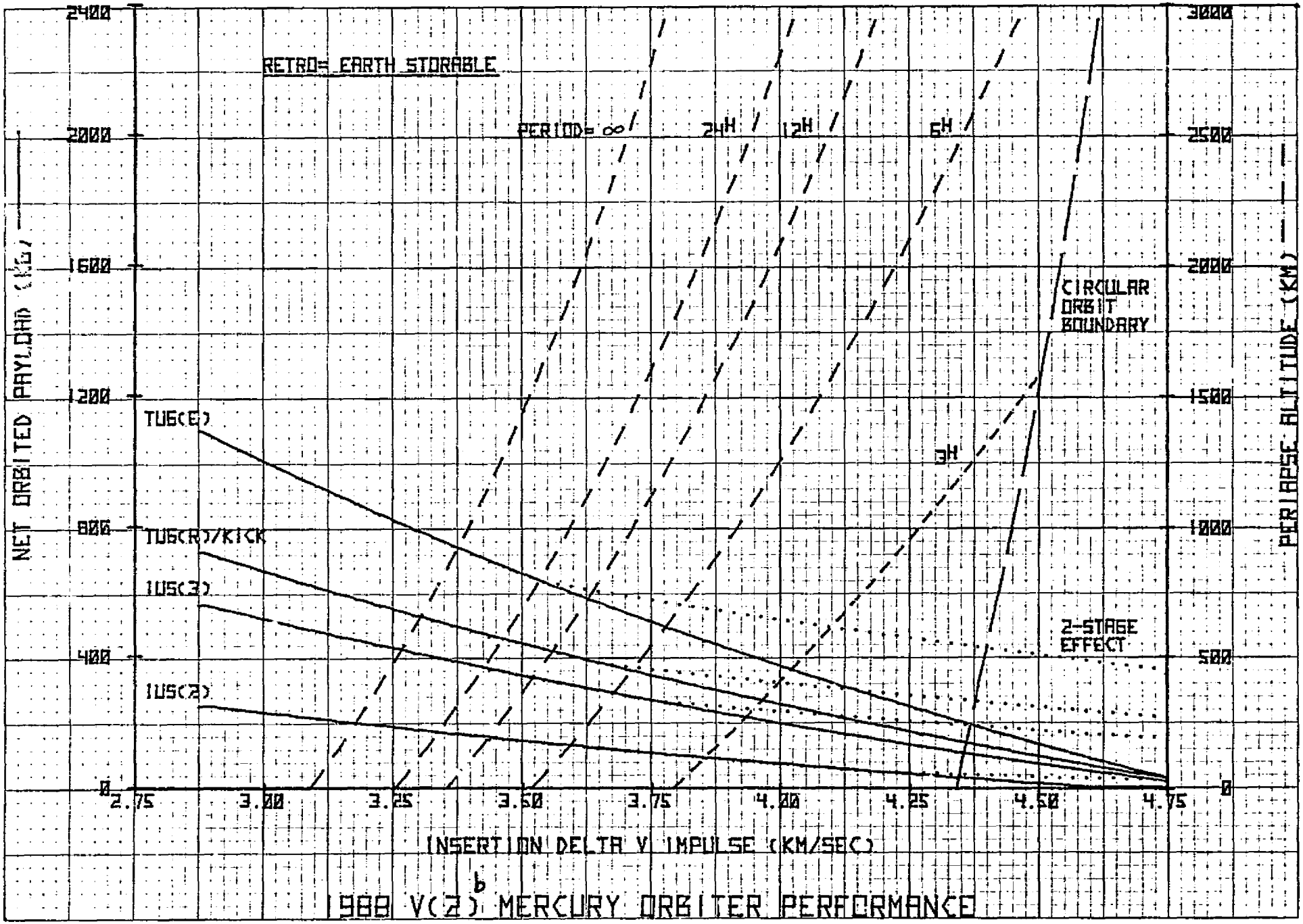

1988 V(2) MERCURY ORBITER PERFORMANCE

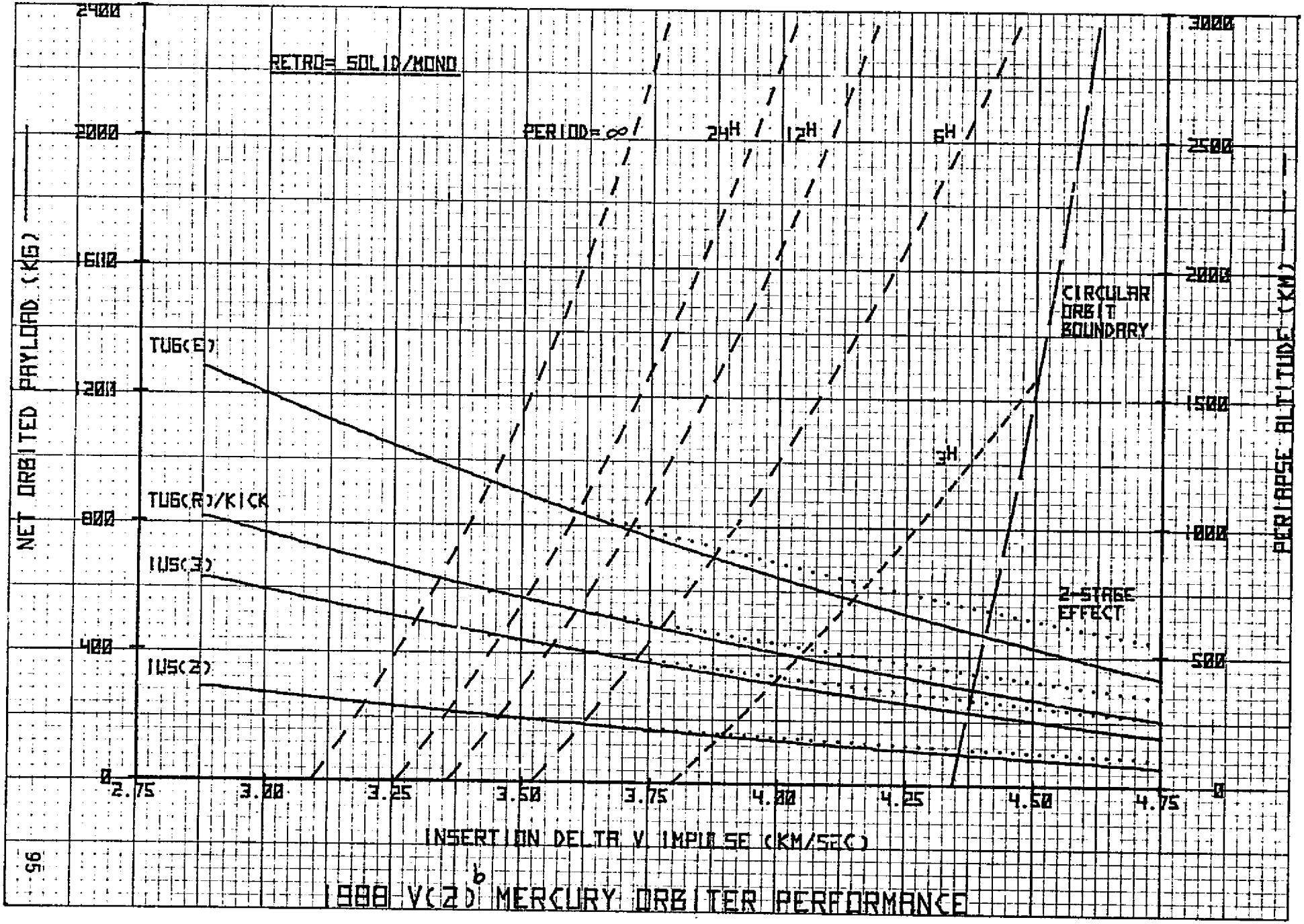

1988 V(2)[b] MERCURY ORBITER PERFORMANCE

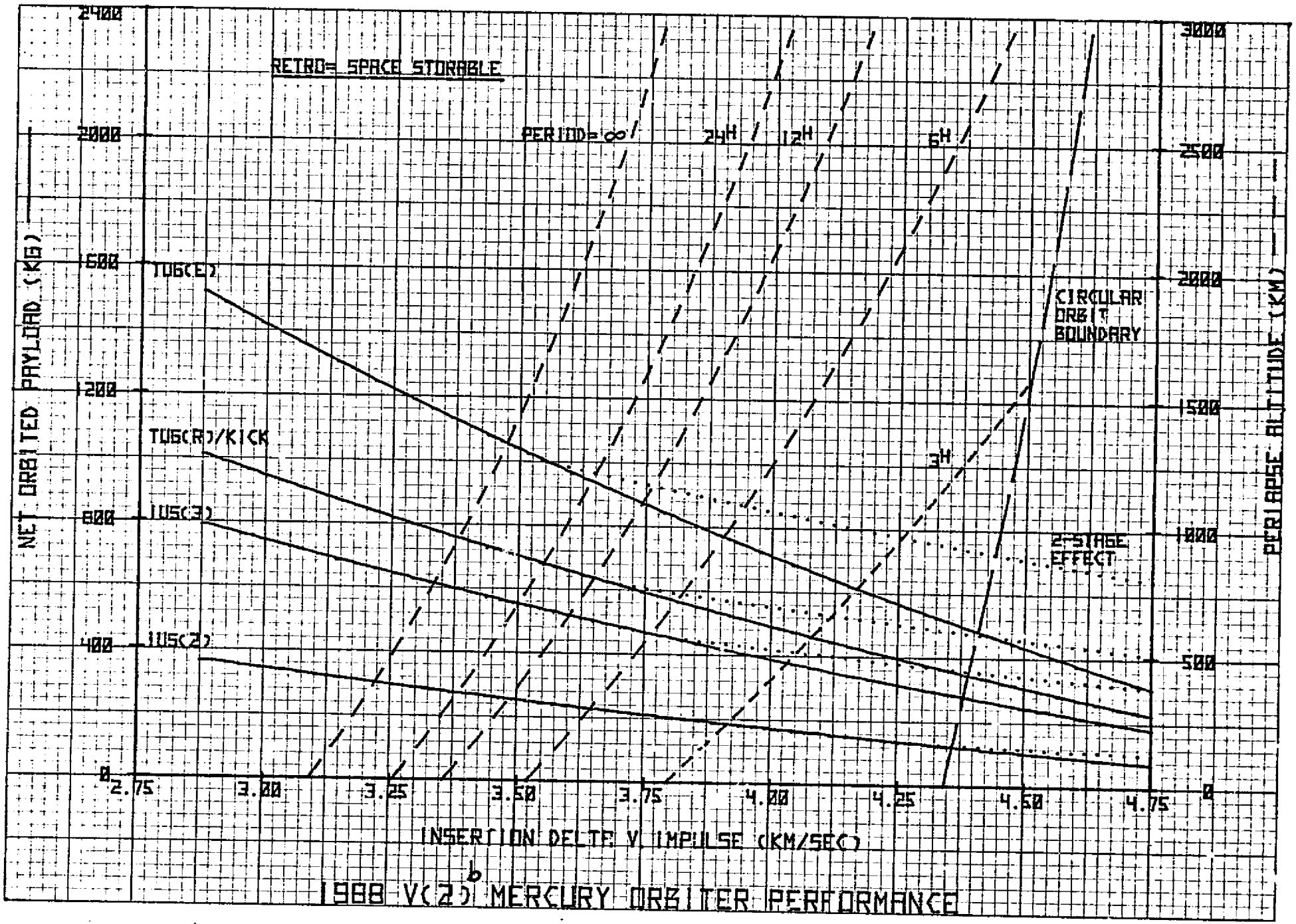

1988 V(2)[b] MERCURY ORBITER PERFORMANCE

1989 V(2) OPPORTUNITY

86

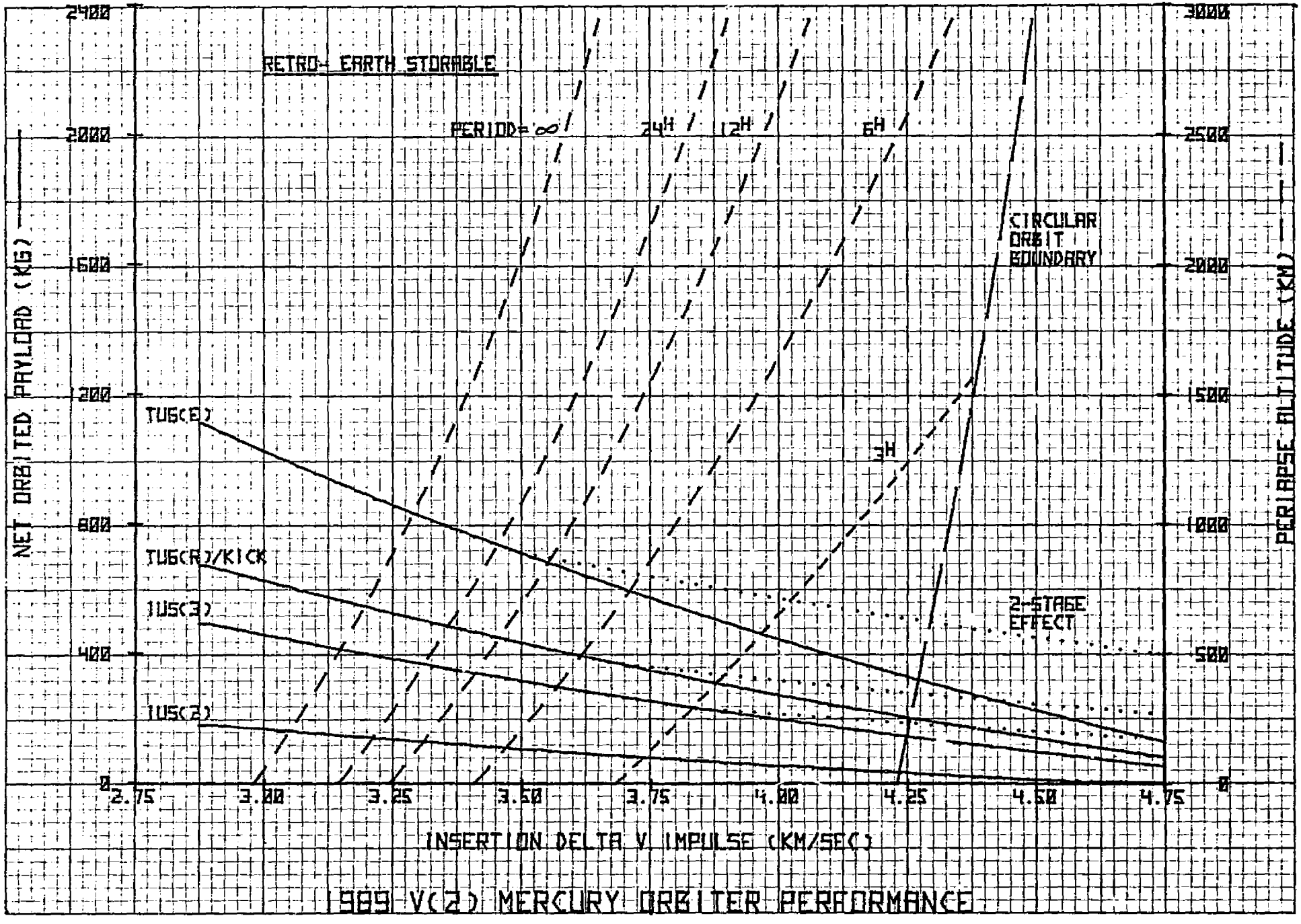

1989 V(2) MERCURY ORBITER PERFORMANCE

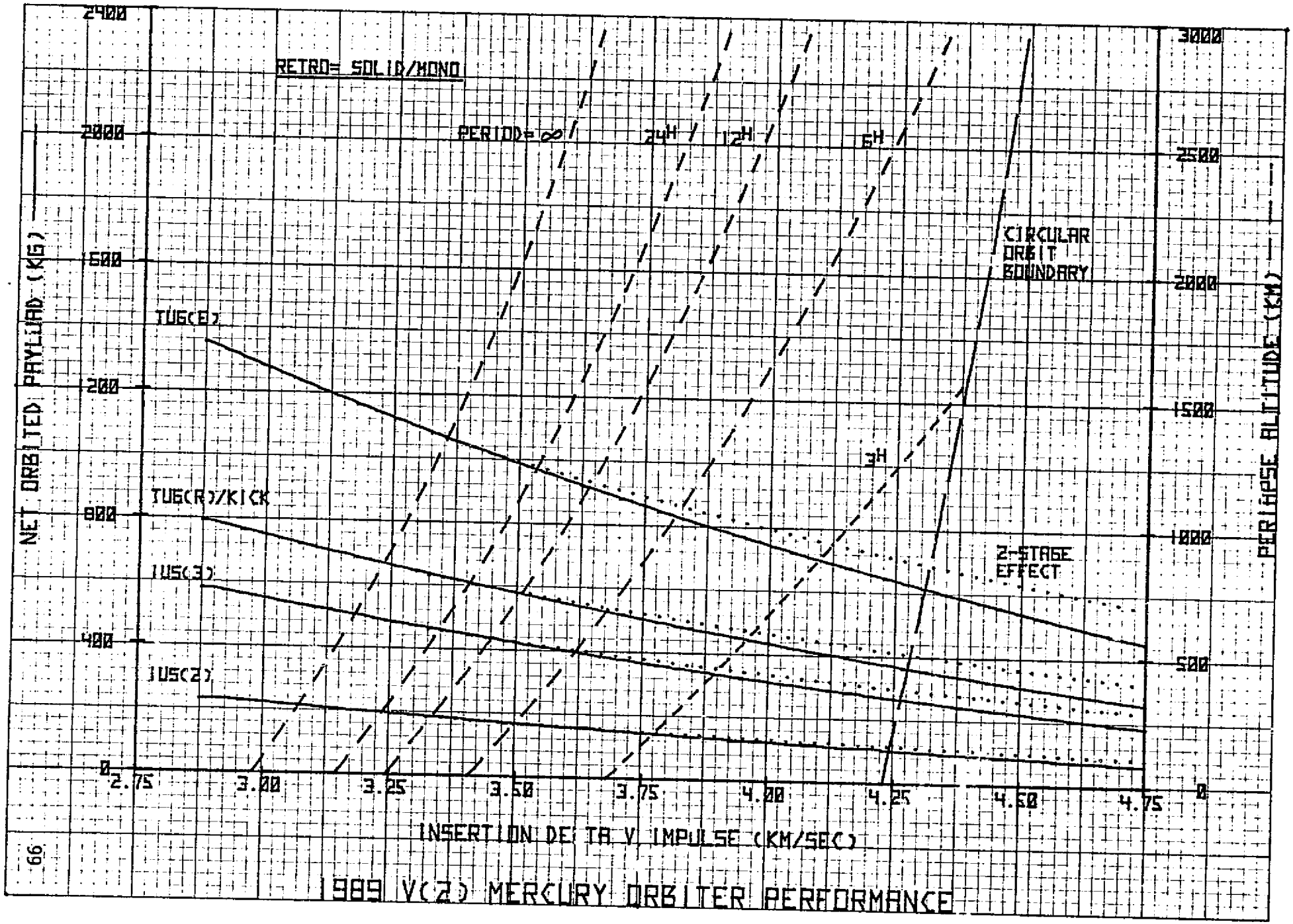

66

1989 V(2) MERCURY ORBITER PERFORMANCE

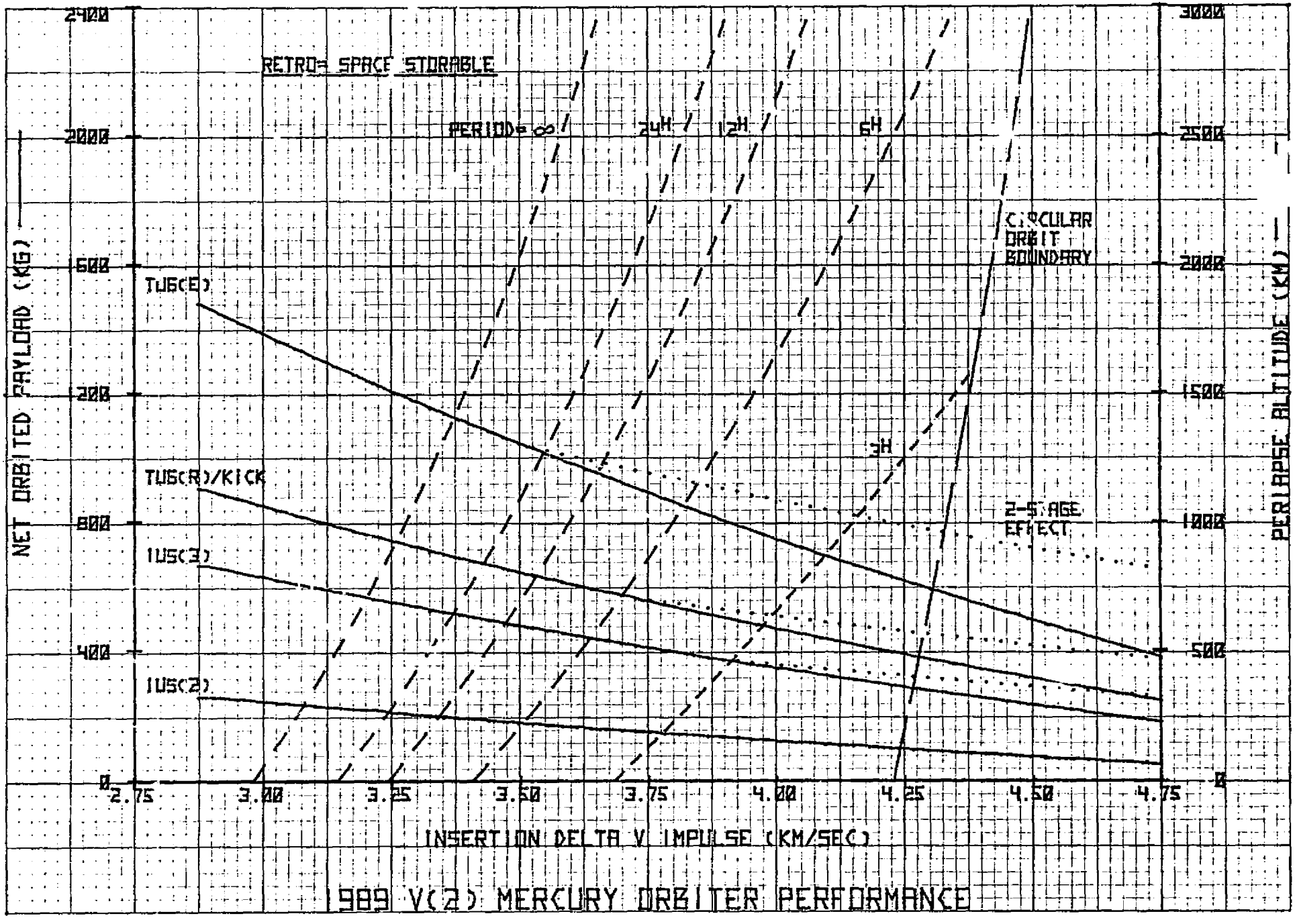

1989 V(2) MERCURY ORBITER PERFORMANCE

1991 V(2) OPPORTUNITY

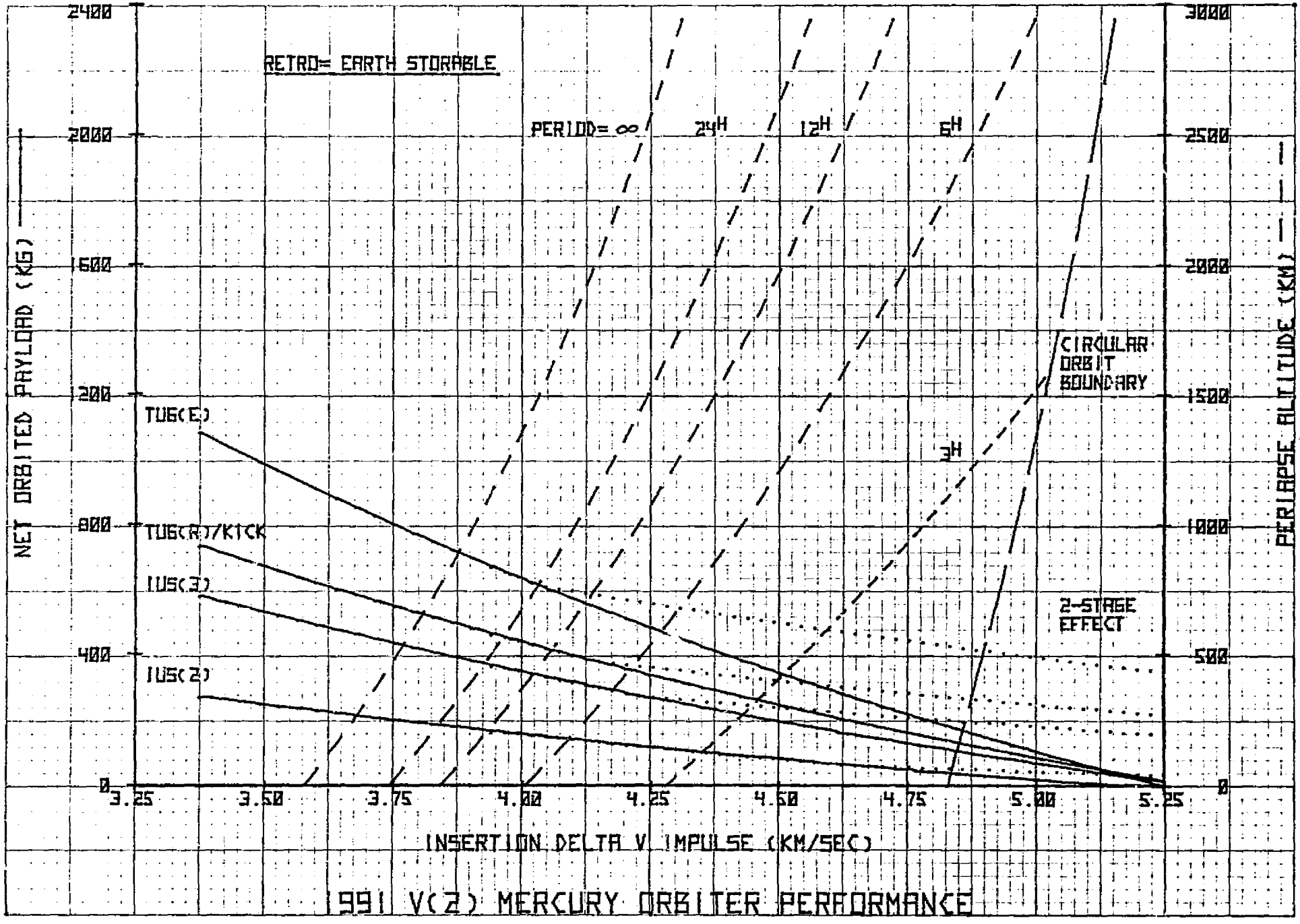

991 V(2) MERCURY ORBITER PERFORMANCE

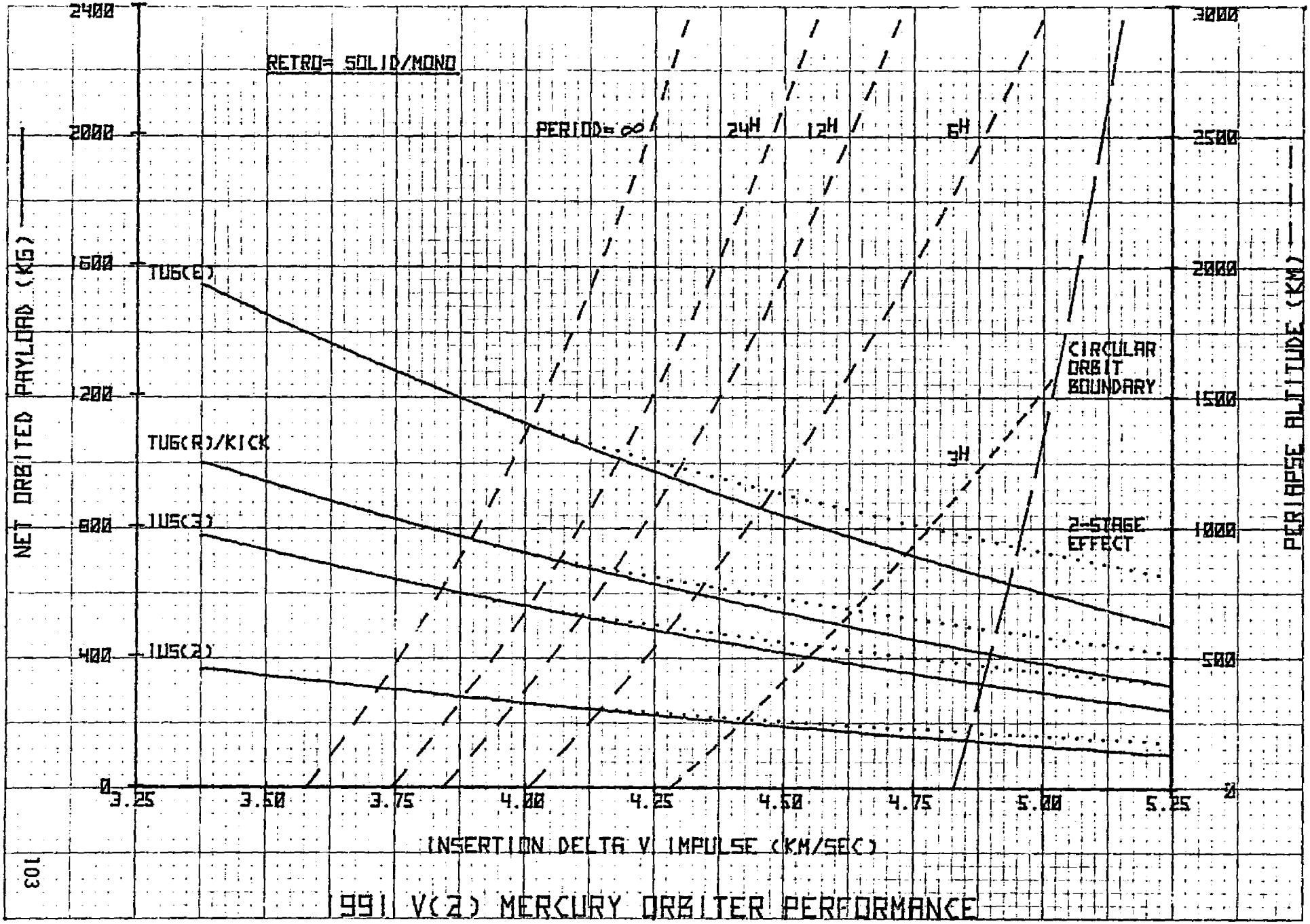

103

1991 V(2) MERCURY ORBITER PERFORMANCE

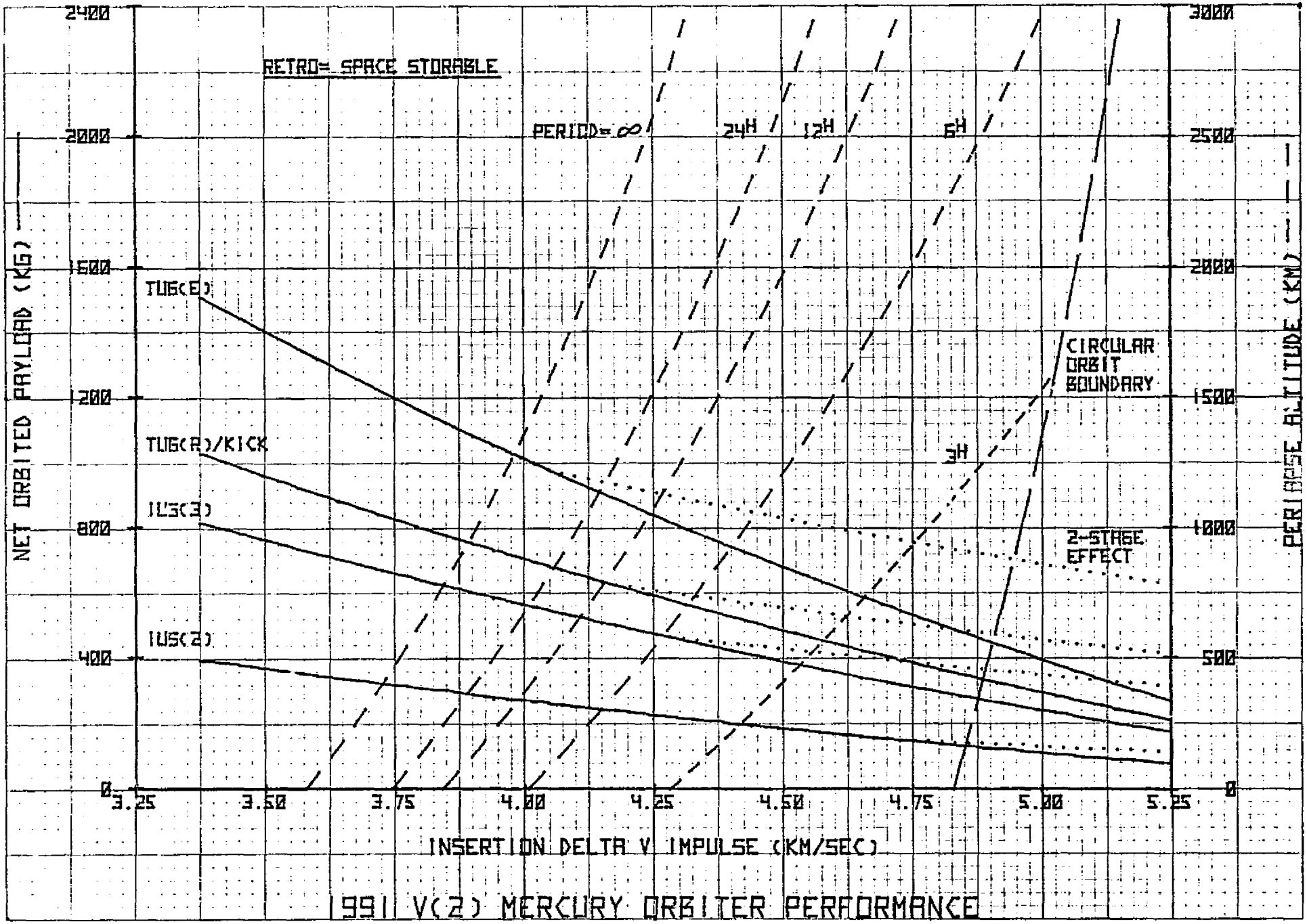

1991 V(2) MERCURY ORBITER PERFORMANCE

1994 V(2) OPPORTUNITY

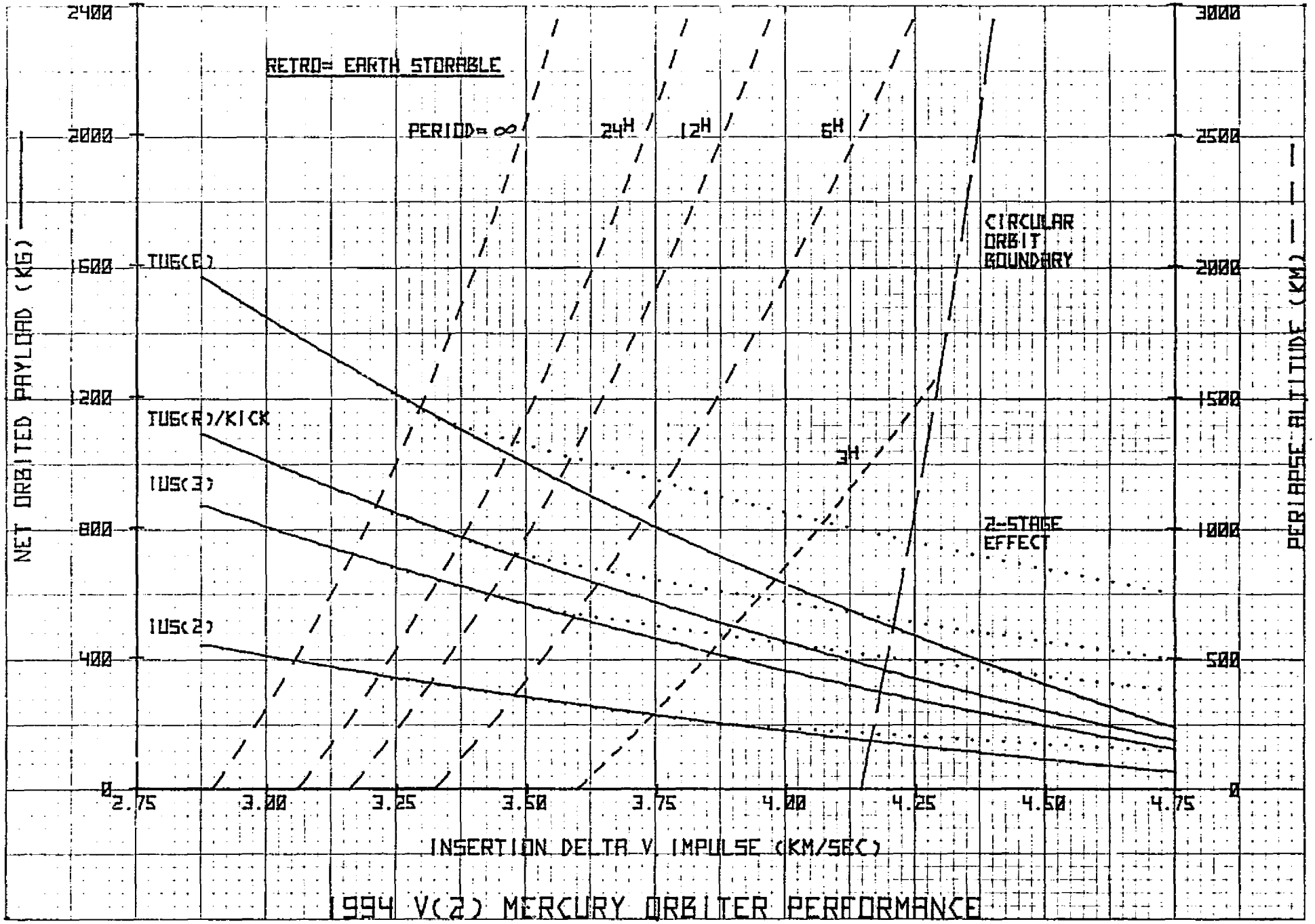

1994 V(2) MERCURY ORBITER PERFORMANCE

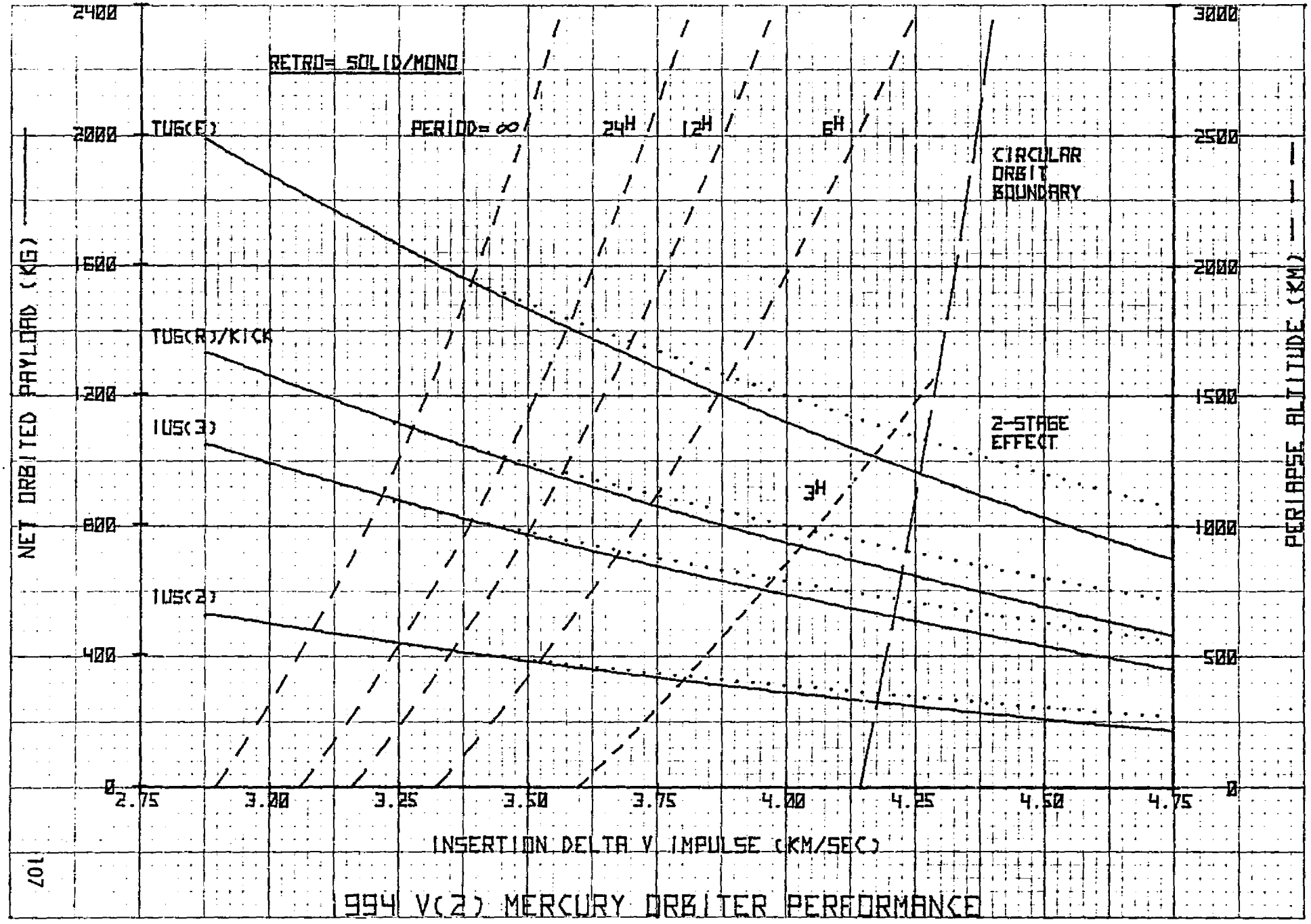

994 V(2) MERCURY ORBITER PERFORMANCE

108

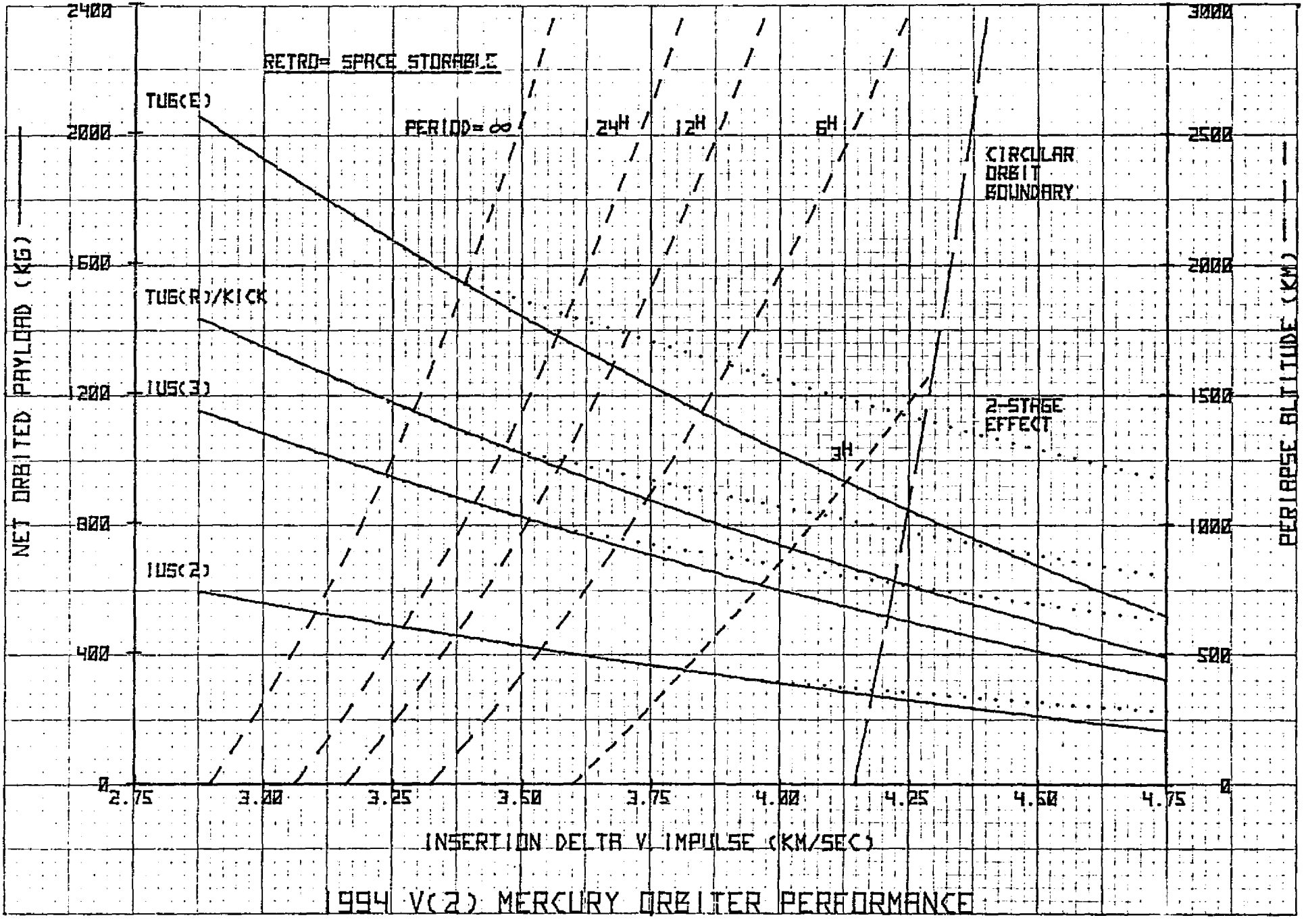

1994 V(2) MERCURY ORBITER PERFORMANCE

1996 V(3) OPPORTUNITY

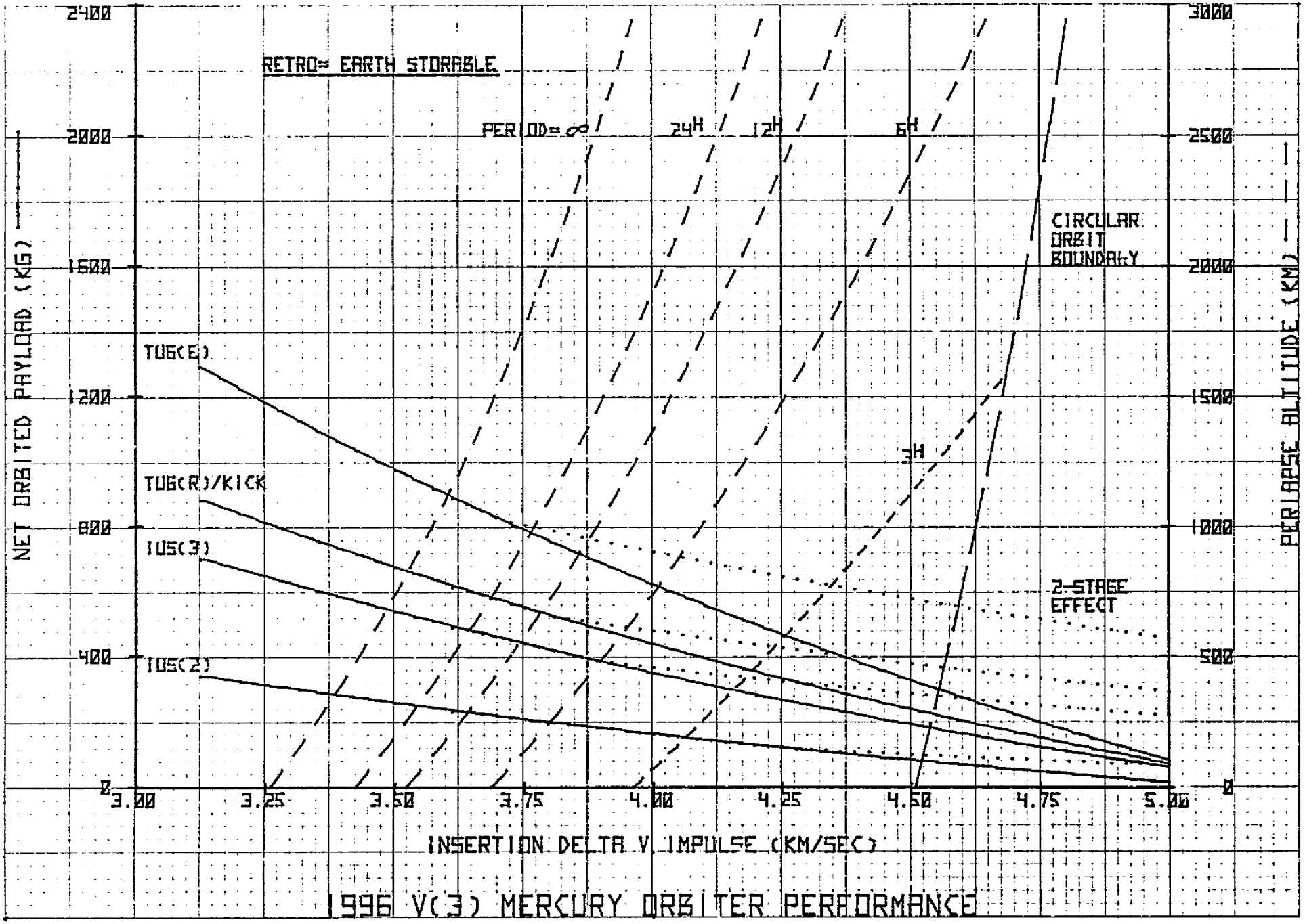

1996 V(3) MERCURY ORBITER PERFORMANCE

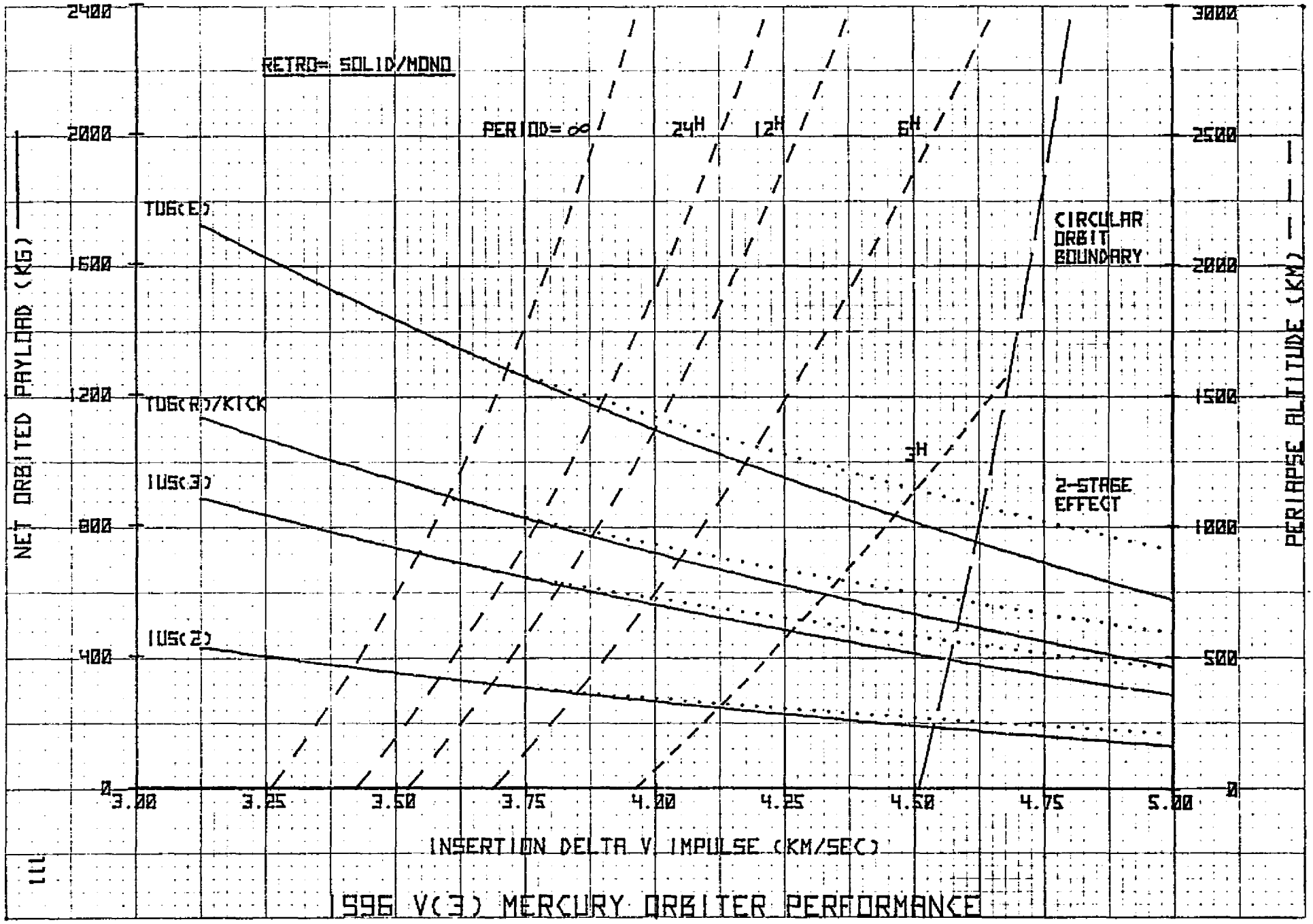

111

1596 V(3) MERCURY ORBITER PERFORMANCE

112

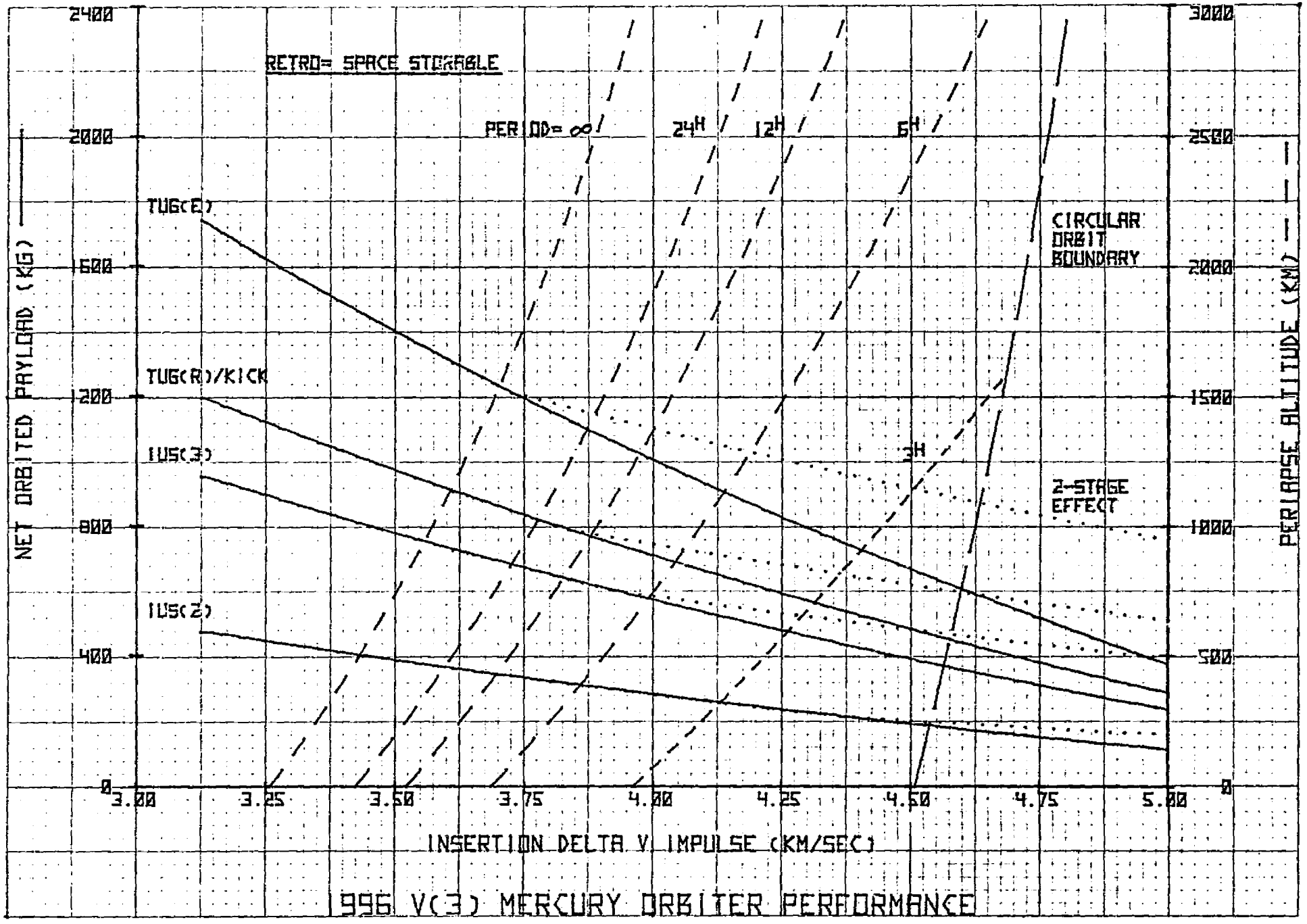

1996 V(3) MERCURY ORBITER PERFORMANCE

1999 V(4) OPPORTUNITY

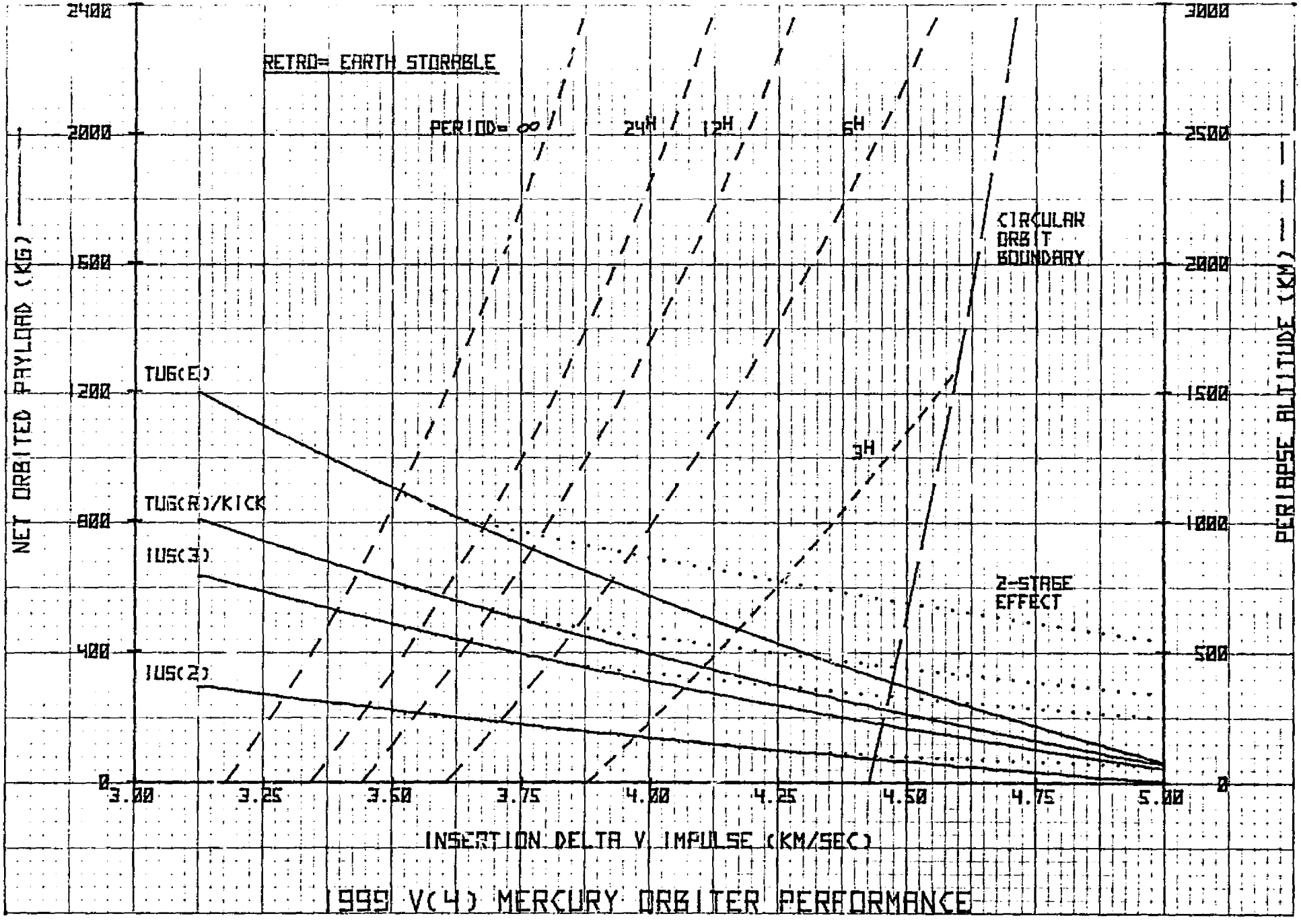

1999 V(4) MERCURY ORBITER PERFORMANCE

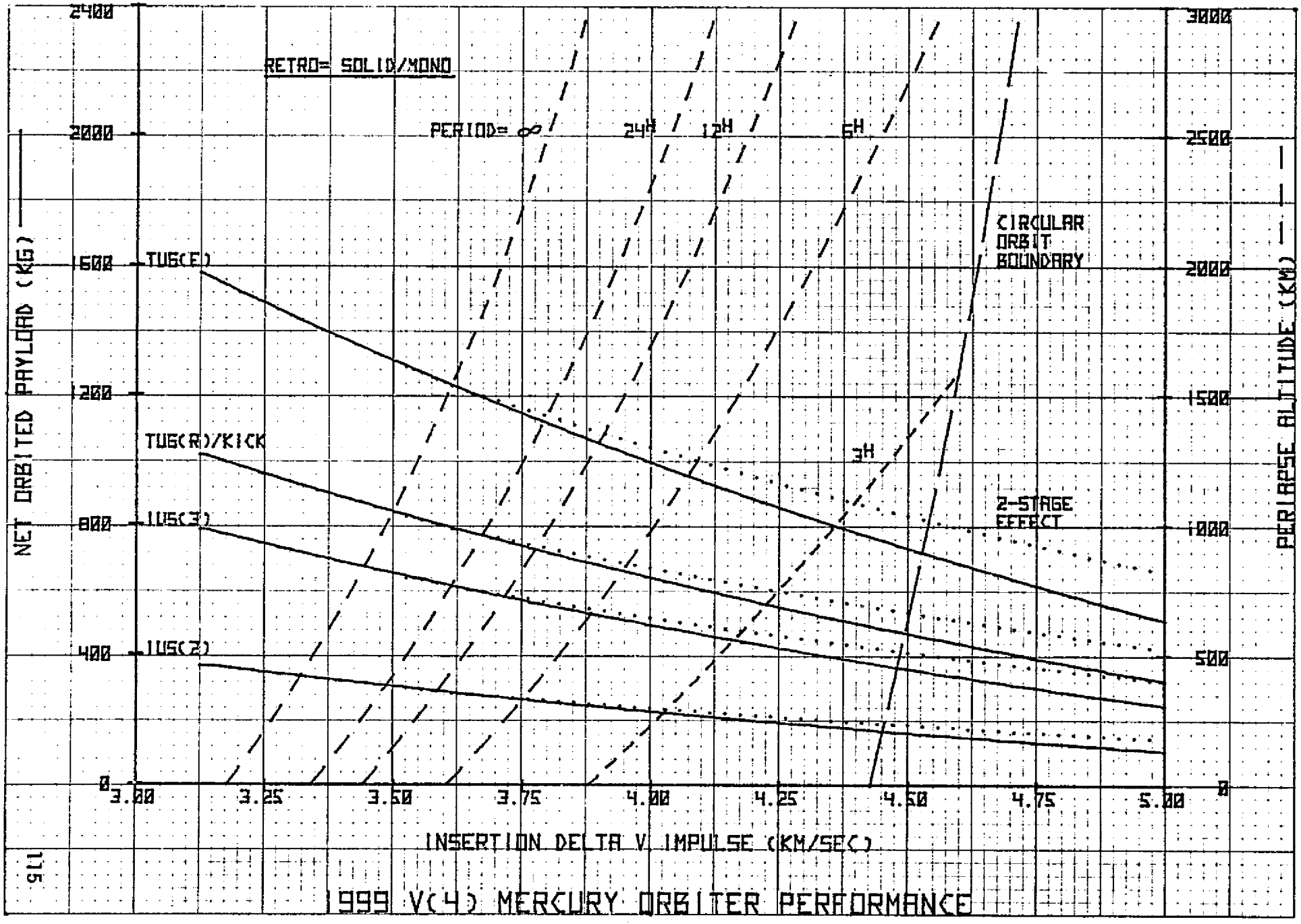

1999 V(4) MERCURY ORBITER PERFORMANCE

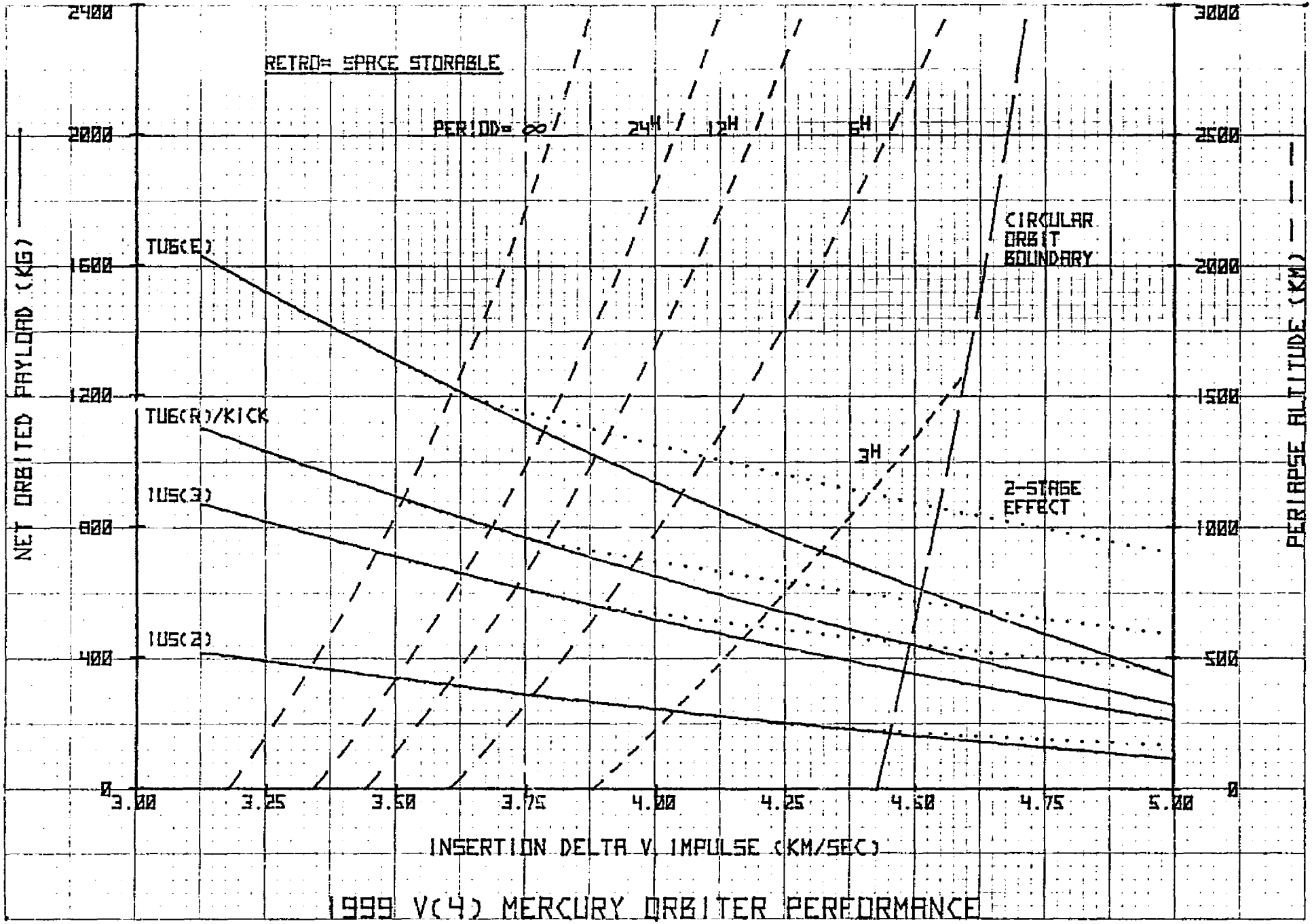

1999 V(4) MERCURY ORBITER PERFORMANCE